



**Politecnico
di Torino**

Politecnico di Torino

FACOLTÀ DI INGEGNERIA MECCANICA E AEROSPAZIALE

Corso di Laurea Magistrale in Ingegneria Aerospaziale

**Satellite structural critical components static test and FEM model
correlation**

Candidato:

Elisa Stasi

Matricola S265796

Relatore:

Prof. Marco Gherlone

Correlatore:

Ing. Luigi Manfredi

List of Figures

1.1	Example of satellite in orbit - <i>Courtesy of TAS-I</i>	6
2.1	Design limit load factor of Soyuz Launcher [1]	9
2.2	Isogrid typical structure [2]	13
3.1	Sandwich panels representation [4]	19
3.2	Particular of honeycomb structure [5]	20
3.3	Qualitative chart of different honeycomb materials [5]	21
3.4	Insert section [6]	23
3.5	Standardized insert diameters [6]	27
3.6	Standardized insert heights [6]	27
3.7	Illustration of typical loads applied to inserts [6]	29
3.8	(a)Rivet shearing, (b) bearing of the hole, (c) ripping, (d) breaking of the plates [7]	34
3.9	Double lap shear joint [8]	35
3.10	Adhesive graphics [8]	36
4.1	Campaign planning scheme - <i>Courtesy of TAS-I</i>	38
4.2	Cylindrical sandwich configuration - [9]	39
4.3	Insert pull-out Test [9]	41
4.4	Insert Shear Test [9]	41
4.5	Bearing characterization [9]	43
4.6	Standard single lap shear specimen [10]	44
4.7	Double Lap shear test on the CFRP laminate [11]	44
4.8	Double shear test on CFRP-Aluminum plate [11]	45
5.1	(a) CAD model - <i>Courtesy of TAS-I</i> , (b) FEM model, (c) real sample of Coupon 1	47
5.2	(a) CAD model - <i>Courtesy of TAS-I</i> , (b) FEM model, (c) real sample of Coupon 2	48
5.3	(a) CAD model - <i>Courtesy of TAS-I</i> , (b) FEM model, (c) real sample of Coupon 3	50

6.1	Setup configuration of coupon 1 - <i>Courtesy of TAS-I</i>	52
6.2	Plot of strains for Strain Gauges 1, 2, 5, 6, 7 and 8	54
6.3	Plot of strains for Axial Strain Gauges 9 and 10 and for bi-axial 3 and 4	55
6.4	Location of strain gauges on Coupon 1 [9]	56
6.5	Loading configuration of the three samples of coupon 2 [9]	58
6.6	Strain gauges position on the outer side of the sample [9]	59
7.1	Load effect due to F_x force - <i>Courtesy of TAS-I</i>	67
7.2	Load effect due to F_y force - <i>Courtesy of TAS-I</i>	68
7.3	Load effect due to F_z force - <i>Courtesy of TAS-I</i>	68
7.4	Load effect due to M_y moment and F_z force arm - <i>Courtesy of TAS-I</i>	69
7.5	Load effect due to M_x moment - <i>Courtesy of TAS-I</i>	70
7.6	Load effect due to M_z moment and due to F_y arm effect - <i>Courtesy of TAS-I</i>	71
8.1	General panel instability [12]	75
8.2	Comparison between general and panel instability [12]	75
8.3	Face dimpling, or Intracellular buckling [13]	76
8.4	Different failure mode for face wrinkling [12]	77
8.5	Shear : detail [5]	78
9.1	Coupon 1 - Rupture detail around brackets area - <i>Courtesy of TAS-TO</i>	81
9.2	Numbering of inserts	82
9.3	FEM detail of the failure zone in accordance to the test	86
9.4	Photo of the coupon 2 after pullout test - <i>Courtesy of TAS-TO</i> . . .	88
9.5	Position of the inserts for pullout test	89
9.6	Numbering of the inserts for axial traction test	92
9.7	Axial traction coupon immediately after the test - <i>Courtesy of TAS- TO</i>	93
9.8	Detail of the failure zone - <i>Courtesy of TAS-TO</i>	93
9.9	Result of the bending test and general view of the insert area - <i>Courtesy of TAS-TO</i>	96
9.10	(a) Detail of the first insert, with the broken skin, (b) an insert which reached plastic deformation, (c) difference between two con- secutive insert locations, where the cleats break in two distinct ways - <i>Courtesy of TAS-TO</i>	97
9.11	Numbering of inserts - <i>Courtesy of TAS-TO</i>	100
9.12	Bearing of the hole - <i>Courtesy of TAS-TO</i>	101
10.1	Strain gauges readings for Qualification and Ultimate load with re- spect to FEM qualification prediction values	109

List of Tables

3.1	AA2024 Aluminium alloy mechanical properties, Dural - <i>Courtesy of TAS-I</i> [3]	14
3.2	AA7075 Aluminium alloy mechanical properties, Ergal - <i>Courtesy of TAS-I</i> [3]	15
3.3	Ti6Al4V Titanium alloy mechanical characteristics - <i>Courtesy of TAS-I</i> [3]	15
3.4	Mechanical properties of Aluminium core honeycomb - <i>Courtesy of TAS-I</i> [3]	16
3.5	UD Lamina property - <i>Courtesy of TAS-I</i> [3]	17
3.6	Fabric properties- <i>Courtesy of TAS-I</i> [3]	18
3.7	Insert table according to ECSS normative [6]	25
3.8	SPI2 comparison with test results	30
4.1	Sandwich cylinder configuration and edgewise expected values [9]	40
4.2	Sandwich shear web configuration and edgewise expected values [9]	40
4.3	Insert SPI-2 characterization [9]	42
6.1	Table of test sequence - [9]	53
6.2	Comparison between FEM prediction results and test results, for strains coming from Qualification Load; last column reports the strains from Ultimate Load test results	53
9.1	Insert margin of safety of coupon 1	83
9.2	Margin of safety of the lamina around inserts location of Y shear web	84
9.3	Margin of safety of the honeycomb around inserts location of Y shear web	84
9.4	Margin of safety of the lamina around inserts location of X shear web	85
9.5	Margin of safety of the honeycomb around inserts location of X shear web	85
9.6	Honeycomb MoS for elements around the rupture zone	87
9.7	Laminate MoS for elements around the rupture zone	87
9.8	Positive MoS highlights that the laminate stays unbroken	90

9.9	Collapsing of the first and second inserts leads to the rupture of the following	91
9.10	Margin of safety, which demonstrates the integrity of the inserts, despite the failure occurred in that area	91
9.11	Margin of safety for laminate around insert area	94
9.12	Margin of safety of the honeycomb around the insert area	95
9.13	Margin of safety of the inserts	95
9.14	Honeycomb MoS indicates an intact core after the test	97
9.15	Margin of safety of the skins around the insert area	98
9.16	Margin of safety of the inserts	98
9.17	Margin of safety of the cleat	99
9.18	MoS of the inserts	102
9.19	Margin of safety of the honeycomb around the insert area	103
9.20	Margin of safety of the laminate around insert area	104
9.21	Upper fork margin of safety for aluminum in the insert area	105
9.22	Lower fork margin of safety for aluminum in the insert area	105
9.23	Bearing results for cylindrical sandwich panel around inserts	106
9.24	Margin of safety for adhesive joint 1 and 2	107

Chapter 1

Introduction

The scope of this Master's Thesis is the mechanical characterization of main structural components of the of Spacecraft Structure HE-R1000 Platform. The Mechanical characterization of the main components of Spacecraft Structure reported in the present academic Thesis have been realised by developing a finite element model, analytical procedure of calculations implemented on the literature theory, and more important by tests realised in TAS-TO facility. HE-R1000 Product High Efficiency Radar is a satellite platform developed in Thales Alenia Space Italia as Earth Observation Product family able to accommodate a deployable antenna Synthetic Aperture Radar, SAR payload operating in X-Band. The control of asset of the satellite will be managed by dedicate Momentum Gyro which, thanks to sensors, spinning rotor and one motorized gimbal tilt the rotor's angular momentum. As the rotor tilts, the changing angular momentum causes a gyroscopic torque that rotates the spacecraft. This system will confer a high agility to the spacecraft around the three axis and it will assure high surveillance to these "dancing satellites", intelligence and missions. This Observation satellites will be equipped by a deployable new generation antenna, SAR, with a diameter of 5 meters which will open its 24 petals once in space. The satellite will be placed on circular Earth Orbit LEO with the scope of mission of Earth observation as ocean monitoring for maritime safety, natural disaster and humanitarian aid.

The HE-R1000 architecture is mainly divided in Primary Structure and Secondary Structure to satisfy all mission and structural requirements.

Even though there are many different configurations, specifically studied for every mission, it is possible to identify a common satellite design.



Figure 1.1: Example of satellite in orbit - *Courtesy of TAS-I*

The Primary Structure is composed by sandwich panels in Carbon fiber skins and aluminium honeycomb instead the Secondary Structure is made both, skin and honeycomb in aluminium.

A spacecraft structure must resist the loads induced by the launcher, while maintaining the functional performances required. The structure will be the core around which subsystems are assembled and in this contest, it has to be compatible with the standard manufacturing process and use standard components, when possible. These requirements must be the basis of the preliminary structure design, in order to minimize structural weight, reduce costs but preserve the correct reliability level at the same time. In this chapter the loads and the structures will be analysed, as a way to give a general overview of a standard satellite design.

As mentioned above, launch generates the highest loads for the majority of spacecraft structures, but loads coming from emergency conditions, of any nature, and the basic key events, such as manufacturing, payload separation, docking, should be taken into account during the preliminary project.

The main structures employed can be divided into two categories, Primary and Secondary; the Tertiary structure can be taken into account for large satellites, and some new generation ones have more complex structures, related to their unique purpose or working environment: among these, it is possible to find manned spacecraft structures.

A SDM has been developed in TAS-I, Structure Development Model. A test campaign was carried out with the purpose of statically qualifying the product HE-R1000. Main purpose of the campaign is to qualify HE-R1000 from the structure point of view, in particular it focuses on:

- Demonstrating structural performance to confirm that the design concept is

consistent with HE-R1000 mission requirement

- Demonstrating structural performance to confirm that the SDM manufactured hardware complies with the design

Chapter 2

Satellite Design

2.1 Design requirements

Guide requirements for satellite structures are mainly two: mass requirement and strength/stiffness requirement. The design has to find the best compromise between the requirement of minimum possible mass and highest stiffness, it has to be avoided dynamic coupling with launch vehicle. Guide requirements for stiffness are expressed in terms of first resonance frequency and they are generally:

- Lateral frequency requirement > 15 Hz for both in-plane directions
- Axial frequency requirement > 40 Hz

The Design Concept of Spacecraft Structure shall be compliant with the requirements contained in the Spacecraft Mission Requirements Specification. Generally, the requirements are articulated in two main groups: Functional Requirements and Environmental Requirements. The Functional requirements include all specifications to assure the functionality of Structure in several environment as:

- On-Ground:
 - Provide the mechanical interface of equipment, external appendages
 - Provide handling/lifting points for fully equipped and loaded S/C Configuration for vertical and horizontal operations
 - Provide the adequate electrical grounding between the structural parts and between Structure and equipment and external appendages, in order to prevent risk of electrostatic discharges.
 - Provide the optical systems device for alignment of appendages and equipment with S/C Mechanical Build Axes within an opportune tolerance

- The S/C Structure shall implement a mechanical passive Micro- mete- oroids and Orbital Debris Protection in addition, a passive and active Thermal Control(Thermal blanket, heat pipes, heaters,etc)
- Adequate protection shall be designed to the structure in order to avoid material degradation in radioactive environment, in particular atomic oxygen.

The Environmental Requirements include all specifications to assure the capability of Structure, payloads and appendages to withstand the thermo-mechanical loads generated by flight dynamic environment of the launcher in the lift-off and ascent phases. In particular,

- Mechanical Environment:
 - quasi-static and dynamic loads resulting from the launcher in lift-off and ascent phases. The Spacecraft structure shall withstand all Design Limit Loads Factors reported by launcher Flight diagrams. The S/C Structure would be verified in relation to minimum and maximum Lateral and longitudinal (compression and tension) QSL.

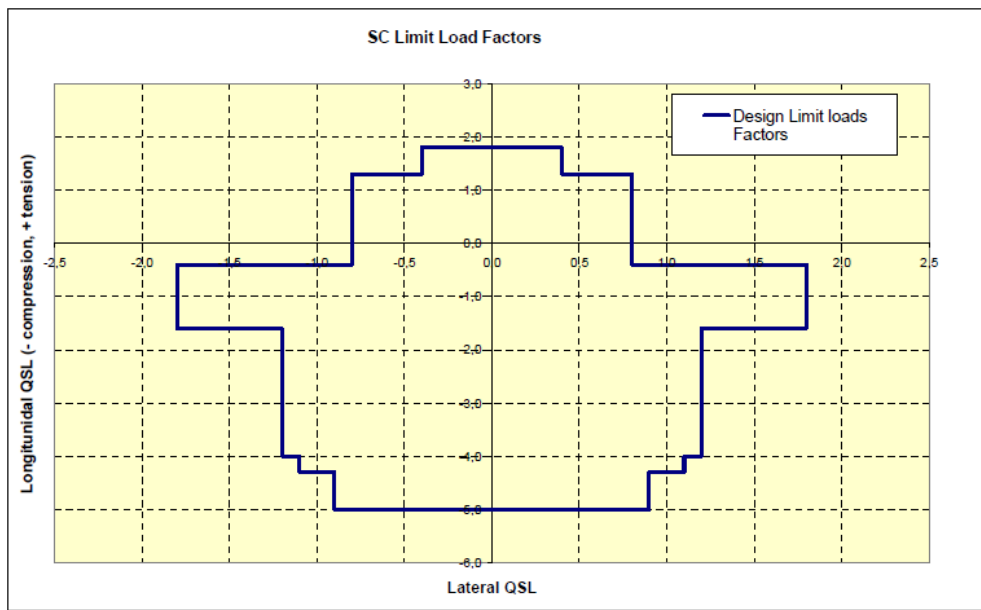


Figure 2.1: Design limit load factor of Soyuz Launcher [1]

- The S/C Structure shall be verified against the thermal loads coming from the launch phases and on orbit mission. In particular, structural integrity under specified on-orbital conditions for the required life-time

have to be maintained. More important, the thermo-elastic distortion of the main parts of structure shall be lower in order to assure the payload, Antenna, pointing accuracy. In addition, on orbit manoeuvring loads shall be sustained by the Structure and appendages.

2.2 Primary and Secondary Structure

Main requirements of the projects are lateral and axial stiffness, combined with the low mass of the structure; minimization of the structure distortion on-orbit is another main requirement and, with the previous ones, they usually lead to the employment of unidirectional modulus carbon fiber, or CFRP.

2.2.1 Primary Structure

The main structure, also called primary structure, is the one whose failure implies the total loss of the satellite. Payloads and satellite's equipment are attached to the primary structure and the structure itself transmits loads to the base of the satellite via appropriate design components. The LVA ring, Launch Vehicle Attachment ring, is the interface between the primary structure and the launcher. The primary structure sees a cylinder, or a cone, as main component, to which all the others parts of the platform are connected; propellant tanks are located inside the cylinder, and due to their dimension it is possible to establish the mission life. Shear webs connect the primary structure to external panels, while the main platform, the top and the bottom floors are perpendicular to the cylinder; the main platform accommodates equipment and protects them from radiations. The top floor is connected to the primary structure from the Earth facing side, in order to allow the positioning of broadcast antennas.

From the mechanical point of view, the cylinder guarantees axial and lateral stiffness, while the shear webs ensure stiffness against lateral bending. The box stiffness, necessary to protect the internal satellite equipment, is provided by top/bottom decks: they permit to reach the adequate axial stiffness necessary to satisfy the requirement. In other words, the primary structure guarantees the maximum contribute to axial and lateral stiffness of the entire satellite structure.

Another important factor is the type of loads the structure is transferring: the Primary structure, for example, transfers quasi-static and dynamic inertia loads toward the launcher interface, through the LVA, during the flight phases; the cylinder and the shear webs are deeply involved into load bearing, thanks to their positioning along the load path, starting from the top and moving toward the bottom, where the LVA is located.

The primary structure is usually made up of CFRP panels, Composite Fiber Reinforced Polymer; in particular, sandwich with CFRP facing allows to obtain a good ratio between mass and strength, and mass and stiffness, if a correct laminate lay-up is chosen.

2.2.2 Secondary structures

Secondary structures are connected to the primary one and they only have to support themselves; in a correct design project, a failure in this kind of structure does not involve the integrity of the entire satellite, although it could cause severe impacts on the mission.

Typical examples of secondary structures are lateral panels, frames, baffles, solar panels and thermal blanket support; some of these parts' main issue is to offer adequate support from the stiffness point of view, while others are supposed to avoid load concentrations and keep small deflections, such as solar panels. Another important task of the secondary structure is to bear acoustic loads, seen as pressures, during the lift-off; however, lateral panels mainly co-operate with the primary structure to reach the optimal lateral and torsional stiffness.

2.3 Other typical non-conventional structure

In addition to sandwich panels, that will be more accurately explained in the next page, it is presented a set of non-conventional structures employed.

- *Monocoque Cylinder*: realized either from metal sheet or by sandwich construction, this is a symmetric shell whose strength is limited by the buckling stress. It has no frames and it can carry only loads which are uniformly distributed over its cross section, indeed any other concentrated load will cause a local failure; for these features, this kind of structure is only suitable for stiffness-critical design. For a low weight, it is recommended a sandwich structure or a isogrid (this last one is heavier)
- *Frames and trusses* : Frames are structures capable of carrying shear loads and bending through their joints and members; truss, on the contrary, can carry only axial loads and to have a stable arrangement it has to form triangles: other forms of positioning lead to instability. If the cross section is rectangular, triangular or square, truss are efficient, while they became less useful in sections which present a section more circular. Typical construction materials are aluminum and titanium alloys or graphite/epoxy. composite.
- *Skin-Frame structures*: It is possible to identify skin surrounding a skeletal framework: this last one is composed of stringers and lateral frames able to

transmit shear to the skin, which is allowed to buckle, since in that case the shear is carried by diagonal tension. This structure results unstable unless it is closed with skin, or include radially deep frames (it is enough to have diagonal members triangularly disposed), however it is very versatile as far as it concerns its shape, and it is usually made up of aluminum, magnesium and titanium alloys.

- *Cylindrical Skin-Stringer*: as particular case of cylinder, this structure includes stringers, whose aim is to stabilize the skin: as a consequence, it also help to bear the load, in fact they carry the majority of axial load and bending moment and at the same time they react to the radial component of diagonal tension loads. It is important to ensure close riveting or to apply threaded fasteners between the skin and the members, otherwise it will not act as a unique structure.
- *Stiffened Skin*: in this particular configuration, stiffeners, whose purpose is to increase the buckling stress of the skin, are located really close one to each other; sometimes it could be necessary to include some intermediate ring frames to keep the stiffeners stable.
- *Semi-monocoque structure*: unlike the stiffened skin, this structure has no stiffeners or stringers, but only ring frames applied in order to rise the buckling stress of the skin.
- *ISOGRID Panels*: it is a one-piece structure, consisting of a network of load-bearing ribs and protective skin directly carved from a solid aluminium plate. This kind of structure can be up to 40% more efficient than skin stringer structures, furthermore eliminating fasteners and fasteners beef-up areas it is possible to reduce costs related to assembly time.

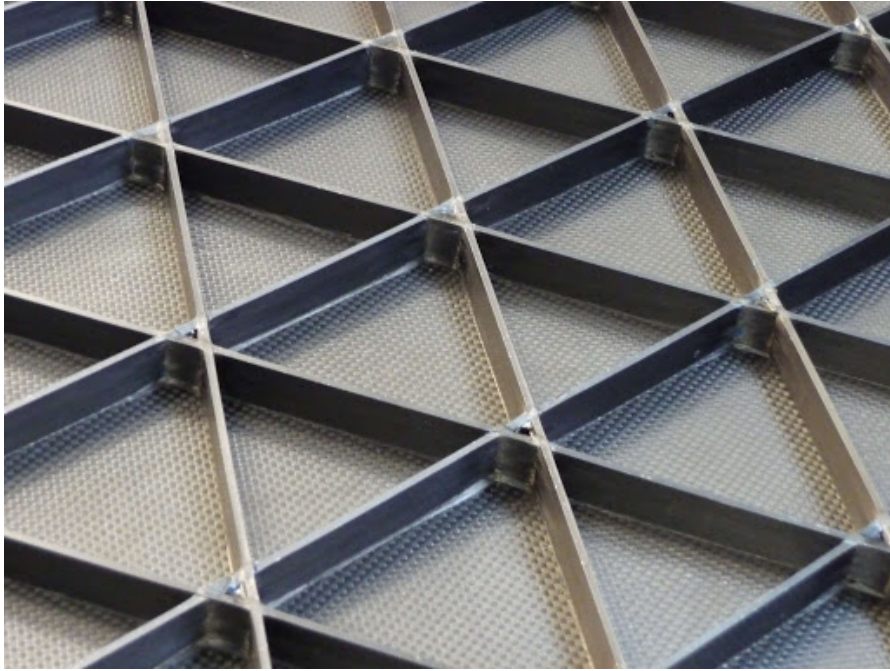


Figure 2.2: Isogrid typical structure [2]

Chapter 3

Materials and Component Description

For the aerospace field, materials and their manufacturing are fundamental for the success of the mission: not by chance, there are severe and strict regulations about the requirements the different structures must satisfy, of which a large part is related to materials they are made of.

In this paragraph it will be done a presentation of the principal materials and structures used for the realization of a standard satellite, starting from the sandwich panels to the description of inserts, junctions and cleats.

AA2024 T3 Sheet		Thickness [mm]	0.25<t<6.35	
Modulus of Elasticity in Tension		E=72400 MPa		
Modulus of Elasticity in Compression		E _c =73774 MPa		
Poisson's Ratio		ν = 0.33		
Density		ρ =2795 Kg/m ³		
Coefficient of Thermal expansion		α =23.2e-06 1/K		
Basis A				
Allowables:		L	LT	
Ultimate Tensile Strength	F _{t_u} [MPa]	461	461	
Tensile Yield Strength	F _{t_y} [MPa]	406	399	
Bearing		e/d =1.5	e/d=2.0	
Ultimate Bearing Strength	F _{br_u} [MPa]	689	875	

Table 3.1: AA2024 Aluminium alloy mechanical properties, Dural - *Courtesy of TAS-I* [3]

AA7075 T7351 Sheet		Thickness [mm]	12.5<t <25.4	
Modulus of Elasticity in Tension		E=71016 MPa		
Modulus of Elasticity in Compression		E _c =73084 MPa		
Poisson's Ratio		ν = 0.33		
Density		ρ =2795 Kg/m ³		
Coefficient of Thermal expansion		α =23.6e-06 1/K		
Basis S				
Allowables:		L	LT	
Ultimate Tensile Strength	F _{t_u} [MPa]	468	475	
Tensile Yield Strength	F _{t_y} [MPa]	393	393	
Bearing		e/d =1.5	e/d=2.0	
Ultimate Bearing Strength	F _{br_u} [MPa]	710	910	
Bearing Yield Strength	F _{br_y} [MPa]	555	667	

Table 3.2: AA7075 Aluminium alloy mechanical properties, Ergal - *Courtesy of TAS-I [3]*

Principal materials employed in aerospace field are Aluminum alloys, carbon fiber and Titanium alloys (table 3.3); among Aluminium alloys, the most used are series 2000, in particular AA2024 (called also Dural, ex Avional), series 6000 (AA6061) and series 7000, like AA7475 and AA7074 also known as Ergal, whose mechanical characteristics are shown in tables 3.1 and 3.2

Ti6Al4V Plate		Thickness [mm]	50.8<t ≥101.6	
Modulus of Elasticity in Tension		E=110320 MPa		
Modulus of Elasticity in Compression		E _c =113078 MPa		
Poisson's Ratio		ν = 0.31		
Density		ρ =4430 Kg/m ³		
Coefficient of Thermal expansion		α = 1/K		
Basis S				
Allowables:		L	LT	
Ultimate Tensile Strength	F _{t_u} [MPa]	896	896	
Tensile Yield Strength	F _{t_y} [MPa]	814	814	
Bearing		e/d =1.5	e/d=2.0	
Ultimate Bearing Strength	F _{br_u} [MPa]	1420	1793	
Bearing Yield Strength	F _{br_y} [MPa]	1110	1317	

Table 3.3: Ti6Al4V Titanium alloy mechanical characteristics - *Courtesy of TAS-I [3]*

For the honeycomb, only Aluminum series 5000 is utilized, specially AA5056 and AA5052. Other materials extensively used in satellite structures are carbon fibers, CFRP materials, in particular prepreg in epoxy resin and carbon yarns:

the classical application of these prepreg is done by building the layup according to the design, and than the piece is cured in autoclave by means vacuum bag in pressure and temperature cycle.

Designation	Density	Min. plate shear					
		Min. Compressive		"L" direction		"W" direction	
		Strength	Modulus	Strength	Modulus	Strength	Modulus
	[kg/m ³]	[MPa]	[MPa]	[MPa]	[MPa]	[MPa]	[MPa]
3/16 5056 0.002	91.3	5.06	1861	3.3	648	1.9	248
3/16 5056 0.0007	32.04	0.83	310	0.72	186	0.34	90
3/16 5056 0.001	49.66	1.79	669	1.38	310	0.76	138
3/16 5052 0.0025	110.53	5.52	1965	3.72	786	2.26	320
OX 3/16 5056 0.0015	73.4	4.88	1793	2.33	354	2.08	257
3/16 5056 0.0025	110	7.00	1965	4.68	790	3.15	360

Table 3.4: Mechanical properties of Aluminium core honeycomb - *Courtesy of TAS-I* [3]

In this document, for coupons and for HE-R1000 construction have been used carbon fiber filament with high modulus and strength, pre-impregnated in the epoxy resin: The Mechanical characterization of CFRP materials for HE-R1000 and related coupons are confidential data of TAS-TO, tables 3.5 and 3.6

UD Lamina Property			
Thickness Tape:		. mm	
Tensile Modulus longitudinal direction		$E_{tx} =$ [GPa]	
Compression Modulus longitudinal direction		$E_{cx} =$ [GPa]	
Shear Modulus		$G_{12} =$ [GPa]	
Poisson's Ratio		$\nu_{12} =$	
Density		$\rho =$ Kg/m ³	
Coefficient of Thermal Expansion		$\alpha_1 =$ $\alpha_2 =$	
	Direction	A-Basis	B-Basis
Ultimate Tensile Strength X_t [MPa]	0°		
Ultimate Tensile Strength Y_t [MPa]	90°		
Ultimate Compressive Strength X_c [MPa]	0°		
Ultimate Compressive Strength Y_c [MPa]	90°		
Interlaminar Shear Strength ILLS [MPa]	-		
Ultimate Shear Strength	-		

Table 3.5: UD Lamina property - *Courtesy of TAS-I* [3]

Fabric		Propriety	
Thickness Tape:		mm	
Tensile Modulus longitudinal direction		$E_{tx} =$ [GPa]	
Compression Modulus longitudinal direction		$E_{cx} =$ [GPa]	
Shear Modulus		$G_{12} =$ [GPa]	
Poisson's Ratio		$\nu_{12} =$	
Density		$\rho =$ Kg/m ³	
Coefficient of Thermal Expansion		$\alpha_1 =$ $\alpha_2 =$	
	Direction	A-Basis	B-Basis
Ultimate Tensile Strength X_t [MPa]	0°		
Ultimate Tensile Strength Y_t [MPa]	90°		
Ultimate Compressive Strength X_c [MPa]	0°		
Ultimate Compressive Strength Y_c [MPa]	90°		
Interlaminar Shear Strength ILLS [MPa]	-		
Ultimate Shear Strength	-		

Table 3.6: Fabric properties-*Courtesy of TAS-I* [3]

It is preferred the adoption of carbon fiber and titanium alloys for satellite structure, because they ensure the adequate strength and stiffness, but also a high thermal stability, due to their low CTE, Coefficient of Thermal Expansion

3.1 Sandwich Panels

There are two principal kinds of sandwich panels, the first one whose core is composed of foam or expanded foam, while the second one holds the so-called honeycomb: this is the structure of interest of this section and its characteristics and features will be explained below.

Other big difference consists of the material the skins are made of, typically Aluminium or CFRP

3.1.1 General description

To give a definition, a structural sandwich is a layered construction formed by bonding two facings, normally really thin, to a core whose thickness is higher than skin's one. Consequently, it is possible to achieve high ratios of stiffness-to-weight structures, as long as materials and geometry are wisely chosen; the rigidity of the

sandwich is ensured by facings, indeed they carry bending and in-plane extensional loads. On the other hand, the core carries the shear loads, it has low compressive strength so it is necessary to place inserts where concentrated loads are applied; it is also important for the stabilization of the faces against local buckling. Sandwich panels undergo large shear deformation, so it is not possible to use the Theory of De Saint-Venant, appropriate corrections will be necessary.

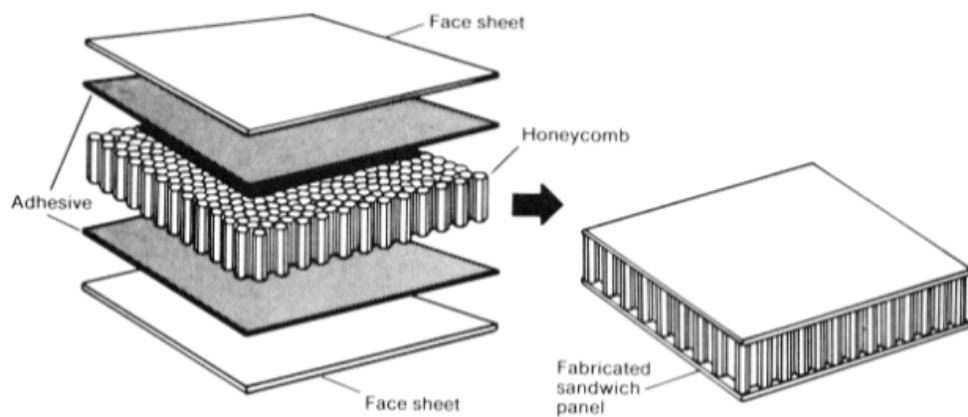


Figure 3.1: Sandwich panels representation [4]

Adhesion between these two components is fundamental to have a safe and functioning structure, capable of transmitting loads from one facing to the other.

3.1.2 Honeycomb

A honeycomb core, as the real bee's one, is a set of hexagonal cells; as said above, the primary function of the core is to stabilize the skins and to carry shear loads, but at the same time it is important to keep the entire structure as lighter as possible. For this configuration a large size of cells is not recommended, indeed the adhesive and the skin could result sunken in the hole of the cell: this phenomenon is known as dimpling and must not happen. On the contrary, a small cell size will raise the density of the core, but it will provide smooth surfaces and improved mechanical features. The size of the cell plays a secondary role from the mechanical point of view, in fact its main purpose is to ensure the bonding between the skins and the core itself, through the adhesive. Another significant factor is the thickness of the foils, which influences density, global mechanical characteristics and ultimate strength to which the panel is subject when it undergoes different local instabilities.

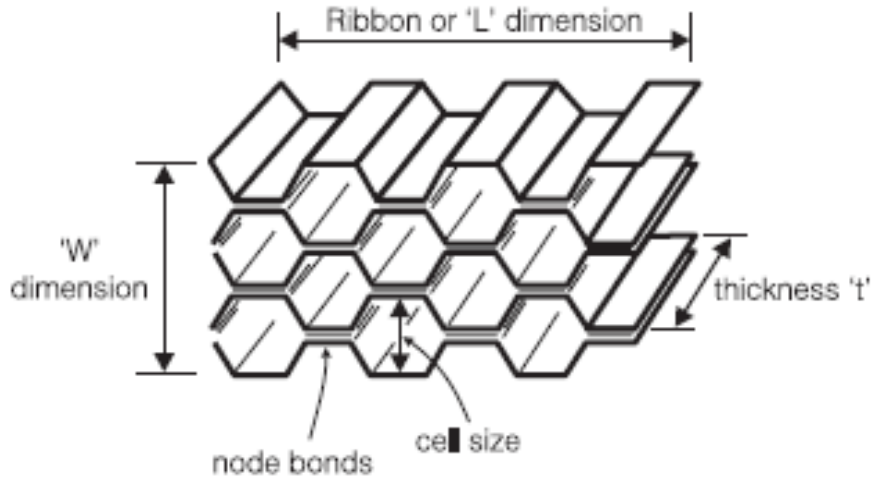


Figure 3.2: Particular of honeycomb structure [5]

As shown in figure 3.2, it is possible to identify three different directions in the honeycomb structure, the first one is usually called T, which develops along the Thickness, the other ones, L and W, are respectively Length and Width of the core.

Along the L direction it is possible to reach the highest shear strength, compared to W, where the values are significantly lower; this difference is due to the fact that cells have a double foil along L direction, so that the shear strength increases. In this case there would be two elastic modulus, E_1 and E_2 , a shear modulus G_{12} and the Poisson coefficient ν_{12} , independent of each other. Conversely, if the wall thickness of the cell along L direction had only one foil, and the hexagon was regular, it would be possible to identify an isotropic behavior, with a single elastic modulus E and a single shear modulus G. Most common shape of cells is the hexagon, but it is possible to find other configurations, such as the over expanded (OX) or the flex-core. The over expanded configuration is often used in cylindrical panels: the cells are flattened hexagonal along the L direction so that, once expanded, they reach the desired length with the correct curvature and it increases shear strength in W direction; it is important to remember that the acronym OX is referred to the nominal hexagonal shape before the expansion. The flex-core configuration has a particular cell shape which enables the panel to reach exceptional bending.

Most common materials employed to realize the honeycomb core are aluminium alloys, such as 3003-H19, 5052-H39, 5056-H39 and 2024-T81; the first one is the cheapest and cannot be used in aerospace applications, principally due to the fact that is not heat treatable. The 5052-H39 and 5056-H39 alloys are the most suitable

in aerospace field, they are available with an anti-corrosive coating too. Finally, the 2024-T81 is the most heat resistant.

For completeness, it is quoted another famous material, called *Nomex*, patented by DuPont, which consists of discontinuous aramid fibre expanded and then impregnated with phenolic resin: its particular quality is to resist to very high concentrated loads without permanent damage; in summary, thanks to its characteristics, *Nomex* is the second most used material for honeycomb for aerospace scope.

Other honeycomb materials employed, but less frequently, are *Korex*, *Kevlar*, *Fiberglass*, *Carbon*; each of them is characterized by different strengths and stiffness, of which is given a qualitative graph, in figure 3.3 in function of the density of the material.

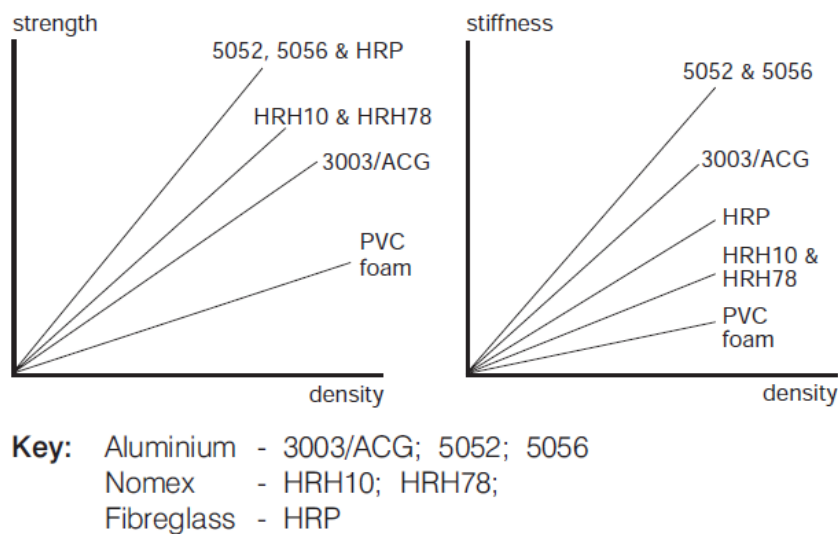


Figure 3.3: Qualitative chart of different honeycomb materials [5]

3.1.3 Skins

Skins are the most resistant part of the sandwich structure, although stabilized by the core; on their own, skins have no self rigidity and they have to withstand the majority of flexural stress. For these reasons, once an axial force is applied to one of the extremity of a generic beam, one of the face will respond to traction, while the other to compression; in other words, skins have the same aim of the flange of an I beam.

The skins, being the most external part of the sandwich, could have other functions, related to aerodynamic or to abrasion resistance; due to this, it is possible to find skins with little differences one to each other, in terms of coating, processing or just thickness.

For what concerns materials, it is possible to use any kind of laminate as long as it respects the requirements. It is important to take into account fragility, failure modes, durability, flammability and all the other characteristics that could be influenced by the work environment of the sandwich panel. Not secondary, it is important to consider the compatibility of these materials with inserts, joints and other components that come into contact with the skins. First material employed was Aluminum, but to meet current needs of the aeronautic field, many new materials have been proposed, studied and consequently used as sandwich skins; some of these solutions contemplate aramid/epoxy, carbon/epoxy composite, but for the satellite under analysis, CFRP skins have been decreed the most suitable material to employ, and with the correct lamination it has been possible to match the requirements with a significant saving in terms of weight, compared to Aluminum skins.

3.2 Inserts

In the following pages, an overview of the principal characteristics of inserts will be given, including the different types involved in the construction of the coupons and the standards to refer to, during the project and the potting phases.

3.2.1 Insert description

According to the ECSS-E-HB-32-22A normative, an insert is part of a detachable fixation device, whose purpose is to enable connection of honeycomb sandwich structures with brackets, boxes, profiles, etc.

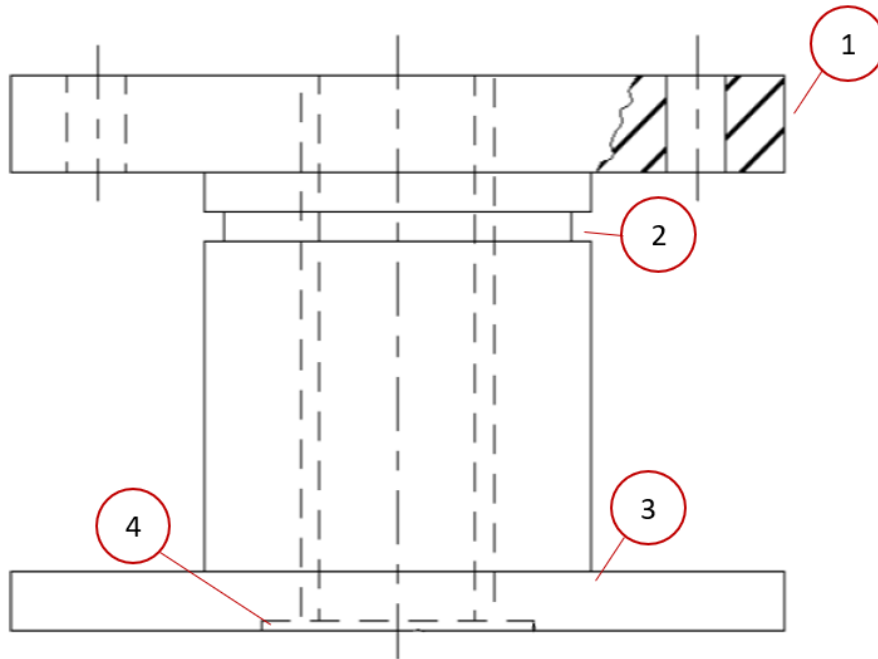


Figure 3.4: Insert section [6]

An insert can be split up into two elements, a fixed and a removable one, and it is connected to the sandwich structure via the potting compound, for example a resin epoxy system.

The figure 3.4 shows a standard insert section and its most common characteristics.

1. Upper flange: the upper flange is usually in line with the skin exterior surface and it hosts injection and venting holes, used to pot the insert.
2. Recess for screw locking
3. Lower flange
4. Protecting plate for closure, used to seal off the insert and protect from external agents and corrosion

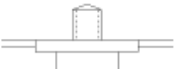
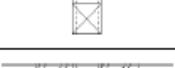
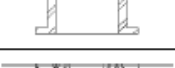
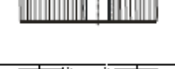
Other concept is the insert system, composed of the insert itself, the sandwich structure and the potting material used to keep the insert in place. Analysing each of these parts, the insert sees a male threaded element, like a screw, and a female threaded element: this last one can be fixed or replaceable; the sandwich is made of a core, two faces and the adhesive used for the bonding. The typical potting material is epoxy resin and it can be both applied for the potting activity and for the bonding of the core of the sandwich with the two skins.

Based on the method of integration employed, it is possible to distinguish three different classes of inserts:

- Group A - These inserts are joint during the sandwich structure production and it is particularly suitable for thin panels; it is not possible to apply them in those situations where specific locking demands are required, furthermore it has to be taken into account that it results difficult to keep the insert in place during the sandwich production, when the resin is still liquid and retains some mobility. As a solution, the insert has a large diameter and a margin of 3-6 mm is considered to guarantee alignment issues.
- Group B - This group of inserts is the most used, cured with epoxy resin and applied into existent sandwich panel; this insert resumes the one described before, in figure 3.4, but it is now given a more detailed view. The standard configuration sees a hollow cylindrical body with flanged ends. The upper flange has two little holes used for the insertion, the first one is used for the injection of the resin, while the second one is for venting: the operator inserts the resin in the first hole and continues until it overflows from the venting one. To avoid contamination from the resin to the lower flange, a thin sheet is applied for protection, while a little recess in the upper part allows the deformation of the thread via compression, to ensure the locking of male - female screw. Flanges and discs, with resin, collaborate in transferring the loads not only through the adhesion shear forces between resin and insert; it is for this reason that the cylinder and the flanges have rough surfaces, to increase the shear load capability when subjected to torsion.
- Group C - this type of insert is used when screwing into a sandwich panel is required; however, this practise is not recommended and it must be avoided, when possible. Screwing directly into the panel, in fact, does not allow to have a clear contact with the core, and as a consequence the load-carrying capability is compromised, and torque moment carrying is deputy to adhesive only.

An important subdivision considers the height of the insert: if the inserts is as high as the sandwich panel, it is called *fully potted*, while it is called *partially potted* if it is not.

In the table 3.7 are pictured some insert for each of the three treated categories.

Type	Shape	Diameter (mm)	Material	Potting Considerations	Torque Locking	Thread Locking	Floating Nut Exchange Capability	Standards	Comments
Type A: Bonding during sandwich manufacture									
1		17 to 30	Al	Full bonded with core filler	None or square shape	e.g. Lockite	No	-	The bore hole is drilled after sandwich bonding. Only for small core height.
Type B: Potting (or equivalent non-standard procedure)									
2		11 to 22	Al (St) (Ti)	Partially or fully potted	Planes or riffls	Deformation of tread	No	NAS 1832 NSA 5135 PA 3825 ENN 3GG/386	Al insert can be used with St or Ti screws. Most common type.
3		11 to 22	Al (St) (Ti)	Partially or fully potted	Planes or riffls	Deformation of tread	No	-	Rarely used
4		11 to 14	Al	Fully potted only	Planes or riffls	e.g. Lockite	No	NAS 1832 TAN 16489 PAN 3827 NSA 5071	Available with and without thread.
5		6 to 14	St Ti	Partially or fully potted	Planes or riffls	e.g. Lockite	No	ERNO No. R 000/095.000	Rarely used.
6		3 to 6	St Ti	Partially or fully potted	Planes or riffls	e.g. Lockite	No	-	Only for very low loads. Rarely used.
7		19 to 70	Al	Partially or fully potted	Planes or riffls	e.g. Lockite	No	-	For high loads
8		19 to 25	Al: Insert Ti: Nut	Partially or fully potted	Planes or riffls	Deformation of thread	Yes	NAS 1835 PAN 3829 ENN 379 NSA 5072	Extended and heavy type for applying floating nuts and exchanging capacity.
9		7 to 20	CFRP / Al	Carbon fibre tube bonded into core	N/A	e.g. Lockite, helicoils.	No	No	Carbon fibre tube inserts, [See also: A.3 and F.6]
10		-	-	-	-	-	-	-	[See also 10.3] [Ref. [5-2]]
Type C: Mechanically clamped or screwed									
11		14 to 22	Al (St) (Ti)	-	Adhesive bonding	Deformation of thread	No	TAN 16485	Low pull-out strength, if no connection with core.
		14 to 22	Al (St) (Ti)	-	Adhesive bonding	-	No	-	-

Key: St: steel; Ti: titanium; CFRP: carbon fibre-reinforced plastic

Table 3.7: Insert table according to ECSS normative [6]

3.2.2 Standard materials and Potting dimensions

Regarding the materials, Aluminium Alloys, Titanium Alloys and Steels are the most used and available on commerce, but the AA 2024 is the preponderant Aluminium alloy which the inserts are made of; this alloy is typically followed by a T85 treatment, which involves heat treatment and aging, natural or artificial: the inserts investigated in this document fall into this group. For completeness sake, it is specified that Titanium alloy TiAl6V4 is used for those applications where improved strength is required, while carbon or stainless steels are not used in aerospace field, due to sublimation problems caused by cadmium, which always covers steel inserts.

There exist four principal types of potting methods, some of them more effective than others. The *casting*, for example, could be very good for fully potted inserts, but it is not practicable, because it does not guarantee the adequate resin surplus, needed due to resin shrinkage. In the same way, casting is not suitable for partially potted inserts because sandwich panels have to be turned over before curing and the resin would run off.

Another process is *foaming*, which does not require any device to be applied and it is used only for fully potted inserts, because the expansion of the foam can not be totally controlled; this procedure is generally performed during the sandwich manufacture process.

The *paste application* method is not advisable because it does not enable visible inspection of the filling of honeycomb cells, so it is not frequently used, even though it is quite simple to perform, in fact only a spatula is required. Finally, *injection* is the method with the best results either for full and partial potting; the main difference in the choice of the devices is related to the number of inserts to pot. The compressed air cartridges is cheaper when a huge number of inserts is involved, while manual injection via medical squirter is used for small number of inserts or for repairing. In both cases it is not possible to handle the panels immediately after potting.

A standardization is in use for diameters and heights of the inserts, which are the most important parameters too. In the following figures, standard diameters and heights are shown, in reference with the different regulations. In particular, it shows that some diameters are preferred to others, such as the ones that follow geometrical progression

$$a \cdot q^n \tag{3.1}$$

where a and q are two constants: $a=8,96$ and $q=1,25$. On the contrary, for the heights there is no preference, because they should fit every possible sandwich structure. It is possible, however, to find a linear dependency between insert standard diameters and corresponding heights.

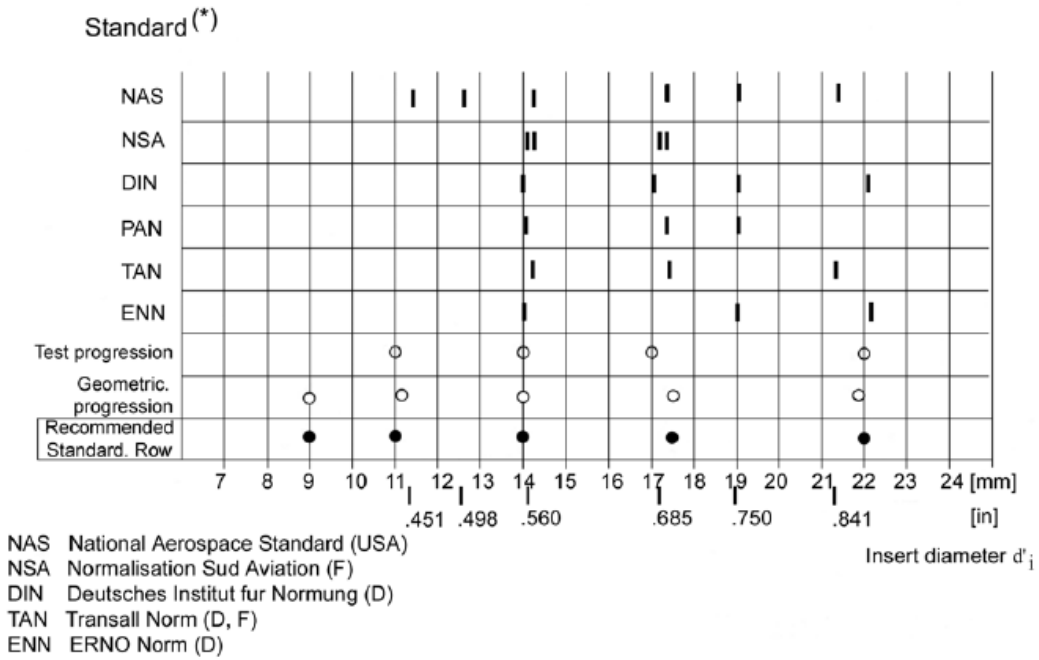


Figure 3.5: Standardized insert diameters [6]

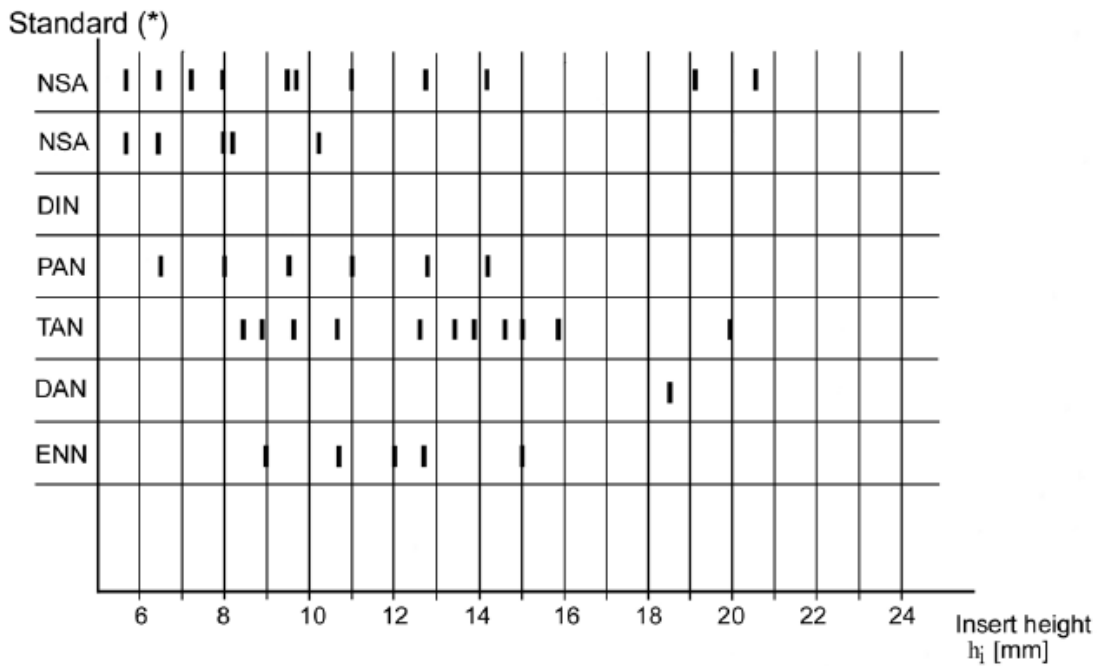


Figure 3.6: Standardized insert heights [6]

While the insert dimensions do not influence the load capability, the same can not be said of the potting: it has fundamental dimensions that must be identified and analyzed.

1. b_p is the effective potting radius and it describes the radial influence zone of the potting; it considers the double foil cell walls of the honeycomb, close to the potting, as a potting part itself and it is defined as the average distance of the nearest single cell walls surrounding the potting, from the point identified as the centre of the insert. Being an analytic dimension, it depends on the insert radius b_i , the side of the cell S_c and the position of the centre of the insert in relation to the hexagonal cell. This value can be calculated as minimum or as typical, and for each of these two there is the further subdivision for perforated or non perforated core

$$b_p = \frac{1}{n} \sum b_n \quad (3.2)$$

- Minimum value - perforated core

$$b_{pmin} = 0,93192b_i + 0,874S_c - 0,66151 \quad (3.3)$$

- Minimum value - Non-perforated core

$$b_{pmin} = 0,9b_i + 0,7S_c \quad (3.4)$$

- Average value - perforated core

$$b_{ptyp} = 1,002064b_i + 0,940375S_c - 0,7113 \quad (3.5)$$

- Average value - Non-perforated core

$$b_{ptyp} = b_i + 0,8S_c \quad (3.6)$$

2. b_R is the real potting radius of the circle whose area is identical to the effective area F_R of the potting, which is clearly not round.

$$b_R = \sqrt{\frac{F_R}{\pi}} = \sqrt{\frac{N_{PC}F_C}{\pi}} \quad (3.7)$$

In this equation it appears the term F_c , which is the sectional area of the core of a singular cell, computable as

$$F_c = 0,95 \times 0,75 \times S_c^2 \cos\alpha \quad (3.8)$$

S_c is the nominal size of the cell and it is a quite standard number, so that F_c assumes the value of $8,4mm^2$ if $S_c = 3,2mm$ and the value of $19mm^2$ if $S_c = 4,8mm$. The real potting is an important measure for the calculus of the tensile failure of the potting, as it will see. For this dimension is provided a minimum and an average value too:

- Minimum value

$$b_R = b_i + 0,36S_c \quad (3.9)$$

- Average value

$$b_{Rtyp} = b_i + 0,5S_c \quad (3.10)$$

When talking of the height of the potting, the first distinction to do is the full or partial potting: the first one is the case in which $h_p = c$ when $c \geq h_i \geq c - 7mm$; when the core height is higher, so $c > h_i + 7mm$, it is the case called *partially potted*. The insert height h_i is a fundamental quantity, minimum potting height for partial potting depends on it, from the equation

$$h_{pmin} = h_i + 7mm \quad (3.11)$$

where the value of 7 mm comes from the fact that bore hole should be 3 to 4 mm deeper than the insert height and the connection underneath the insert must be done at least with 3 mm of potting resin. The average value of the height is h_{ptyp} , calculated as

$$h_{ptyp} = h_{pmin} + A \tanh\left(\frac{c - h_{pmin}}{h_{pmin}}\right) \quad (3.12)$$

with $A=2,5$ mm for $S_c = 3,2mm$ and $A=5$ mm for $S_c = 4,8mm$

Concerning the loads, inserts can withstand four principal kinds of loads: Out of plane, in plane, moment and torsion. As shown in figure 3.7, the out of plane load corresponds to a force of traction, or compression, along the axis of the insert (1), while the in-plane load can be associated to a shear load, a force applied to the insert on the plane perpendicular to its axis (2). The moment is substantially a bending moment (3) and torsion is the moment around the insert's axis (4).

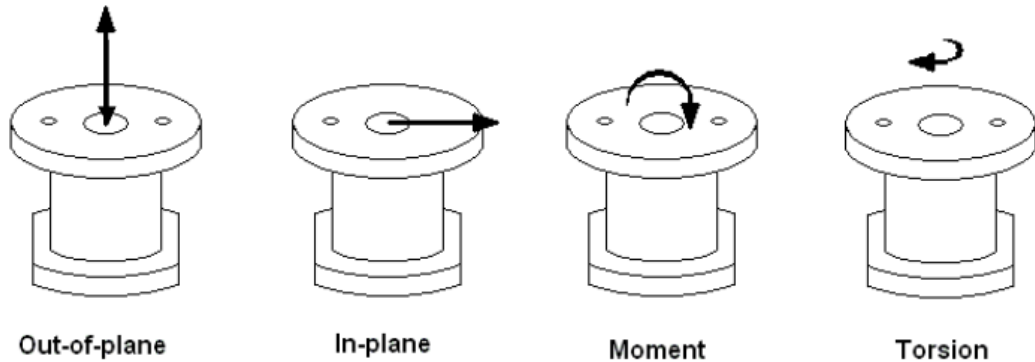


Figure 3.7: Illustration of typical loads applied to inserts [6]

The principal insert analyzed is the type SPI2, fully potted through the thickness, which connects cylinder with tank interface, but also cylindrical panel sandwich with shear webs; it was tensile tested and to shear loads too, to verify the ultimate strength for both pull-out and in-plane configurations. This procedure is done to compare the results with the insert calculus, in order to be able to predict the ultimate failure load and to acquire data heritage useful for future applications: in this way, next time this type of insert is used, it will not be necessary to test them. The calculation of this values is close to test results, with a percentage error less than 15%, in agreement with regulations, figure 3.8

Cylinder - Tank Interface --- SPI_2				
	SPECIFICATION	EXCEL	TEST RESULTS	ERROR
Pull Out Load [N]	5500	4605,21772		
Shear Load 0° [N]	6800	10431,5882		
Shear Load 90° [N]	6800	10431,5882		

Table 3.8: SPI2 comparison with test results

The values for bending and torsion loads have not been tested because less influential than axial and shear loads, for the calculation requested, and because design gives preference to axial and shear loads on inserts.

3.2.3 Maximum allowable in tension and compression

In this section, calculation of the tensile/compressive allowable of the insert is reported; the tensile allowable is expressed as P_{ssT} and from theory it is the minimum value between the critical load for fully potting configuration P_{FPcrit} and the critical tensile load for partially potted configuration P_{PPcrit} . The generic critical load is the minimum between the critical load for fully potted insert P_{FPcrit} , critical tensile load for partially potted inserts $P_{PPcritT}$ and compressive critical load for partially potted inserts $P_{PPcritC}$. For this analysis only geometrical and design parameters are involved, external loads are not applied.

The critical load for fully potted insert, for example, is given by the equation

$$P_{FPcrit} = \frac{2\pi b_p h_c \tau_{Ccrit}}{\frac{\beta}{\beta+1} K_{max}} \quad (3.13)$$

where b_p is the minimum value for perforated core 3.3, h_c is the height of the core, and β , τ_{Ccrit} and K_{max} are quantities calculated as written below:

$$\beta = h_c / f \quad (3.14)$$

$$\tau_{Crit} = 1.36\tau_{wt} \quad (3.15)$$

$$K_{max} = \frac{b_p}{r_{\tau max}} \left[1 - \left(\frac{r_{\tau max}}{b_p} \right)^{0.5} e^{(\alpha 1)(b_p - r_{\tau max})} \right] \quad (3.16)$$

β is a geometrical component, the ratio between honeycomb height and face thickness, τ_{wt} is the core typical allowable shear in W-direction, which is multiplied by 1,36 according to the ESA PSS-03-1202 regulation. K_{max} includes a series of constants and equations coming from the regulation too, where

$$r_{\tau max} = \frac{b_p}{\left[1 - e^{-0.931714(\alpha 1 b_p)^{0.262866}} \right]} \quad (3.17)$$

and

$$\alpha 1 = \frac{1}{f} \left[\frac{G_c}{E_f} 12(1 - \nu_f^2) \left(\frac{\beta}{2} + 1 + \frac{2}{3\beta} \right) \right]^{0.5} \quad (3.18)$$

is a variable of the Bessel function. The tensile critical load for partially potted inserts is composed of three components: P_{FA} is the load part carried by the upper surface, P_{Scrit} is the load part carried by shear stresses in the core around the potting, and P_{NcritT} is the load part carried by normal stresses in the core underneath the potting, for tensile case.

$$P_{FA} = \frac{P_{FPcrit} - 2(\pi r_{\tau max})h_c \tau_{Crit}}{2} \quad (3.19)$$

$$P_{Scrit} = 2\pi r_{\tau max} h_{pmin} \tau_{Crit} \quad (3.20)$$

$$P_{NcritT} = \pi r_{\tau max}^2 \sigma_{ccritT} \quad (3.21)$$

where h_{pmin} in this case is equal to h_s , the height of the sandwich, because the insert is through the thickness and it is $h_s = h_c + 2f$, and σ_{ccritT} is the tensile strength of aluminium core. In particolare, it is calculated as

$$\sigma_{ccritT} = \sigma_{0critT} \frac{\gamma_c}{\gamma_0} \quad (3.22)$$

with σ_{0critT} the tensile strength of core material, γ_c the core density and γ_0 the density of core material. For the compressive load, the equation is similar to the tensile one, but instead of P_{NcritT} , P_{NcritC} is added, so the equation results

$$P_{PPcritC} = P_{FA} + P_{Scrit} + P_{NcritC} \quad (3.23)$$

where σ_{ccritC} is the minimum compression strength of core material, given as input.

3.2.4 Maximum allowable shear load

The maximum allowable for shear load is Q_{ss} and it comes from the equation

$$q_{ss} = 8b_{pmin}^2\tau_{wt} + 2fb_{pmin}\sigma_{fy} \quad (3.24)$$

where b_{pmin} is the minimum effective radius explained before, and σ_{fy} is the allowable at yield of the skins. This result value is in agreement with the test one, while bending and torsion allowable are calculated only, the reference value is the one coming from the regulation in this case.

3.2.5 Maximum allowable in bending and maximum allowable for torsional load

The maximum allowable in bending is M_{ss} and it is easily

$$M_{ss} = P_{ss}b_i \quad (3.25)$$

where b_i is half of the insert diameter. The maximum allowable for torsion load is

$$T_{ss} = 4\pi b_{Rmin}^2 t_0 \tau_{0crit} \quad (3.26)$$

In this case, the real pottig radius b_{Rmin} is used, t_0 is the cell sheet thickness and τ_{0crit} is a given input.

3.2.6 Margin of safety for the inserts

Two different margins are calculated, depending on the load configuration: PQ is a quantity used to develop the first margin, and it includes the maximum allowable in tension/compression and the shear allowable. The margin is

$$Mos = \left(\frac{1}{PQ^{0.5}} \right) - 1 \quad (3.27)$$

and it has to be positive to consider the insert as intact. The quantity PQ is

$$PQ = \left(P_{app} \frac{SF}{P_{ss}} \right)^2 + \left(Q_{app} \frac{SF}{Q_{ss}} \right)^2 \quad (3.28)$$

and it compares the applied load to the corresponding allowable, with the Safety Factor, equal to 1 in case of design safety factor. PQMT is more complete quantity, which involves the bending and torsional component, resulting in the equation

$$PQMT = \left(\frac{P_{app}}{P_{ss}} \right)^2 + \left(\frac{Q_{app}}{Q_{ss}} \right)^2 + \left(\frac{M_{app}}{M_{ss}} \right)^2 + \left(\frac{T_{app}}{T_{ss}} \right)^2 \quad (3.29)$$

and the respective margin of safety is

$$MoS1 = \left(\frac{1}{PQMT^{0.5}} \right) - 1 \quad (3.30)$$

As for the previous one, this margin too has to be positive to leave the insert unbroken.

3.3 Joints

Principally, joints can be mechanical or bonding type, but their main issue, in any case, is to connect panels with components and brackets, primary and secondary structure.

Junctions can be bolted, bonded or through cleats, but there are four important type of joints analysed:

- Type 1: connection between primary panels structure. This type of connectors have been verified in these areas
 1. LVA Ring to Thrust cylinder
 2. Shear web to Thrust cylinder
 3. Shear web to Horizontal Platform cleats
- Type 2: connection between Primary and Secondary structure, in particular
 1. Shear web - lateral panels cleats
 2. Horizontal platform - lateral panels cleats
 3. PLM upper platform - PLM lateral cleats
- Type 3: connection Secondary to Secondary structure and it concerns the interaction of the lateral panels with the external frame, made of rods, and between lateral panels each others
- Type 4: Primary to Tertiary structure connection, which means the joints between primary structure and different appendiges.

3.3.1 Mechanical Joints

Some pros and cons have to be taken into account using mechanical joints: they are easy to use and to inspect, practical from the point of view of thicknesses, and no residual stresses are detected, however the parts to be connected have to

be drilled, or somehow damaged from their integrity; moreover, a concentration of stresses is noticed around the insert zone, which determines a low fatigue resistance. Finally, a limited stiffness and a corrosion disposition close the primary analysis of their characteristics.

The most common mechanical joint is riveting, whose principal aim is to withstand shear stresses, so they have to be excluded, as a solution, every time the axial load overcomes the 5% of the shear ultimate load. To correctly evaluate the joint, friction between plates is ignored. The breaking of the riveted joint depends on the shape and diameters of the head of the rivet, the thickness of the plates, the materials of both rivets and plates, and so on; the main failure modes for a round head rivet are rivet shearing, bearing of the hole, ripping and tensile failure of the sheet. In the first case, rivet shearing, the tensile shear stress on the section reaches the allowable one and exceeds it, while the bearing failure is a contact problem, non-linear in kind and regards the pressure of the rivet upon the sheet. The ripping can be avoided if a correct distance between the rivet and the free edge is chosen, and the breaking of the plate happens in those areas where the hole is absent, between the rivets. In the following figure 3.8, an illustration of the possible failure of a rivet is explored

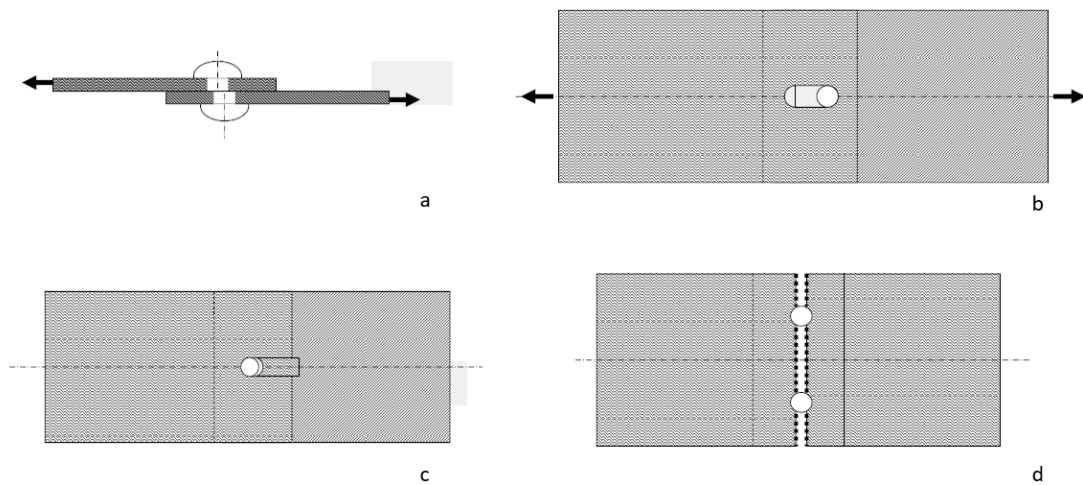


Figure 3.8: (a) Rivet shearing, (b) bearing of the hole, (c) ripping, (d) breaking of the plates [7]

3.3.2 Adhesive joints

Adhesive joints show high stiffness and good fatigue resistance, they are light and do not lead to fretting problems, they result as a continuous surface because the

plates are not drilled, and there is no stress concentration. Their limits concern the difficult inspection of the components and the thicknesses, which can not be too high. The removal of the adhesive means the breaking of the joint, and they easily decay due to environmental causes; furthermore, if the sheets connected are made of different materials, residual stress can be identified.

In this case too, loads are transferred through shear stresses along the joint line, but the stress distribution study is complicated, and for this subject, the Hart-Smith theory is considered.

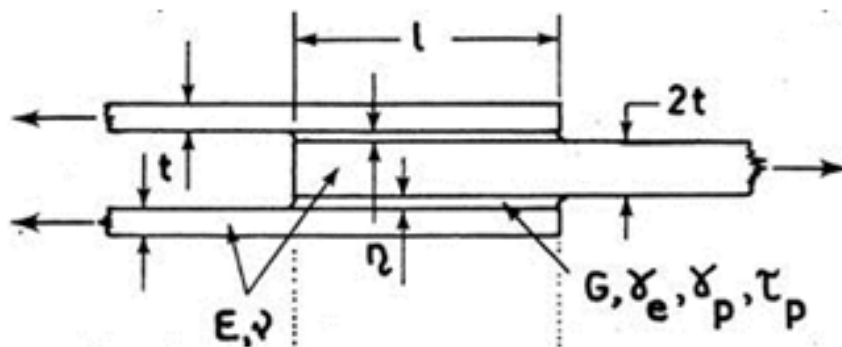


Figure 3.9: Double lap shear joint [8]

For the double lap shear joint, as reported in figure 3.9, l is the length of overlap, t is the thickness of the plates and $2t$ the thickness of the third component, the one between first and second plate (it can be of a different thickness too). Every component has its own Elastic modulus and Shear modulus, and for the adhesive γ_e is the gradient of the elastic part of the curve, while γ_p is the gradient of the plastic part of the curve. In the figure 3.10 the adhesive behavior and properties are reported, next to the adhesive shear stress and shear strain. The plastic part allows to have a leveling of tensions at the edge of the adhesive and it can be seen in the horizontal line for the mean shear stress τ

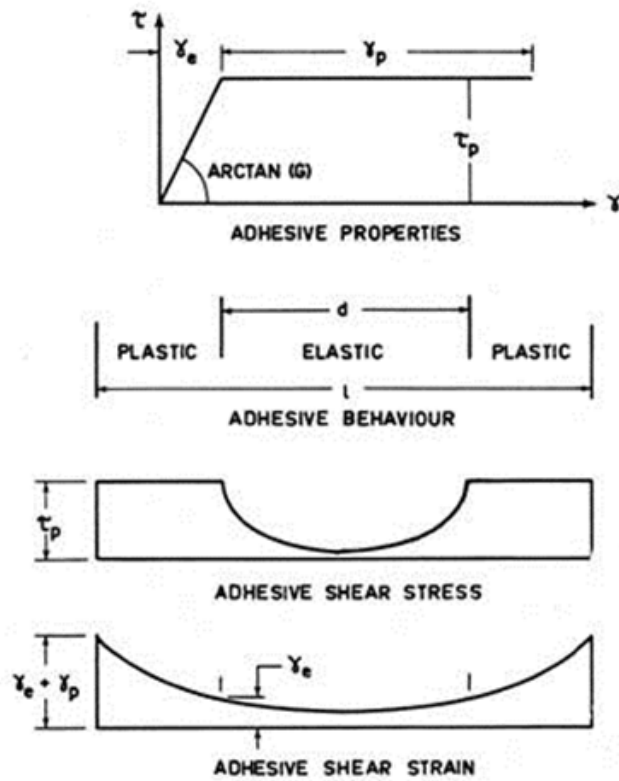


Figure 3.10: Adhesive graphics [8]

If the joint is balanced, $\tau(x) = \tau(-x)$ the behavior of the τ is symmetrical; increasing the length of overlap decreases pressure peaks on the joint, even though beyond a certain length they uniform, which means that a optimum overlap length exists: it is not useful adding adhesive when not necessary, because it just adds weight to the structure.

Chapter 4

Planning of experimental tests

The test campaign has been divided into three principal phases: Development test, Verification test and Qualification test, of which a schematization is given in figure [4.1](#)

4.1 Development testing

Development testing consists in the characterization of materials, structures, joints and every component could be part of the satellite. This type of test is done before verification and qualification testing, because the aim of the test is to understand the mechanical and physical proprieties of materials, as CFRP material and adhesive, in order to have an adequate data base for FEM analysis and analytical calculations. In a second moment, the activities are aimed to characterize the main structural basic components in order to have a confidential data base of allowables to use for analysis and design definition. For this purpose, an extensive test campaign includes sandwich characterization as edgewise compression tests, potted insert tests and edge insert (cleats) tests. These tests are executed according to ASTM regulations.

4.1.1 CFRP Lamina Mechanical Characterization

CFRP Lamina Mechanical characterization are tests previously conducted, the results are confidential data for TAS-TO and they are, full-fledged, fundamental part of the campaign test

4.1.2 Sandwich Characterization

Main purpose of these tests is to verify the performance characteristics of the laminates prepared and involved, compared to predictions made using the engi-

neering properties for elementary UD and Fabric materials and the laminate plate theory; the sandwich layup test samples are compound of hardware face sheets materials, face sheet lay-ups, adhesive film, honeycomb core and representative manufacturing process.

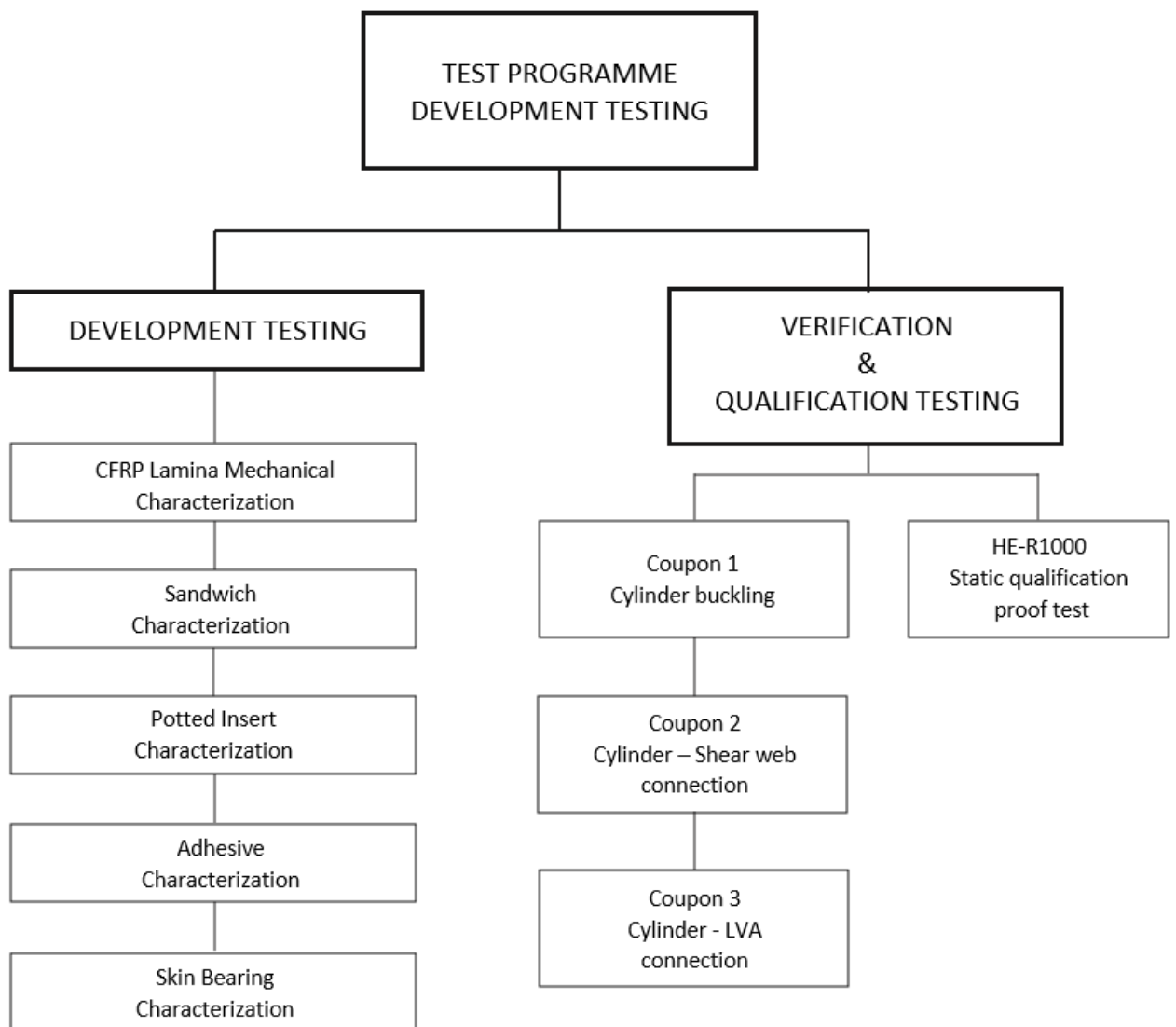


Figure 4.1: Campaign planning scheme - *Courtesy of TAS-I*

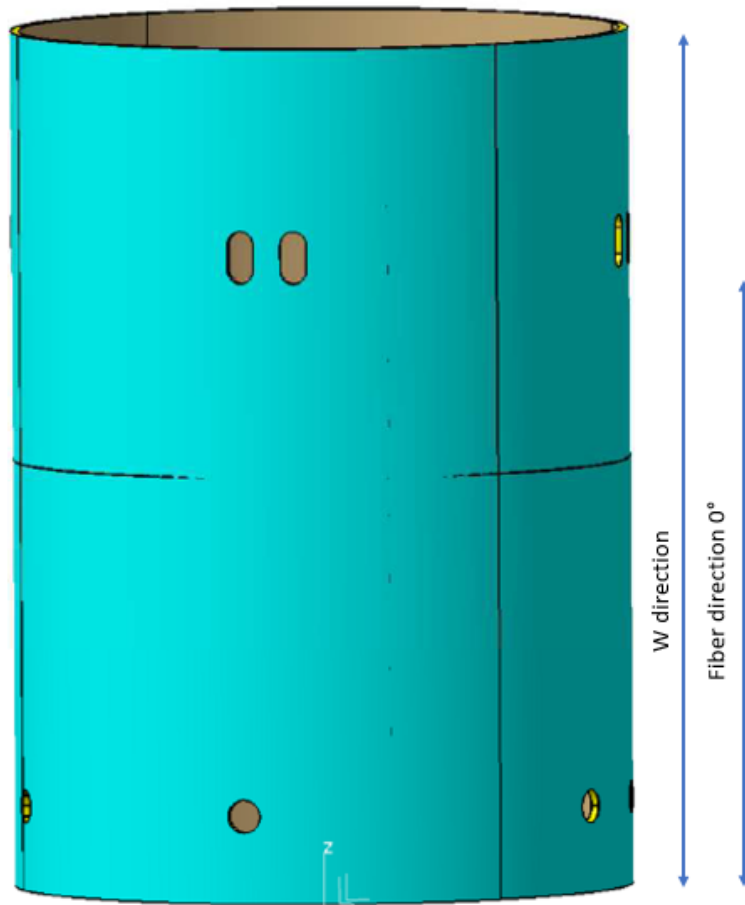


Figure 4.2: Cylindrical sandwich configuration - [9]

Characterization tests of sandwich structures, edgewise sandwich coupons, are done according to ASTM C364; for the CFRP edgewise coupons of HE-R1000 load values are required L and W direction. Edgewise coupons has been tested in flight configuration, which indicates its composition (compound, type of honeycomb, skins..), while for the coupon's dimensions, these are regulated according to the ASTM previously cited; the edgewise test results for sandwiches are in agreement with the expected values, in table 4.1

Sample definition	Fabric:	TAS – I DESIGN		
	UD:	TAS – I DESIGN		
	Laminate:	TAS – I DESIGN		
	Honeycomb:	OX 3/16 5056 0.0015P		Thickness = 0.91 mm
	Sandwich panel thickness:	14.02 mm		Thickness= 12.20 mm
Manufacturing	Co-cured with Redux 312L			
Sample typology	Flat: L-direction // 0°CFRP direction			
Test Environment	Room Temperature			
Loading direction	L,W			
Pre-conditioning	N.A.			
Test Measurement	Load Direction	Reference	Number of Samples	Expected value (Average)
Compression Strength [MPa]	L-direction	ASTM C364	5	Min 200
Compression Modulus [GPa]	L-direction	ASTM C364		Min 75
Compression Strength [MPa]	W-direction	ASTM C364	5	Min 75
Compression Modulus [GPa]	W-direction	ASTM C364		Min 12

Table 4.1: Sandwich cylinder configuration and edgewise expected values [9]

For the shear web sandwich configuration, edgewise results are reported below 4.2

Sample definition	Fabric:	TAS – I DESIGN		
	UD:	TAS – I DESIGN		
	Laminate:	TAS – I DESIGN		
	Honeycomb:	3/16 5056 0.001P		Thickness = 0.91 mm
	Sandwich panel thickness:	28.00 mm		Thickness= 26.18 mm
Sample typology	Flat : L-direction // 0°CFRP direction see Appenx1			
Manufacturing	Honeycomb cured: Foam 490A Pre-cured skin bonded with Redux 312L Sandwich panel thickness: 28.00 mm			
Test Environment	Room Temperature			
Loading direction	L,W			
Pre-conditioning	N.A.			
Test Measurement	Load Direction	Reference	Number of Samples	Expected value (Average) MPa
Compression Strength [MPa]	L-direction	ASTM C364	5	Min 190
Compression Modulus [GPa]	L-direction	ASTM C364		Min 80
Compression Strength [MPa]	W-direction	ASTM C364	5	Min 70
Compression Modulus [GPa]	W-direction	ASTM C364		Min15

Table 4.2: Sandwich shear web configuration and edgewise expected values [9]

4.1.3 Potted Insert Characterization

This characterization does not follow any international regulation or ASTM, but pull-out and shear tests had been carried out according to TAS-I internal test procedure, using dedicated tooling and fixtures which do not induce premature failures in the samples; however, some standard samples must be produced. Following insert configurations characterized the in-plan and out-of-plane (pull-out) shear capabilities, figures 4.3, 4.4

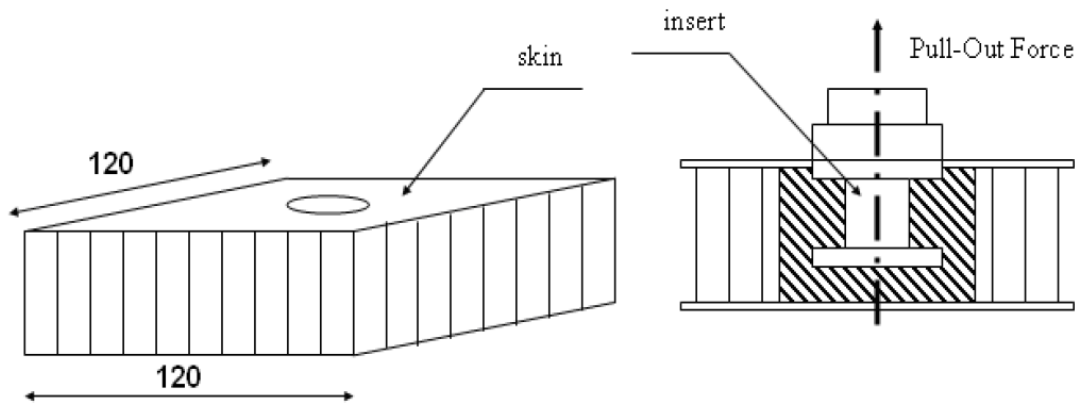


Figure 4.3: Insert pull-out Test [9]

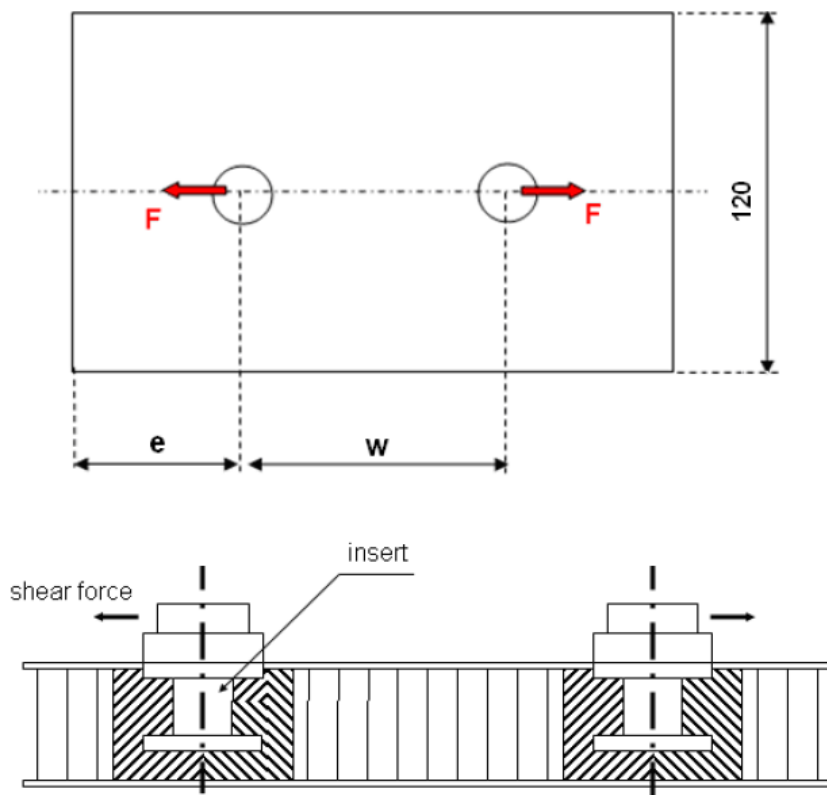


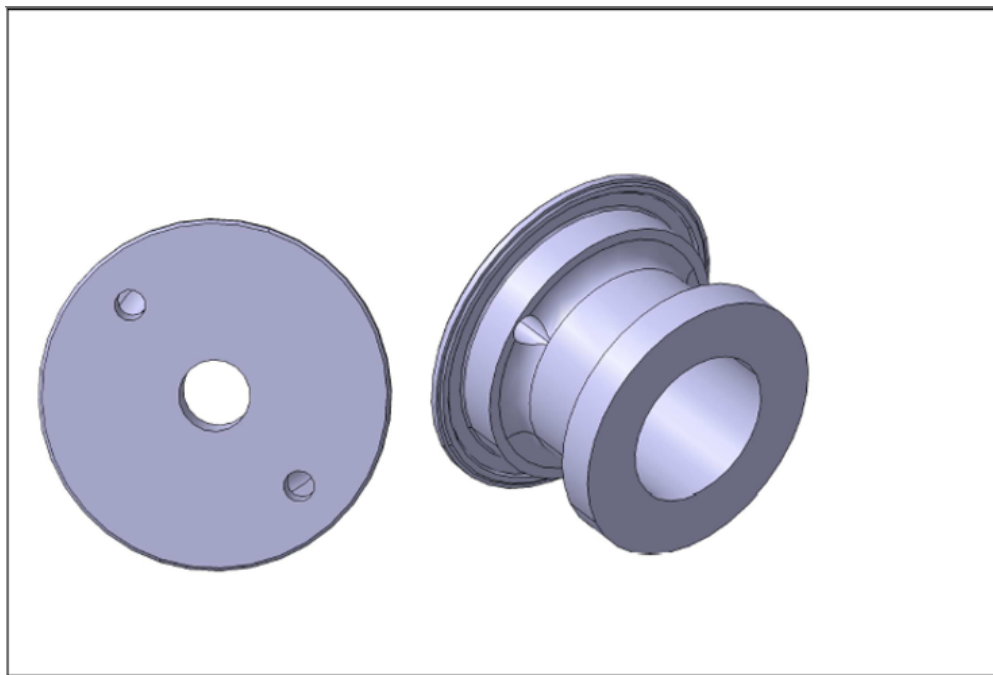
Figure 4.4: Insert Shear Test [9]

Tests have been carried out to evaluate the deterioration of the insert shear

capability in the following conditions:

1. Reduced edge/distance $\frac{e}{d} = 1.5$
2. Reduced distance of pitch $w = 4d$

The insert SPI-2, table 4.3 is the most considered in this thesis, it principally connects Cylinder and shear web interfaces, and it was subjected to all the earlier described tests, while for its construction the ESA-PSS-03-1020 regulation was taken into account.



Sample definition	Fabric: TAS - I DESIGN UD: TAS - I DESIGN Laminate: TAS - I DESIGN Honeycomb: OX 3/16 5056 0.0015P Sandwich panel thickness: 14.02 mm	Thickness = 0.91 mm Thickness = 12.20 mm		
Hole diameter	Diam. 21 mm toll. 0/+0.03			
Test Environment	Room Temperature			
Pre-conditioning	N.A.			
Test Measurement	Load Direction	Reference	Number of Samples	Expected value (N)
Pull Out Load	Normal to sandwich surface plane	ESA-PSS-03-1020	5	Min 5500
Shear Load	In-plane 0° fiber direction		5	Min 6800
Shear Load	In-plane 90° fiber direction		5	Min 6800

Table 4.3: Insert SPI-2 characterization [9]

4.1.4 Skin Bearing characterization

The aim of the test is to evaluate the bearing strength capability of CFRP laminate in presence of in-plane shear load. The bearing test must follow the ASTM D5961 regulation to have validity and dedicated specimens have been manufactured with the following characteristics, and later tested.

Laminate: **TAS – I DESIGN** Thickness = 0.91 mm

Hole diameter: 6 mm

Edge distance $e/d = 1.5$

Number of samples = 3 dir 0° + 3 dir 90°

Figure 4.5: Bearing characterization [9]

Bearing is the ovalization of the hole, and it involves the shear stress and geometrical factors: for this type of sandwich, with this configuration, the ultimate strength reached is $\sigma_u = 459 MPa$, result coming from tests.

4.1.5 Adhesive Characterization

The adhesive characterization is done through single/double Lap Shear Test in order to determine the apparent shear strength of the adhesive and it consequently allows to verify the conformance of its curing process. The Single Lap Shear test is performed using standard specimens in aluminum alloy, AA2024 - T3 ALCLAD of 1,6 mm of thickness, bonded with adhesive from the same batch of the associated production panel, and cured in the same autoclave load, according to ASTM-D-1002 regulation.

The specimens should give a cohesive failure mode (i.e. failure located within the adhesive) at values meeting minimum requirements. The figure 4.6 shows a sketch of a standard single lap shear specimen

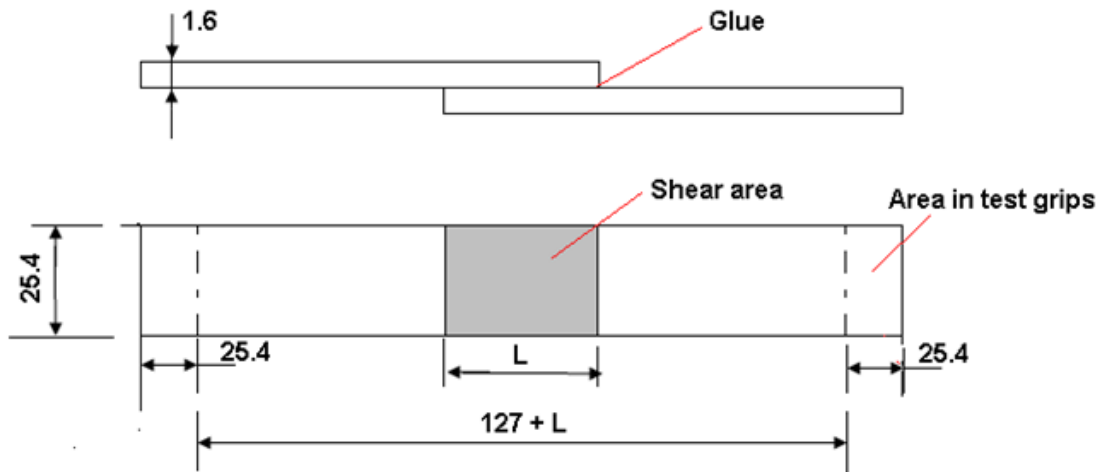


Figure 4.6: Standard single lap shear specimen [10]

For a further verification of mechanical performances of CFRP/CFRP bonded joints, Redux 312L/EA9321 adhesives shall be tested by means of standard double lap shear tests, according to ASTM-D-5868, and they will be performed in two different configurations:

- CFRP - CFRP monolithic laminate bonded with two monolithic laminate. Adhesive employed is 312L, fig. 4.7

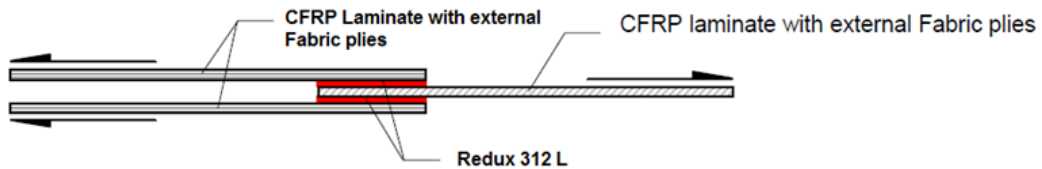


Figure 4.7: Double Lap shear test on the CFRP laminate [11]

- CFRP monolithic laminate bonded in two aluminum 7075 T7351 plate. Adhesive used is Hysol EA9321, fig. 4.8

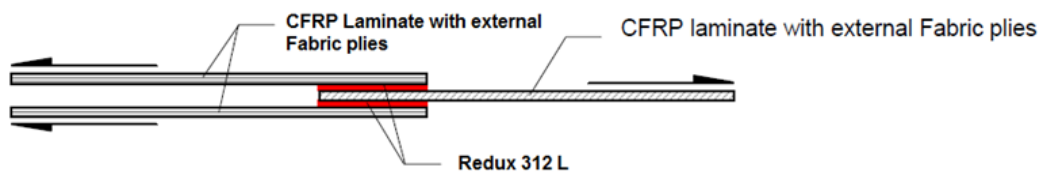


Figure 4.8: Double shear test on CFRP-Aluminum plate [11]

4.2 Verification and Qualification testing

This phase of the planning involves the verification and qualification testing of the coupons, better shown in the chapter below, and the static qualification proof test of HE-R1000 structure.

Three different type of coupons have been made and tested, each one with a different purpose and configuration:

- Coupon 1 consists of a section of cylindrical sandwich panel with two shear webs, on top of which LURA brackets are positioned; this first coupon is compression tested.
- Coupon 2 has been reproduced three times, each one for a different test configuration, it is a 30° section of cylindrical sandwich panel, with a single shear web; the samples are identified as *Pull Out Coupon*, *Axial Coupon* and *Bending coupon*.
- Coupon 3 investigates the connection between the Cylinder and the LVA ring, in other words it tests the connection with the Launcher attachment; two samples are tested, one for compression and one for tension.

Chapter 5

Coupons mechanical characterization

Different coupons are realized to explore the ultimate load strength and the behavior of the structural component of a generic satellite. A coupon is a structure in 1:1 scale, it can be geometrically similar to the structure but not exactly the same: this difference is justified by the fact that, to investigate the deformation and the failure of the component, it is necessary to isolate parts of the structure which needs appropriate constraints and boundary condition, not obtainable just isolating the component from the satellite itself. The important objective is to test a structure with the same load path whose undergoes the real component, once assembled. Three coupons are presented in this chapter, each of them modeled and tested according to the effective real loads that the structure would withstand.

5.1 Coupon 1

This coupon is realized to test the cylinder buckling, loading the structure with a loading rate of 500 N. The coupon is a section of 150° of a cylindrical sandwich panel, two representative sample shear web are connected through inserts and cleats, to the main cylindrical structure, in +X and -Y position: this location is chosen to give approximately the same stiffness of SDM, the LURA brackets are mounted on the upper ring to apply the axial load. There is complete agreement between the CAD model, the mathematical FEM model and the realized coupon, as seen in fig. 5.1: first of all, a CAD model is produced, from the design requirements, then it is modelled with finite elements to predict stresses and deformations, eventual failures and breaks; finally the coupon is realized and tested following the guidelines of test procedure.

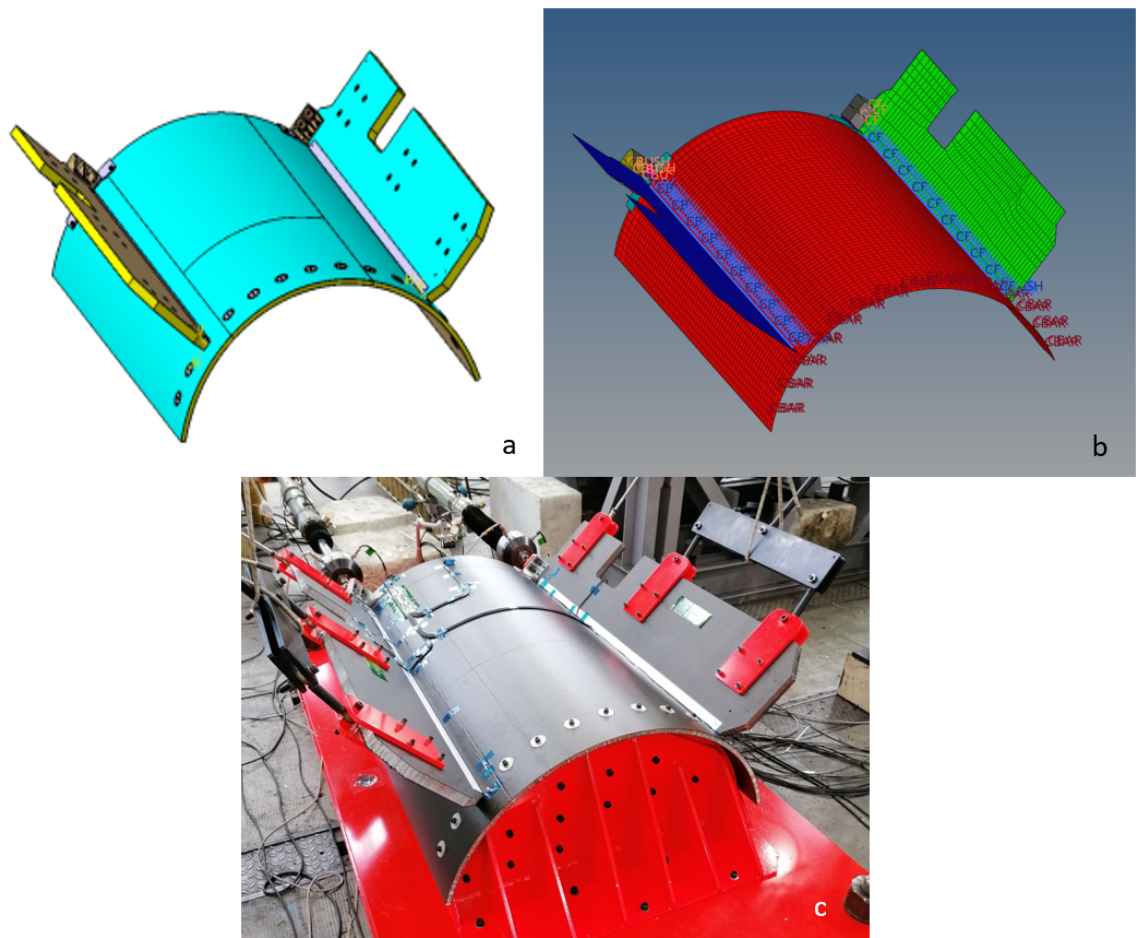


Figure 5.1: (a) CAD model - *Courtesy of TAS-I*, (b) FEM model, (c) real sample of Coupon 1

The connection between shear web panels and the cylinder is the same of SDM but they are not fixed to the ground base, because the cylinder bears the primary path of loads, while the shear web panels present dedicated inserts due to the application of lateral loads. Coupon 1 has been totally instrumented, to collect useful data about deformations and stresses.

5.2 Coupon 2

For this coupon, three samples have been made, to undergo three different tests: the first one was for pull-out testing, the second for axial traction testing and the last one for bending testing; however, the model was the same for every sample, and it is the below reported, fig. 5.2 The test article is a 30° section of cylindrical

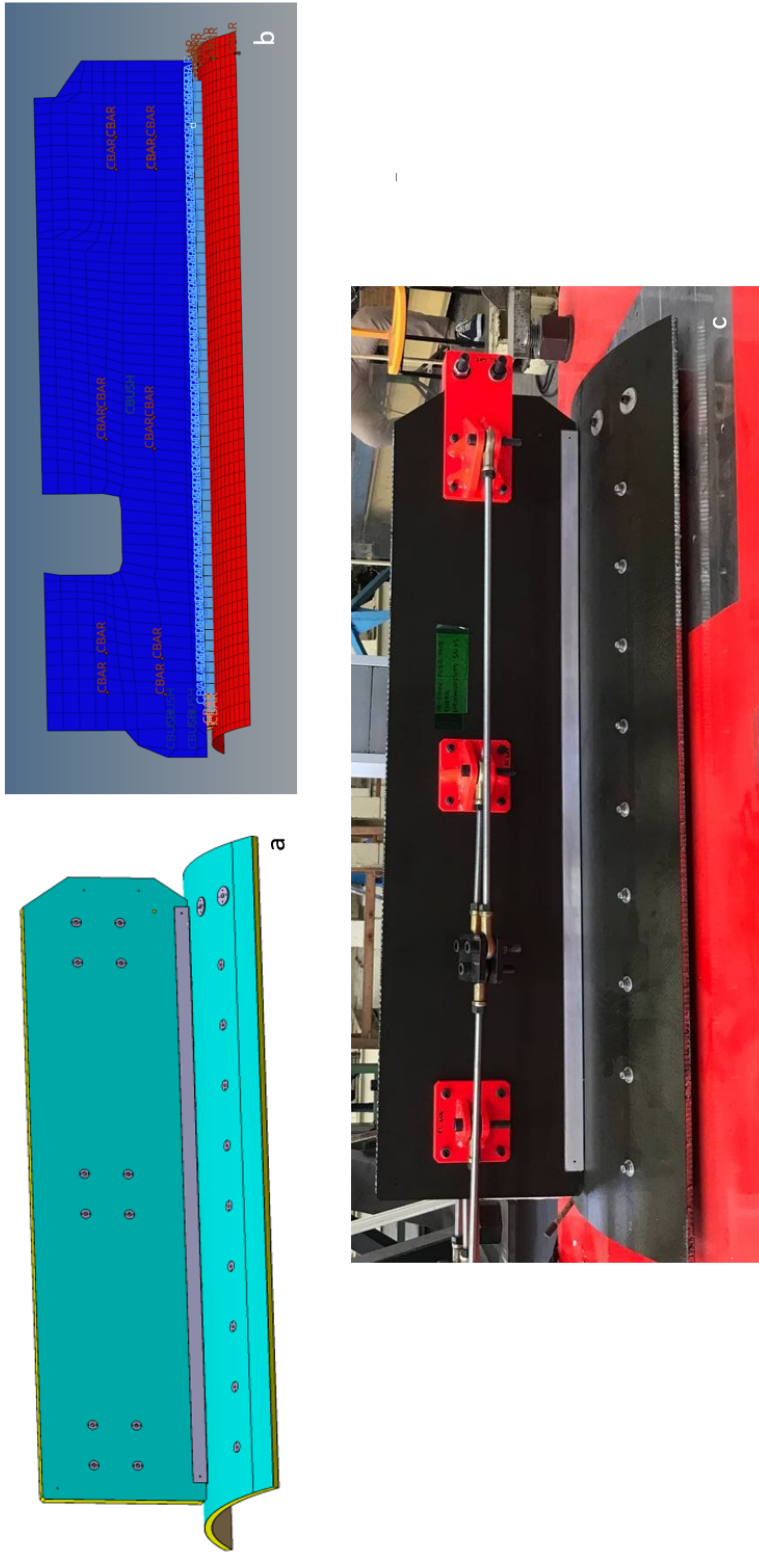


Figure 5.2: (a) CAD model - *Courtesy of TAS-I*, (b) FEM model, (c) real sample of Coupon 2

sandwich panel, with the same manufacture of SDM cylinder; as for Coupon 1, a representative sample of shear web panel approximately with the same stiffness of SDM is connected to the cylinder, as SDM design; on the shear web, some joints are dedicated to the application of the loads. Every coupon is loaded up to qualification design level, recorded and than unloaded; once the junction between Cylinder and Shear Web panel is checked, to assure that no failure occurred, the coupon is loaded up to rupture, to register the final ultimate strength.

5.3 Coupon 3

The aim of the test is the demonstrate the performance of the joint between Cylinder and LVA Ring, verifying the compatibility of the sample to sustain the qualification loads without any sign of yielding or failure; as for the previous ones, once the qualification load is checked, the sample is brought to rupture, to investigate ultimate strength and failure modes. Two samples are produced, one for tensile stress test and a second one for compressive stress test; both of samples are a 60° section of SDM Cylinder-LVA ring connection, with the use of same fasteners. The cylindrical section of the sandwich panel is located between two Aluminum forks, symmetrical positioned with respect to the horizontal centre line.

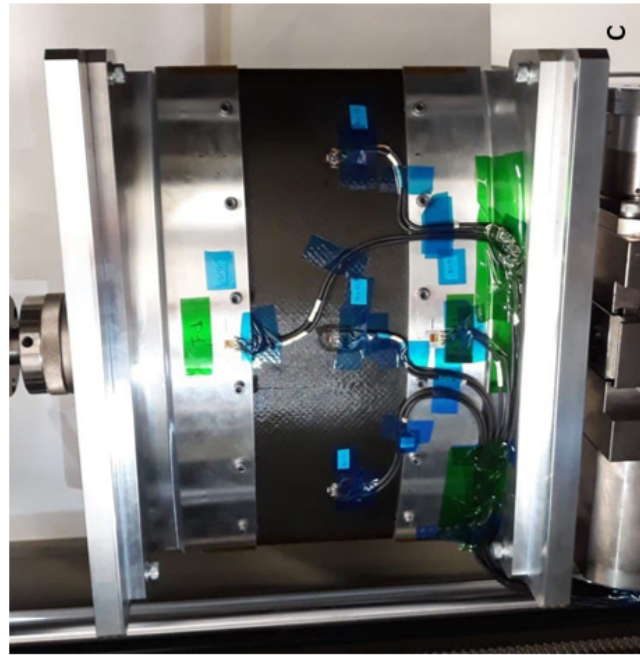
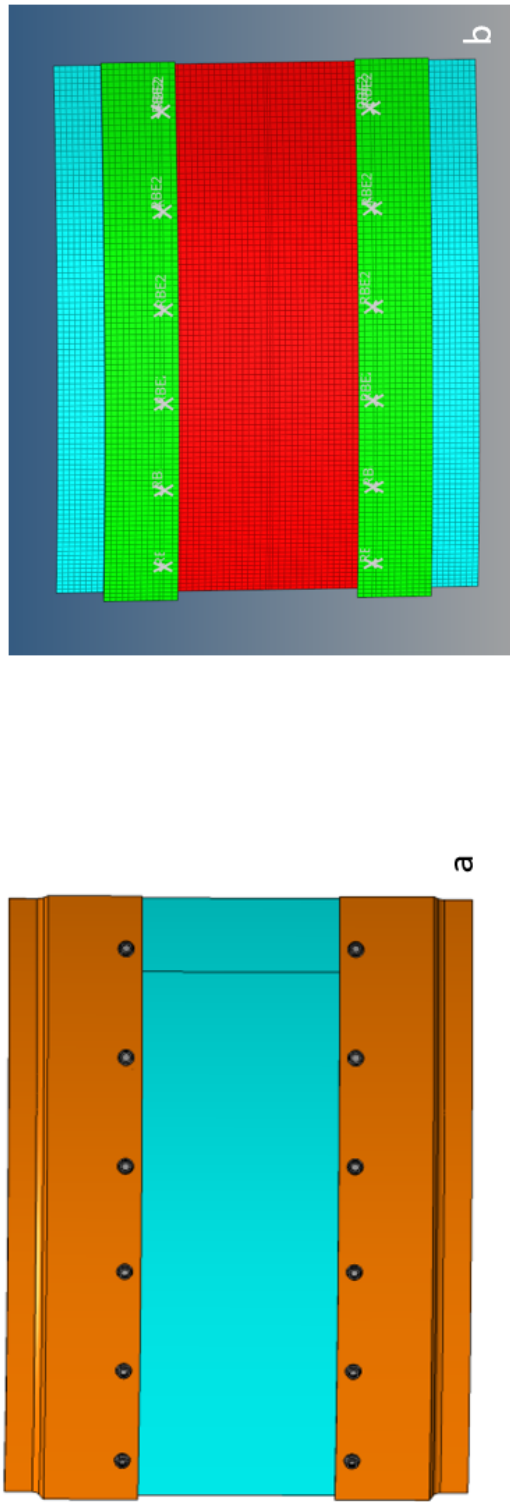


Figure 5.3: (a) CAD model - *Courtesy of TAS-I*, (b) FEM model, (c) real sample of Coupon 3

Chapter 6

Instrumentation and test procedure

In this section, instrumentation used for testing is introduced and procedure tests described, in order to explain how coupons undergo qualification and verification testing.

Only coupons 1 and 3 have been instrumented, with approximately the same equipment, for example fixture to the ground (Test Rig) and LVDT; the Test Article, another way to call the coupon, has to satisfy following requirements to be effectively tested:

- To provide an adequate interface points, to be fixed to the ground
- To provide adequate interface points to allow the connection to hydraulic jack
- Appropriate design to provide very stiff boundary conditions. As far as possible, sliding of connection element and Test Rig unexpected deformations have to be avoided, to preserve the real and correct behavior of the coupon during the test; when this conditions fails, any potential deformation of the frame must be recorder, to remove it during the calculation of the effective displacement.
- Capability to sustain the applied loads during the test, without rupture.

The instrumentation applied, described below, is placed to monitor the foreseen load path in the mot significant location, and in peculiar and critical points underlined by the FEM prediction.

- Acquisition channels for mono and bi-axial strain gauges in order to measure the strain level in the CFRP skins of sandwich panels.

- LVDT, transducer of position, to measure the respective out of plane displacements
- The load cell for each load direction in order to recover the overall loads applied during the test

6.1 Coupon 1

Coupon 1 has been instrumented with 8 mono axial SG, 2 biaxial SG, a LVDT and a load cell, in different location on the Cylinder and Shear Webs; in particular SG7 and SG9 are located on the -Y shear web panel, SG8 and SG10 on the X shear web panel, the rest of them on the cylinder. The fig. 6.1 shows the setup configuration, where the red lower platform is the fixture to the ground, while the red lateral clamps allow the connection with the loading apparatus, which supplies lateral load; on the left of the figure, a double hydraulic jack in attached to the LURA brackets to provide the axial load.

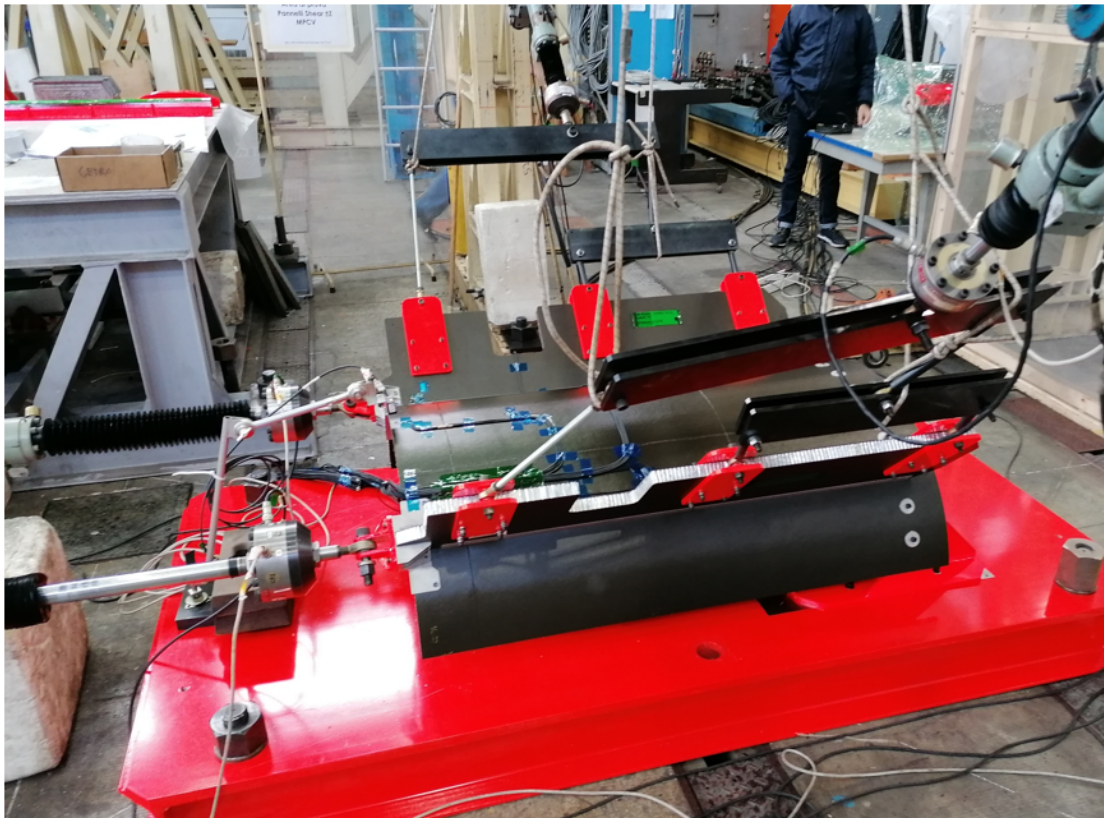


Figure 6.1: Setup configuration of coupon 1 - *Courtesy of TAS-I*

For coupon one, the following loading steps have been executed:

% Step		1	2	3	4	Expected Ultimate Collapse Loads
Qualification Design Load	Axial Load	5511	11023			
	Lateral Load	1966	3933			
Expected Ultimate Collapse Load	Axial Load	Step 1		16534	41887	55000
	Lateral Load			5899	7079	10000

Table 6.1: Table of test sequence - [9]

As reported, the Qualification Design Load is 11023 N in axial direction and 3993N for each shear web panel, while the Expected Ultimate Collapse Load is 55000 N for each LURA bracket and 10000 for each shear web. Before testing, it is appropriate to give prediction values of the strains for the Qualification Load: to do so, it is checked the position of the strain gauges and a corresponding element is found on FEM model. From post processing, strain's values are collected and then compared to the ones resulting from the test, from the strain gauges reading: if the difference between these two values is less than 15%, the model is representative of the reality, and its results can be taken into account. For example, for Coupon 1, the majority of the predicted values are in line with the test result data, except for SG9 and the axial direction of the bi-axial SG number 3, fig. 6.2

NAME	sured Direc	FEM ID	Qualification Level			Ultimate Level
			FEM prevision - Strain $\mu\epsilon$	Test results - Strain $\mu\epsilon$	ERR %	Test results - Strain $\mu\epsilon$
Cyl_SG1	Z - axis (xx)	70017004	-115.7	-131	13.22%	-315.2
Cyl_SG2	Z - axis (xx)	70017466	-182.3	-174	-4.55%	-488.6
Cyl_BX4_a	Z - axis (xx)	70018737	335	59	-82.39%	162
Cyl_BX4_c	ingential (y)		-738.5	-702	-4.94%	-1761
Cyl_BX3_a	Z - axis (xx)	70019076	397.3	421	5.97%	1029
Cyl_BX3_c	ingential (y)		-1193	-1016	-14.84%	-2518
Cyl_SG5	Z - axis (xx)	70017904	-335.1	-302	-9.88%	-881
Cyl_SG6	Z - axis (xx)	70018347	-306.5	-274	-10.60%	-943
SW_SG10	Z - axis (xx)	70040946	-299.6	-313	4.47%	-1005
SW_SG8	Z - axis (xx)	70040086	-317.2	-340	7.19%	-1385
SW_SG9	Z - axis (xx)	70055941	-212.1	-435	105.09%	1556
SW_SG7	Z - axis (xx)	70055086	-352.9	-359	1.73%	-1604.5

Table 6.2: Comparison between FEM prediction results and test results, for strains coming from Qualification Load; last column reports the strains from Ultimate Load test results

A further step is to verify the closure of the strain gauges, which means to plot the graph of the strains during the loading and unloading of the coupon during the Qualification Load test, and verifying if the difference between the zero initial

loading step and the final step, when the coupon is completely unloaded, is part of the sensitivity range of the instrument ($50\mu\epsilon$); if the range exceeds this limit value, then the strain gauge's values are considered not coherent. Plots of the different strain gauges are reported below, fig. 6.2 and fig. 6.3 to verify their reading during the Qualification Load step

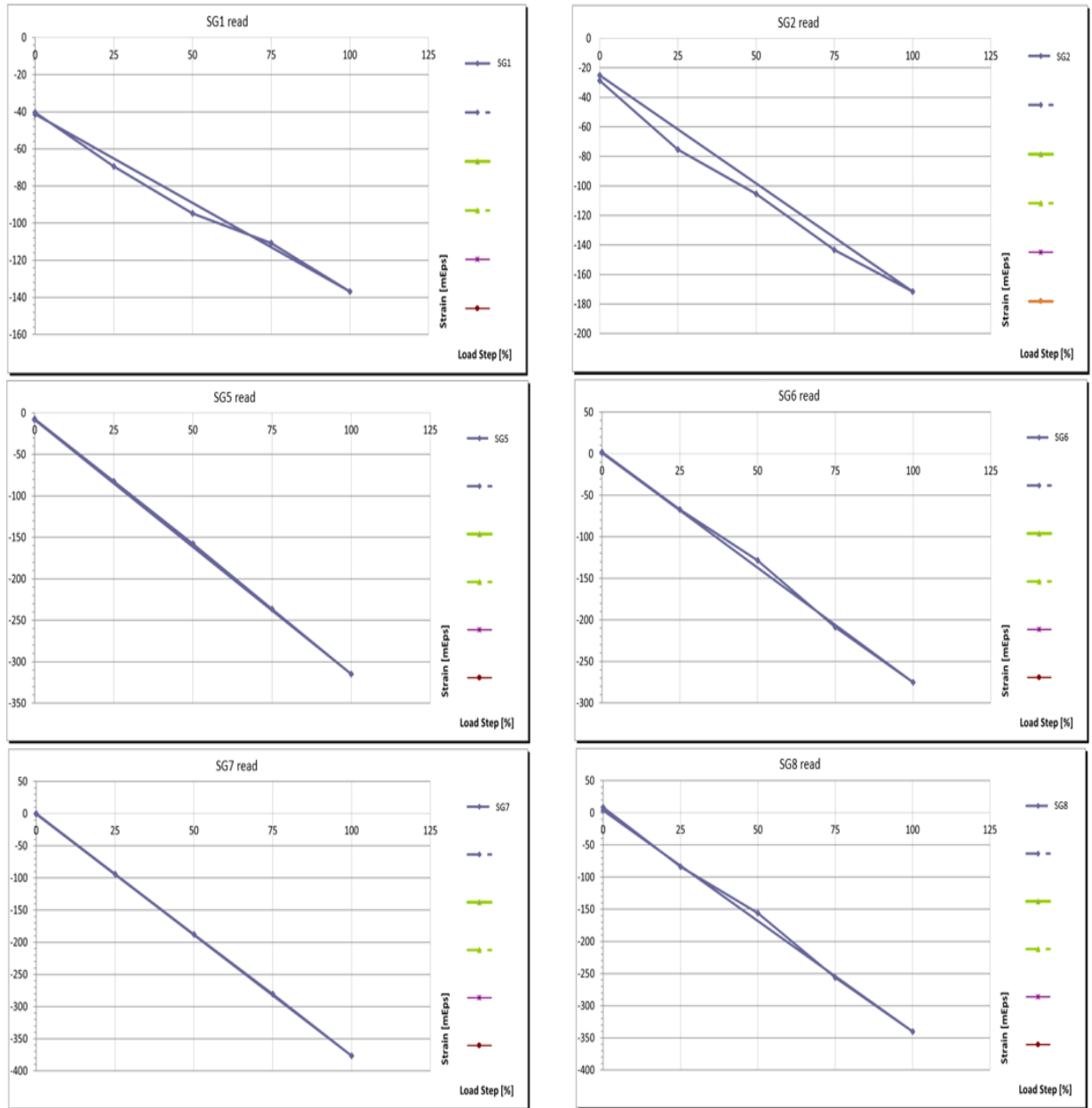


Figure 6.2: Plot of strains for Strain Gauges 1, 2, 5, 6, 7 and 8

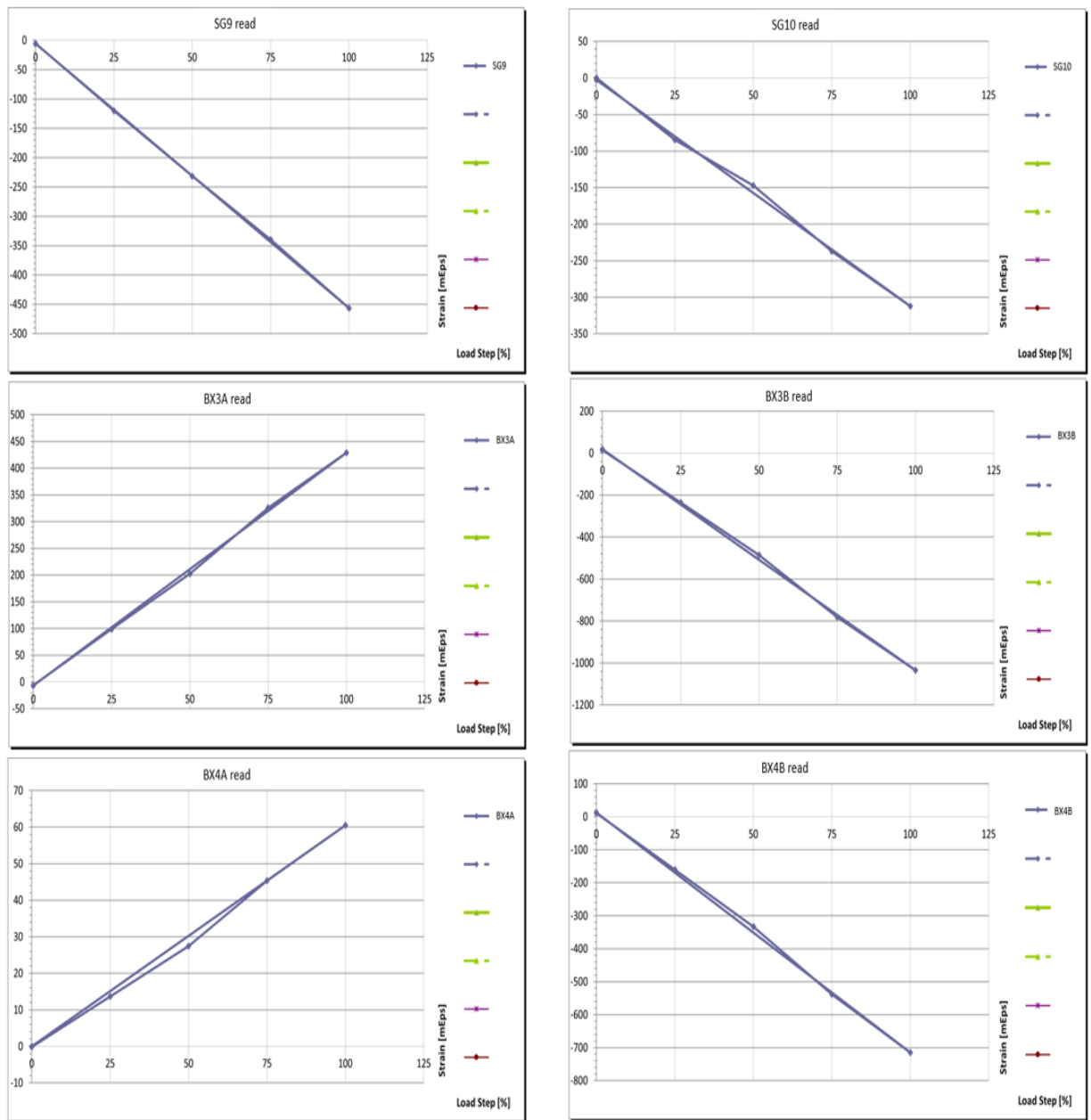


Figure 6.3: Plot of strains for Axial Strain Gauges 9 and 10 and for bi-axial 3 and 4

Strain gauges number 9 and the axial direction of the bi-axial number 4 read a strain values different from the predicted FEM's one: this is not a huge issues if, as in this case, the rest of the instrumentation give results coherent with the mathematical model. A possible explanation to this event could be a FEM element size too big, not capable of representing the effective deformation of the interested

area, or a model which presents local discrepancy compared to the real coupon's behavior.

For the sake of completeness, in the next figure 6.4 the location of strain gauges and other instrumentation is shown, from test specification

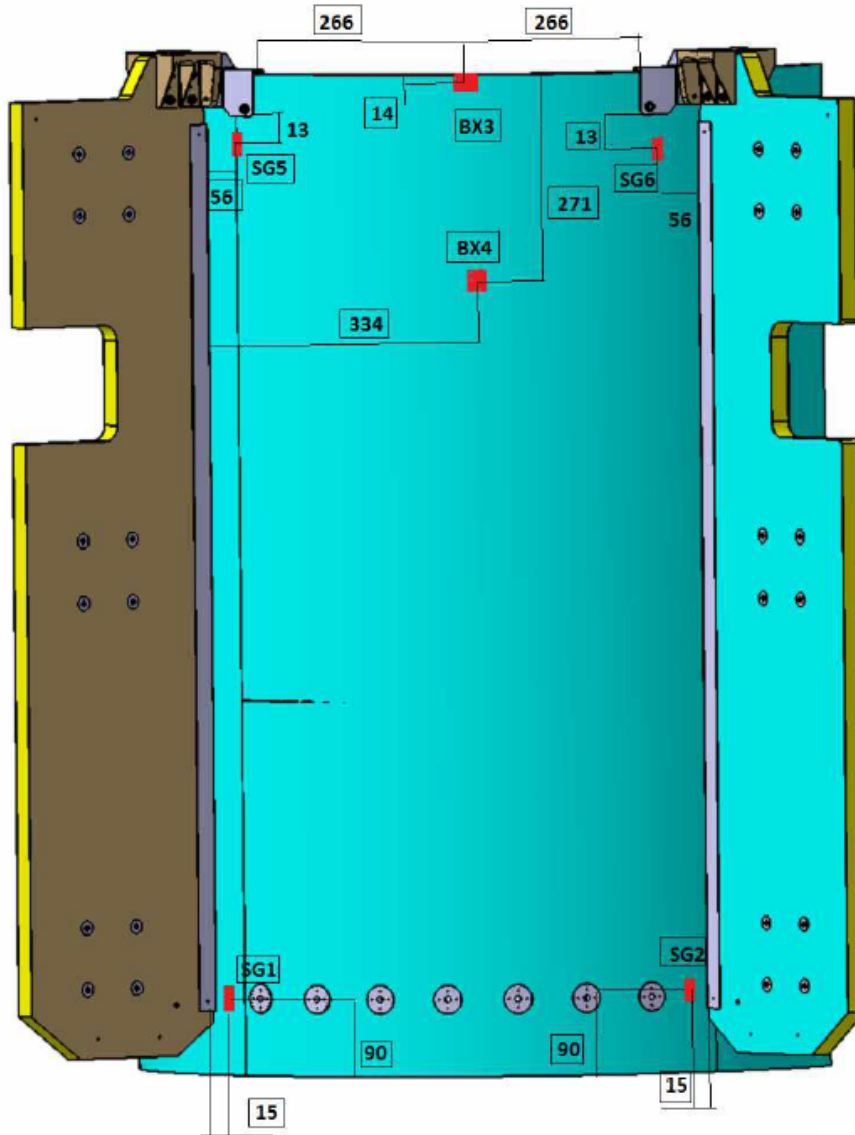


Figure 6.4: Location of strain gauges on Coupon 1 [9]

6.2 Coupon 2

As previously explained, three samples are made for coupon 2, and none of them was instrumented, mainly because the tests they would have undergone were not fundamental from the displacement or deformation point of view: these samples are led to rupture to register the Ultimate Load Strength and validate the Qualification and Ultimate load predicted through FEM model. Edges of the cylindrical section of the sandwich panel are fixed to the ground, while the clamps grip the appropriate points of the Shear Web panel to apply the load. The instrumentation used includes 3 Load cells, one for each test; below, the three load configurations, from the Specific document, fig. [6.5](#)

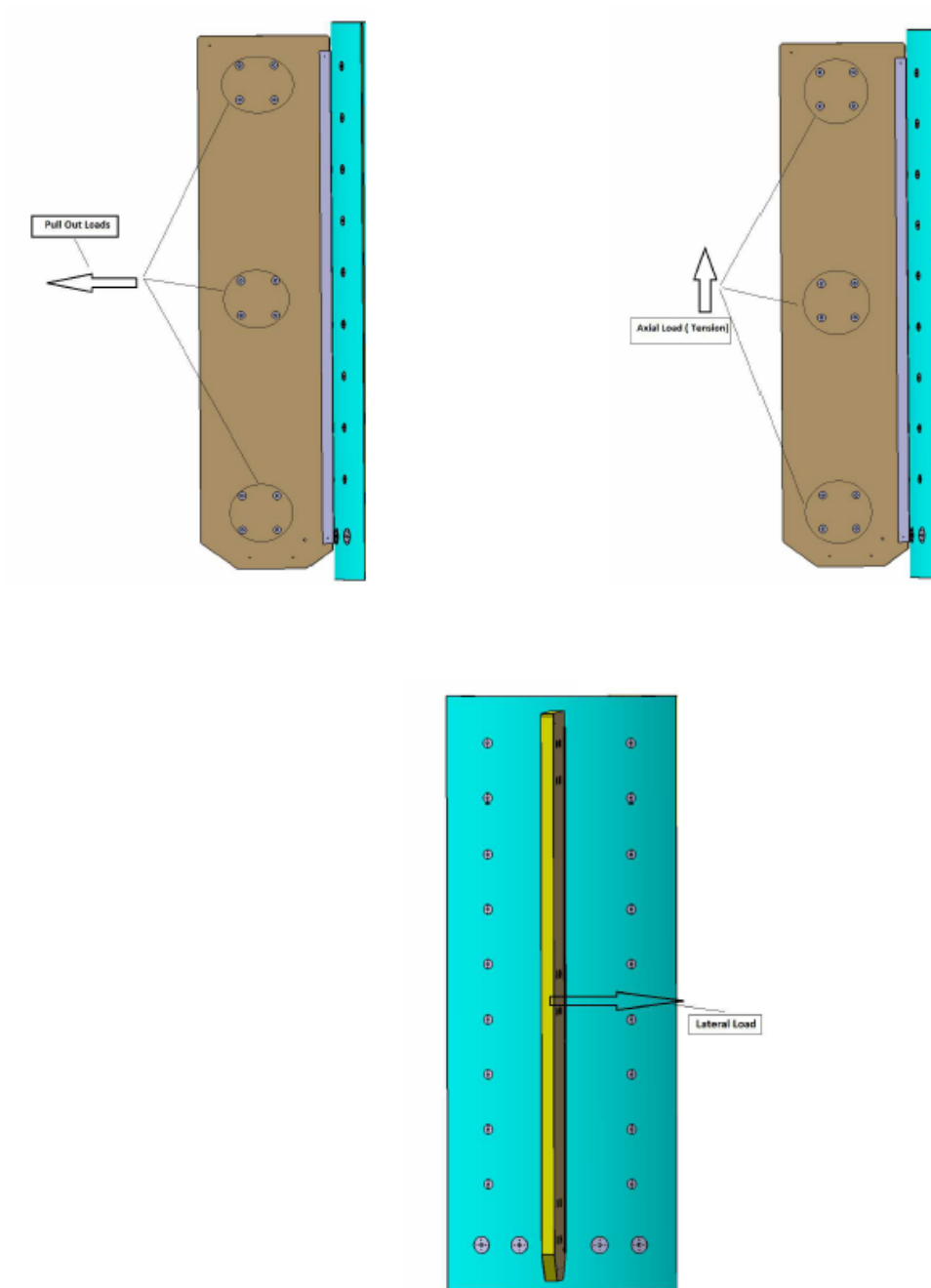


Figure 6.5: Loading configuration of the three samples of coupon 2 [9]

6.3 Coupon 3

The test verifies the capability of the sample to sustain the Qualification Loads without yielding or failure and the Ultimate load the structure is capable to withstand before collapsing. The samples, two 60° sections of cylindrical sandwich panel between two aluminum forks and connected with adequate fasteners, are differently tested, one in tension and the other in compression. For this type of test, a different instrumentation has been used, for what concerns the loading apparatus: the sample is placed between the plates of the INSTRON machine, and this justifies the shape of the aluminum forks, machined for good parallelism to adapt to the plates. As for the previous, the coupon is loaded up to qualification level, the value is recorded and it is then unloaded; once these operations have been done, the junction is checked to evaluate any eventual failure. The sample is finally tested to Ultimate Load and this value is registered, as the failure mode.

The positioning of strain gauges, fig. 6.6, for both sample, is provided for each skin of the sandwich panel, so the inner and the outer side, and the same for the LVA Ring metallic flange; this configuration has the aim of monitoring the symmetry of the loading in the sample and of recording the strain distribution in the CFRP skin of sandwich panel and in the LVA ring metallic part. The strain gauges used are 10 and they are bi-axial type, which means that the measurements are done through 20 channels.

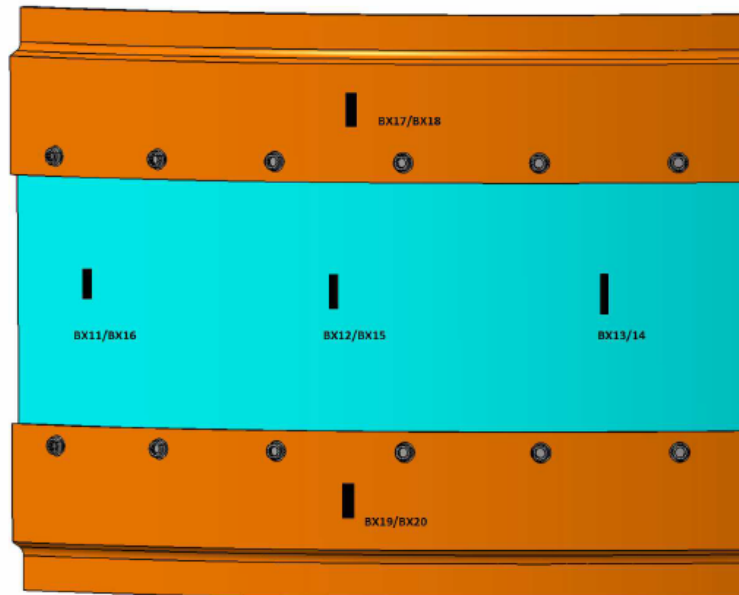


Figure 6.6: Strain gauges position on the outer side of the sample [9]

Chapter 7

Analytical joint calculation

To be able to calculate joint analytical results, international regulations will be followed, specific for each kind of connection. For bolted joints, NSTS 08307 is the reference guide from which the calculus is implemented.

7.1 Bolted Joint

Generally, it is required a preloading for the bolt that is subjected to increased axial tensile load, in order to reduce cyclic stresses and prevent major issues such as joint separation or pressure leakage. There are three principal requirements to be respected, to allow joint's employ, and they concern the strength of the bolt, its fracture and fatigue life and a certain safety factor at limit load. To verify if the strength requirement is respected, the bolt is checked at maximum external load and maximum preload, while the joint separation is checked at maximum external load and minimum preload. The safety factors have to be applied only to external loads.

This regulation only takes into account the fact that the bolt is subjected to axial and shear forces, and it does not withstand moment. However, it is important the calculation of maximum and minimum preloads necessary to meet the requirements. It is not necessary to include safety factors in the different criteria, but it is mandatory to take into account any uncertainty of the preload; to do this, a maximum preload PLD_{max} and a minimum preload PLD_{min} are defined.

Three procedures are available for the calculation of PLD_{max} e PLD_{min} , each one used for the a particular situation:

- Procedure A - This procedure is applied when the applied torque does not overcome the initial torque yield and it is computable through two further sections, the *Typical Coefficient Method* or the *Experimental Coefficient*

Method For the *Typical Coefficient Method*, maximum and minimum preload can be calculated with these formula

$$PLD_{max} = (1 + \Gamma)T_{max}/[R_t(\tan \alpha + \mu_t^{typ}/\cos \beta) + R_e\mu_b^{typ}] + P_{thr}^{pos} \quad (7.1)$$

$$PLD_{min} = (1 - \Gamma)(T_{min} - T_p)/[R_t(\tan \alpha + \mu_t^{typ}/\cos \beta) + R_e\mu_b^{typ}] + P_{thr}^{neg} - P_{loss} \quad (7.2)$$

Other way to write them is:

$$PLD_{max} = (1 + \Gamma)T_{max}/K^{typ}D + P_{thr}^{pos} \quad (7.3)$$

$$PLD_{min} = (1 - \Gamma)(T_{min} - T_p)/K^{typ}D + P_{thr}^{neg} - P_{loss} \quad (7.4)$$

The terms in the previous equations are the minimum and maximum torque T_{min} and T_{max} of the applied range, while T_p represents any prevailing torque; Γ is the uncertainty of the measurement, while positive and negative thermal loads are P_{thr}^{pos} and P_{thr}^{neg} . Finally, depending on the chosen equation, typical coefficient of friction μ_t^{typ} is at the interface between internal and external thread interface, and μ_b^{typ} is the nut-to-joint bearing interface; alternatively, it is possible to use the typical nut factor K^{typ} .

Using the *experimental coefficient method*, it is possible to avoid the uncertainty factor, providing ???

$$PLD_{max} = T_{max}/[R_t(\tan \alpha + \mu_t^{min}/\cos \beta) + R_e\mu_b^{min}] + P_{thr}^{pos} \quad (7.5)$$

$$PLD_{min} = (T_{min} - T_p)/[R_t(\tan \alpha + \mu_t^{max}/\cos \beta) + R_e\mu_b^{max}] + P_{thr}^{neg} - P_{loss} \quad (7.6)$$

or, as for the typical coefficient method

$$PLD_{max} = T_{max}/K^{min}D + P_{thr}^{pos} \quad (7.7)$$

$$PLD_{min} = (T_{min} - T_p)/K^{max}D + P_{thr}^{neg} - P_{loss} \quad (7.8)$$

- Procedure B - This procedure is applied when the torque yield of the bolt is reached during the preload, whose maximum and minimum have to be investigated during an application specific test. Test wrench and the one used for actual hardware must have the same accuracy.
- Procedure C - This method is used when the initial torque yield is reached in any other different way from the previously depicted; the equations are

$$PLD_{max} = (1 + \Gamma)(PLD + TOL) + P_{thr}^{pos} \quad (7.9)$$

$$PLD_{min} = (1 - \Gamma)(PLD - TOL) + P_{thr}^{neg} - P_{loss} \quad (7.10)$$

7.1.1 Typical coefficients of friction/ nut factor and expected preload loss

Some parameters must be taken into account during the selection of typical coefficient of friction, which are specific and different for each application and each bolt: materials which come into contact at the interface between bolt and joint, the surface finish and the lubricants employed. These three items are the same considered for the typical nut factor, but in this case nut type and size is important too.

Regarding the preload loss, it is quite frequent to experience it due to plastic deformation or vibration or the compound action of both; however, the criteria used for the joint analysis do not concern vibrations. The entity of the loss is approximately in a range of 2-10% of the preload level in the bolt, but it is not specified how to calculate this amount; in the specific case in which the bolt stiffness is dependent upon non metallic materials, the preload loss must be precisely determined through an application specific test. It is provided a plausible equation to calculate this value

$$0.05 \times PLD_{max} \quad (7.11)$$

7.1.2 Preloaded bolt strength criteria

This criteria investigate yield loss analysis, for which it is necessary to use yield factors of safety and allowables, while the ultimate load analysis involves allowables and ultimate factors of safety. To be respected, the bolt must not yield in the minimum cross section at yield load and must not fail at ultimate load.

Four types of load can be applied to a preloaded bolt: axial load, shear load, bending load and the combination of these three. The bolt, however, must meet the criteria in each category and the criteria itself has to guarantee that there would not be a destructive yield during the installation of the bolt; for these reasons, bolt, bolt thread and nut has to be revised.

The axial load is calculated through the expression

$$P_b = PLD_{max} + n(SF \times P) \quad (7.12)$$

where n is the stiffness parameter and n the loading-plane factor.

1. Axial load - It is necessary to know PA_t and PA_s , respectively the axial load allowable of the bolt due to tension and the one due to thread shear, and both the minimum cross section of bolt and shear pull-out of threads have to satisfy two criteria.

- Minimum cross-section of bolt

$$MS = PA_t / (SF \times P) - 1 \geq 0 \quad (7.13)$$

$$MS = PA_t/P_b - 1 \geq 0 \quad (7.14)$$

If it is given a minimum tensile load for the bolt, it is possible to calculate the axial load allowables for Yield

$$PA_t = \left(\frac{F_{ty}}{F_{tu}} \times \text{minimum ultimate tensile load}\right) \quad (7.15)$$

and for ultimate

$$PA_t = \text{minimum ultimate tensile load} \quad (7.16)$$

It could be that the ultimate tensile load is not available: in that case, the axial load allowable has to be derived from testing or calculated, for Yield and Ultimate case, as

$$PA_t = A_t \times F_{ty} \quad (7.17)$$

$$PA_t = A_t \times F_{tu} \quad (7.18)$$

A_t , as said before, is the tensile stress area of the bolt and it is based on the minimum cross-sectional area of this last one, and it can be calculated as

$$A_t = 0.7854 \left(D_e^{bsc} - \frac{0.9743}{n_o} \right)^2 \quad (7.19)$$

where D_e is the major diameter of external thread and n_o is the threads/inch

- Shear pull-out of threads

$$MS = PA_s/(SF \times P) - 1 \geq 0 \quad (7.20)$$

$$MS = PA_s/P_b - 1 \geq 0 \quad (7.21)$$

The previous equations are used to determine the margin of safety in those cases where the internal thread is not totally threaded onto the bolt or when it does not guarantee to reach the full ultimate load capability. The term P is the external axial load applied to joint at bolt location when limit load is applied to the structure, P_b is the bolt axial load resulting from yield, ultimate or joint separation.

2. Shear load

$$MS = VA/(SF \times V) - 1 \geq 0 \quad (7.22)$$

In this formula terms V , bolt shear load resulting from limit load, and VA , shear load allowable of bolt, appear and they are used to calculate the margin of safety for shear load

3. Bending load

$$MS = MA/(SF \times M) - 1 \geq 0 \quad (7.23)$$

where M and MA are respectively the bolt bending moment resulting from limit load and its allowable.

4. Combined axial - shear - bending load

$$\left(R_a + \frac{R_b}{K}\right)^2 + R_s^3 \leq 0 \quad (7.24)$$

$$1 \leq K \leq K_y \quad (7.25)$$

where K_y is a plastic bending factor, whose value is 1 in case of minimum preload and it does not exceed the 0.2% of the maximum preload. The terms "R" are a sequence of ratios which compare the load to the respective allowable; the subscript indicate a for axial, b for bending and s for shear

$$R_a = \max \left[\frac{SF \times P}{PA_t}; \frac{P_b}{PA_t}; \frac{PLD_{max}}{PA_t} \right] \quad (7.26)$$

$$R_b = \frac{(SF \times M)}{MA} \quad (7.27)$$

$$R_s = \frac{(SF \times V)}{VA} \quad (7.28)$$

7.1.3 Plastic Bending

This theory is applied if the preceding are not respected but the resulting permanent deformation can still be accepted, providing that the material is ductile enough.

- Bending load

$$MS = \frac{(MA \times K_p)}{SF \times M} - 1 \geq 0 \quad (7.29)$$

where K_p is the new plastic bending factor

- Combined axial - shear - bending load

The same ratios employed for the preload strength criteria are resumed here, but the R_b sees a little difference in the addition of the plastic bending factor K_p

$$R_b = \frac{(SF \times M)}{(MA \times K_p)} \quad (7.30)$$

The criteria to be respected is

$$R_a^2 + R_b + R_s^3 \leq 1 \quad (7.31)$$

7.1.4 Preloaded bolt separation criteria

The joint separation must not occur under the joint limit separation load, and in this case a linear preloaded joint theory is used; it is possible to implement more accurate theory to describe the behavior of the joint, but in any case it has to include minimum preload PLD_{min} and the joint separation load P_{sep} and the analysis must be non linear if the yield of the bolt is reached applying the separation load.

Since it is not always realistic, because it is possible that the joint separation occurs before the joint separation load is reached, it is frequent to use more elaborate preloaded joint/seal design in which every single component analyzed must be considered as critical. The system must include a separation safety factor SF_{sep} while using P_{min} as preload. Known that the separation preload can be calculated as

$$P_{sep} = P \times SF_{sep} \quad (7.32)$$

the following equation is used to chose which case is applicable for the joint separation.

$$P_b = PLD_{min} + nP_{sep} \quad (7.33)$$

If the bolt axial load resulting from the joint separation is lower than tensile yield allowable of the bolt itself, the criteria states

$$MS = \frac{PLD_{min}}{[(1 - n)P_{sep}]} - 1 \geq 0 \quad (7.34)$$

The second case, where P_b ge the tensile yield allowable of the bolt, need a non linear analysis to determine if the joint separation happens, and it has to occur below the separation joint load

7.2 Adhesive Joint

For the adhesive joint, Hart-Smith theory is applied; it includes formulas to evaluate the margins of facings, honeycomb and local buckling too, but they had been calculated separately, so the only result of interest is the margin of the adhesive. To start, some element are introduced, to better explain next calculations:

Allowable minimum joint load N/mm on double lap shear joint

$\eta = 0.1 mn$ is the adhesive thickness, while λ_x and λ_y are used to identify the overlap length and the following allowable.

$$\lambda_x = \sqrt{\frac{G_{adh}}{\eta} \frac{2}{E_x t_f}} \quad (7.35)$$

$$\lambda_y = \sqrt{\frac{G_{adh}}{\eta} \frac{2}{E_y t_f}} \quad (7.36)$$

In particular, d_{plx} is the length of the overlap in x direction, and d_{ply} is the same but in y directions. If their value is higher than a and b, the dimensions of the cleat or the joint over the plate, then it is taken to evaluate the allowables. On the contrary, if it is lower, a and b are used, to be conservative. *immagine del giunto*

$$d_{plx} = \frac{2}{\lambda_x} \left(\sqrt{1 + 2 \frac{\gamma_p}{\gamma_e}} - 1 \right) \quad (7.37)$$

$$d_{ply} = \frac{2}{\lambda_y} \left(\sqrt{1 + 2 \frac{\gamma_p}{\gamma_e}} - 1 \right) \quad (7.38)$$

$$f_{bondx} = \tau_{adh} d_{plx} \quad (7.39)$$

$$f_{bondy} = \tau_{adh} d_{ply} \quad (7.40)$$

The quantities f_{bondx} and f_{bondy} are the adhesive ultimate allowable in x and y directions. Other quantities are used to find these values, such as the edge insert geometrical data a_{ins} , b_{ins} and h_{panel} , which describes the geometrical properties of the cleat; the adhesive properties involved are:

- τ_{adh} Adhesive shear strength
- G_{adh} Adhesive shear modulus
- γ_e Adhesive elastic strain
- γ_p Adhesive plastic strain

Other properties used to calculate load effects in different directions due to forces and moments are facing and honeycomb ones. Facing quantities are face thickness t_f , Elastic modulus in x and y directions E_x and E_y , in-plane shear modulus G_{xy} and Poisson ratio in both directions ν_{xy} and ν_{yx} . The Honeycomb characteristics are its height h_c , equal to panel's height minus twice the facing thickness, the elastic modulus of the core E_c and the Shear modulus G_c .

7.2.1 Applied Forces and Moments

$$F_z = [N], F_x = [N], F_y = [N], M_z = [Nm], M_x = [Nm], M_y = [Nm]$$

7.2.2 Load effect due to Fx Force

The F_x force loads upper and lower surfaces in x direction and it can induce:

- adhesive bonding failure
- face sheet strength failure x direction
- facing instability x direction

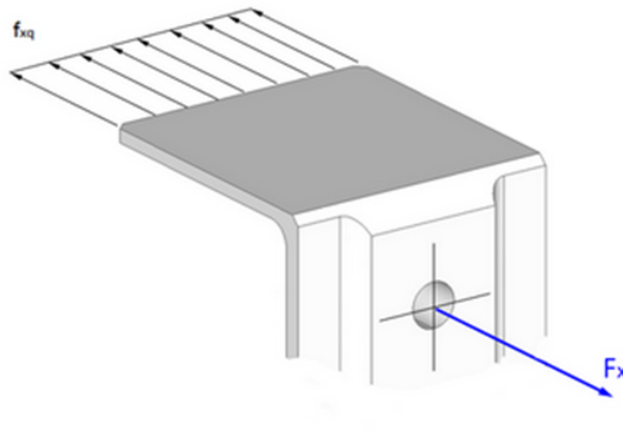


Figure 7.1: Load effect due to F_x force - *Courtesy of TAS-I*

$$f_{xq} = \frac{F_x}{2b_{ins}} \left[\frac{N}{mm} \right] \quad (7.41)$$

7.2.3 Load effect due to Fy Force - applied in the centroid

The F_y force loads the upper and lower surfaces in Y direction and it can induce:

- adhesive bonding failure
- face sheet strength failure y direction
- facing instability y direction

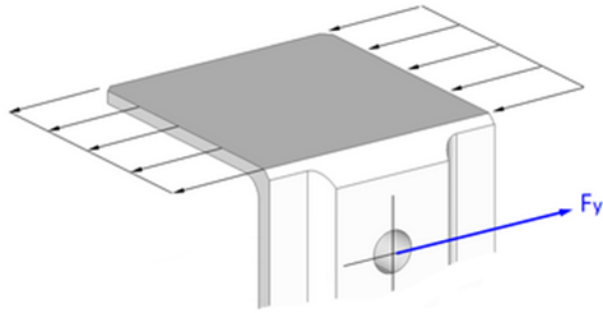


Figure 7.2: Load effect due to F_y force - *Courtesy of TAS-I*

$$f_{yr} = \frac{F_y}{2a_{ins}} \left[\frac{N}{mm} \right] \quad (7.42)$$

7.2.4 Load effect due to F_z Force - applied in the centroid

The F_z force loads the upper and lower surfaces in z direction and can induce:

- shear stress in the facing
- core shear failure in z direction
- flatwise bond failure (tension side only)

$$f_{zp} = \frac{F_z}{2a_{ins} + b_{ins}} \left[\frac{N}{mm} \right] \quad (7.43)$$

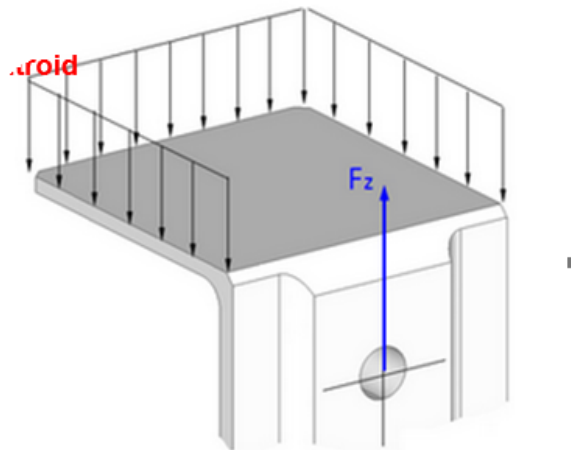


Figure 7.3: Load effect due to F_z force - *Courtesy of TAS-I*

7.2.5 Load effect due to M_y moment and F_z force arm

The M_y moment and F_z force arm effect load the upper and lower surfaces in x direction and it can induce:

- adhesive bonding failure
- face sheet strength failure x direction
- facing instability x direction

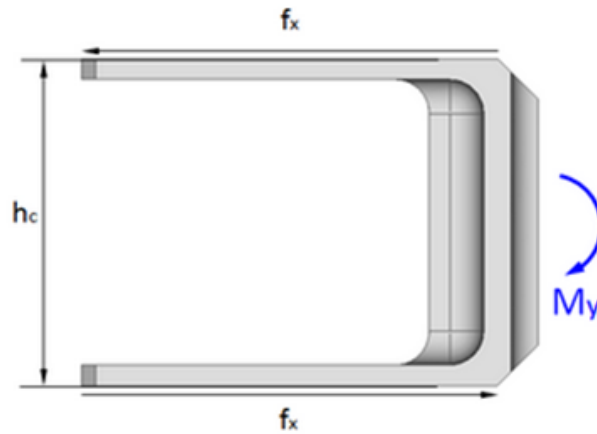


Figure 7.4: Load effect due to M_y moment and F_z force arm - *Courtesy of TAS-I*

$$f_{xn} = \frac{M_y + F_z \frac{a_{ins}}{2}}{h_c b_{ins}} \left[\frac{N}{mm} \right] \quad (7.44)$$

7.2.6 Load effect due to M_x Moment

The M_x moment loads the upper and lower surfaces in y direction and it can induce:

- adhesive bonding failure
- face sheet strength failure in y direction
- facing instability y direction

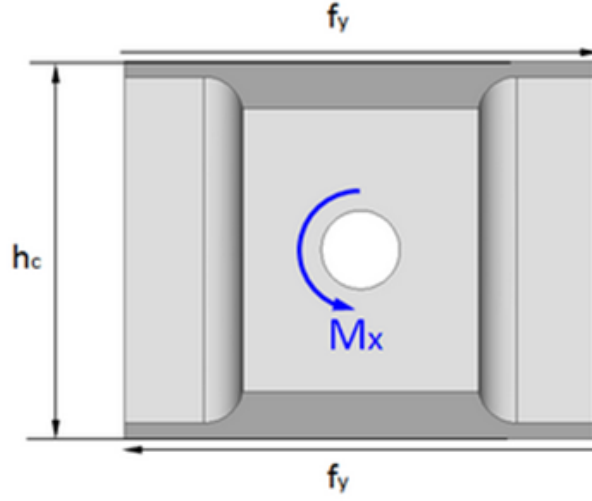


Figure 7.5: Load effect due to M_x moment - *Courtesy of TAS-I*

$$f_{ym} = \frac{M_x}{h_c a_{ins}} \left[\frac{N}{mm} \right] \quad (7.45)$$

7.2.7 Load effect due to M_z Moment and F_y arm effect

The M_z moment and F_y force arm effect load the upper and lower surfaces in x and y directions and it can induce:

- adhesive bonding failure
- sheet strength failure x and y directions
- facing instability x and y directions

$$f_{xt} = \frac{\left(M_z + F_y \cdot \frac{a_{ins}}{2} \right) \cdot \frac{b_{ins}}{2} \cdot \frac{b_{ins}^3}{12}}{2 \left(\frac{b_{ins}^3}{12} + \frac{a_{ins}^3}{6} \right)^2} \left[\frac{N}{mm} \right] \quad (7.46)$$

$$f_{yt} = \frac{\left(M_z + F_y \cdot \frac{a_{ins}}{2} \right) \cdot \frac{a_{ins}}{2} \cdot \frac{a_{ins}^3}{6}}{2 \left(\frac{b_{ins}^3}{12} + \frac{a_{ins}^3}{6} \right)^2} \left[\frac{N}{mm} \right] \quad (7.47)$$

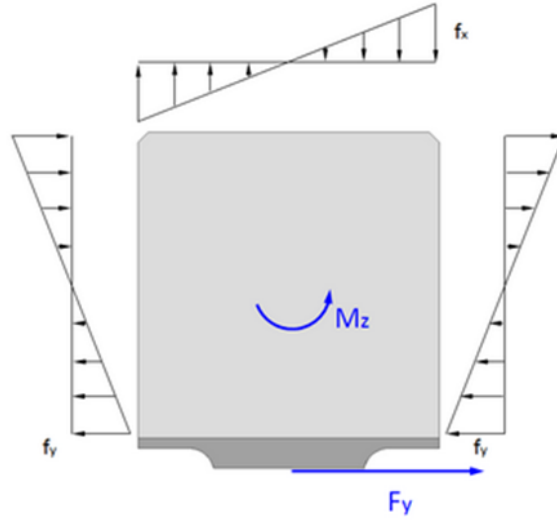


Figure 7.6: Load effect due to M_z moment and due to F_y arm effect - *Courtesy of TAS-I*

Once all the loads have been elaborated, the margin has to be calculated. The different components of the force are added up into f_{xsum} , f_{ysum} and f_{zsum} and then multiplied for the safety factor, but in design case this is equal to 1. The margin is calculated as

$$MoS = \xi - 1 \quad (7.48)$$

where ξ is

$$\xi = \sqrt{\frac{1}{R_1^\alpha} + \frac{1}{R_2^\beta}} \quad (7.49)$$

α and β are two empiric coefficients, whose value is between 1 and 2, while R_1 and R_2 depends on the forces found before and the characteristics of adhesive and joint geometry.

$$R_1 = \frac{f_x}{f_{xa}} \quad (7.50)$$

$$R_2 = \frac{f_y}{f_{ya}} \quad (7.51)$$

Chapter 8

Calculation of sandwich panels and failure modes

8.1 Calculation of Sandwich panels and insert

Once the sandwich structure is clearly identified, it is necessary to calculate those parameters fundamental to evaluate the margin of safety of the laminate, of the honeycomb and of eventual inserts applied.

8.1.1 Face sheet properties and Hoffmann theory

Materials used and their properties, and laminate construction for composite sheets determines the directional properties. When calculated in relation to the inserts, the strength of a sandwich face sheet does not influence the load carrying capability of the insert, while the bending stiffness has a focal role for the tensile and compressive loading of the insert. The bending stiffness B can be expressed by the equation

$$B = \frac{E_f f^3}{12(1 - \nu_f^2)} \quad (8.1)$$

where f is the thickness of the faces, E_f the Young modulus, ν_f the Poisson's coefficient of the materials of the face.

This equation was used for the simplest case of isotropic faces, but for anisotropic face sheets, the calculus of face sheet thickness is given by the formula employed for Aluminium face sheets.

$$f_{Al} = f_{an} \sqrt[4]{\frac{\sqrt{E_x \times E_y}(1 - \nu_{Al}^2)}{E_{Al}(1 - \nu_x \times \nu_y)}} \quad (8.2)$$

The Hoffmann theory is used in this case to calculate the margin of safety of the laminate which the faces are composed of, to evaluate it and states if it breaks under the applied loads; this theory is used for composite face sheets, and take into account the different tensile and compressive allowables in the fiber direction and in the perpendicular one, besides the in-plane shear allowable. To be able to build the margin, some quantities have to be explained

- T_x is the traction allowable along x direction, also intended ad the 0° direction, or the fiber direction.
- T_y is the tensile allowable along the y direction, which means the direction perpendicular to the fiber one, 90° . This is usually really lower than the T_x , because it is essentially the resistance the resin could give to the ply.
- C_x is the allowable to compression along x axis, it it generally lower than the traction one, because fibers better work at under tensile loads
- C_y is the compression allowable in y direction, always perpendicular to the fiber.
- S_{xy}, S_{xz}, S_{yz} are the in-plane shear allowables and they are generally very small values, but still not negligible.

The complete formula of the Failure Index from the Hoffmann theory is

$$FI = \frac{\sigma_1^2}{T_x C_x} + \frac{\sigma_2^2}{T_y C_y} + \frac{\tau_{12}^2}{S^2} + \frac{C_x - T_x}{T_x C_x} \sigma_1 + \frac{C_y - T_y}{T_y C_y} \sigma_2 - \frac{\sigma_1 \sigma_2}{T_x C_x} < 1 \quad (8.3)$$

where for the term S it is used the minimum of the three in-plane shear allowables. In this document, due to a percentage error less than 1%, a simplified version of the equation is used, whose terms are reported below

- $F_1 = \frac{1}{T_x} - \frac{1}{C_x}$
- $F_2 = \frac{1}{T_y} - \frac{1}{C_y}$
- $F_{11} = \frac{1}{T_x \bullet C_x}$
- $F_{22} = \frac{1}{T_y \bullet C_y}$
- $F_{12} = \frac{-0.5}{T_x \bullet C_x}$
- $F_{66} = \frac{1}{S_{xy}^2}$

The simplified FI is given by

$$FI = F_1\sigma_x + F_2\sigma_y + F_{11}\sigma_x^2 + F_{22}\sigma_y^2 + 2F_{12}\sigma_x\sigma_y + F_{66}\tau_{xy}^2 < 1 \quad (8.4)$$

According to theory, if the FI is minor than 1, the laminate crushes, but the margin of safety could be positive, which means that the laminate does not break; it is acceptable if the FI is around the unity, between 1 and 4, but for higher values of the failure index, the MoS became negative and the zone is compromised. To calculate the Margin of Safety for the laminate, two terms group the different factors, a and b

$$a = F_{11}\sigma_x^2 + F_{22}\sigma_y^2 + 2F_{12}\sigma_x\sigma_y + F_{66}\tau_{xy}^2 \quad (8.5)$$

$$b = F_1\sigma_x + F_2\sigma_y \quad (8.6)$$

that combined give the term SR, of which only the positive solution is taken

$$SR = \frac{-b + \sqrt{b^2 + 4a}}{2a} \quad (8.7)$$

The margin is finally given by

$$MoS = SR - 1 \quad (8.8)$$

The margin, to guarantee the integrity of the lamina, must be positive.

8.1.2 Honeycomb Margin of Safety

As done for the laminate, the honeycomb has to be investigated too, to understand if it can withstand the loads. The quantities taken into account to evaluate this index are the in-plane shear stresses, in particular in planes XZ and YZ. The shear stress present in XZ plane has to be compared to the τ allowable in W direction, while the stress in plane YZ is compared to the τ allowable in L direction; RF is the middle value used for the calculus of the margin MoS, that again has to be positive in order to consider the honeycomb intact.

$$MoS = RF - 1 \quad (8.9)$$

$$RF = \frac{1}{\sqrt{\left(\frac{\tau_W}{\tau_{Wallow}}\right)^2 + \left(\frac{\tau_L}{\tau_{Lallow}}\right)^2}} \quad (8.10)$$

8.2 Failure modes - General and panel instability

A sandwich panel could collapse in different ways due to the composition of the structure, which involves skins, core and adhesive and their respective allowable. Different failure modes can be divided in general and local instability: the first ones involve the whole sandwich structure, the second ones are specifically referred to the way core, skins and adhesive interact with each others and the resulting defects. At the beginning, general instability and panel instability will be described.

- *General instability*: this kind of instability is referred to sandwich structures with no stiffeners except at the boundaries. It is meant as general because a total distortion of the structure is recognised: the bending of the composite skins is coupled with transverse shear deformation and as a result it is possible to identify large waves along the entire panel surface, as shown in figure 8.1



Figure 8.1: General panel instability [12]

- *Panel instability*: unlike the other case, panel instability happens when localized stiffeners are applied at locations that differ from the boundaries. However, this mode involves again the over-all bending of the composite coupled with transverse shear deformation, so the result is similar to general instability ones. To better explain the difference between the two failure mode, a sandwich cylinder is taken into account: if the stiffeners are located close to nodal points, they are capable to enforce the these points to stay in positions, which does not happen during general instability, because there is nothing holding the nodal points in place. The figure 8.2 below better explains the distinction between the two instabilities.

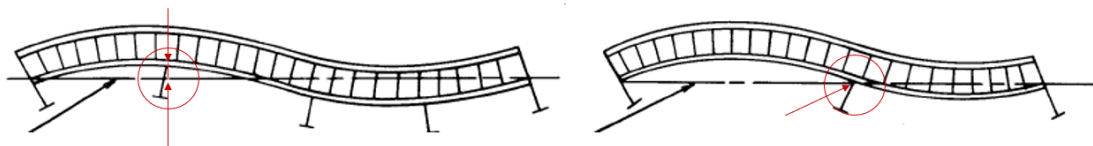


Figure 8.2: Comparison between general and panel instability [12]

8.2.1 Failure modes - Local instability

For local instabilities are meant all those phenomena involving concentrated areas of the panel or in particular load configurations. It is presented a general description of local failure modes, while analytical calculations and results will be presented in the following chapters.

- *Intracellular buckling - Face dimpling*: this type of local instability occurs when the core structure results not continuous, which means that the skins immediately above the cell start collapsing down inside these last ones, creating the visible effect of a dimple. This instability does not deform the walls of the cell, but involves only the slipping of the above surfaces within the cells.

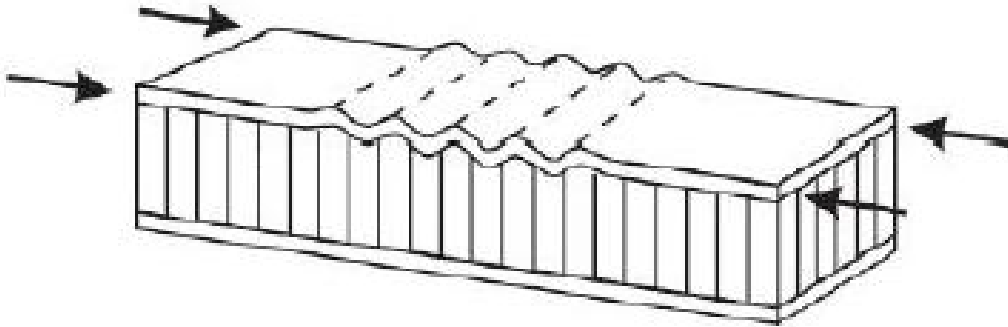


Figure 8.3: Face dimpling, or Intracellular buckling [13]

To evaluate this kind of failure, the critical compressive stress can be calculated as

$$\sigma_{cr} = \frac{k\pi^2\eta E_f}{12(1-\nu_e^2)} \left(\frac{t_f}{s}\right)^2 \quad (8.11)$$

where k is a coefficient depending on the geometry of the plate, its boundary conditions and type of loads it withstands, η is the plasticity reduction factor, t_f is the thickness of the faces and s a selected characteristic dimension of the plate; E_f and ν_e are the Elastic modulus and Elastic Poisson's ratio of the facings.

- *Face wrinkling*: this failure mode involves generally a larger area of the panel, not singular cells; in particular, it is recognizable by short waves running on the surfaces of the skins and the straining of the core material in

direction normal to the skins. A further distinction can be identified, in fact the buckling can appear symmetrical or antisymmetrical with the original middle axis of the sandwich. As a result to this failure mode, three types of break could happen: core crushing, tensile rupture of core proper and tensile rupture of the bond. The figure 8.4 shows each of these behaviours, in particular for the core crushing an insufficient strength of the core is noticed, which causes the yielding of the entire panel structure; in the case of tensile rupture of the bond, the main character is the adhesive, that is not capable of performing its function: this type of rupture, however, can be avoided if adhesive is chosen with attention, so that its strength results higher than the core properties. In other words, it is more probable to have a break due to core inadequate strength rather than a rupture caused by bond failure. At last, the tensile rupture of the core happens when the tensile strength of the material of the core is not able to carry the load to which it is subjected, and as secondary result there is a partial removal of the skins from nominal distance.

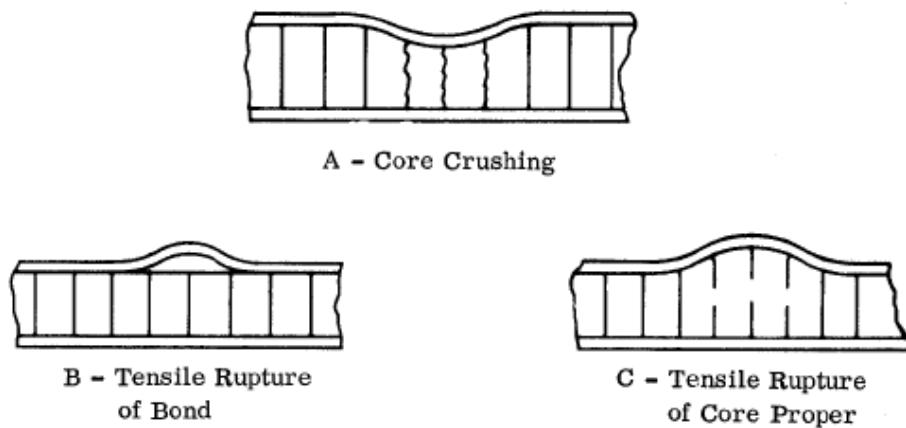


Figure 8.4: Different failure mode for face wrinkling [12]

Face wrinkling stress is obtained from the equation

$$\sigma_{wr} = Q \left[\frac{\eta E_f E_c G_c}{(1 - \eta_e^2)} \right]^{\frac{1}{3}} \quad (8.12)$$

where

- η is the plasticity reduction factor
- E_f is the Young's modulus of facing

- E_c is the Young's modulus of core in the direction normal to facings
- G_c is the core shear modulus
- ν_e is the elastic Poisson's ratio of facings.

At the beginning of the expression, Q is noticed, which is the relative minimum of the equation

$$\frac{\frac{\zeta^2}{30q^2} + \frac{16q}{\zeta} \left(\frac{\cosh\zeta - 1}{11\sinh\zeta + 5} \right)}{1 + 6,4K_\delta\zeta \left(\frac{\cosh\zeta - 1}{11\sinh\zeta + 5} \right)} \quad (8.13)$$

with

$$q = \frac{t_c}{t_f} G_c \left[\frac{(1 - \nu_e^2)}{\eta E_f E_c G_c} \right]^{\frac{1}{3}} \quad (8.14)$$

and

$$K_\delta = \frac{\delta E_c}{t_c F_c} \quad (8.15)$$

The terms appeared in these equations are ζ , a parameter involving the core elastic moduli and the buckling wavelength, t_c the core thickness, t_f the face thickness, δ the amplitude of the initial waviness in facing and F_c the flatwise sandwich strength

- *Shear crimping*: even though it is common recognized as a local failure, shear is non other than a general buckling whose wavelength is so short to be considered as a localized collapse. Shear crimping causes core failure in terms of shear, but it could also affects the bonding between core and faces.

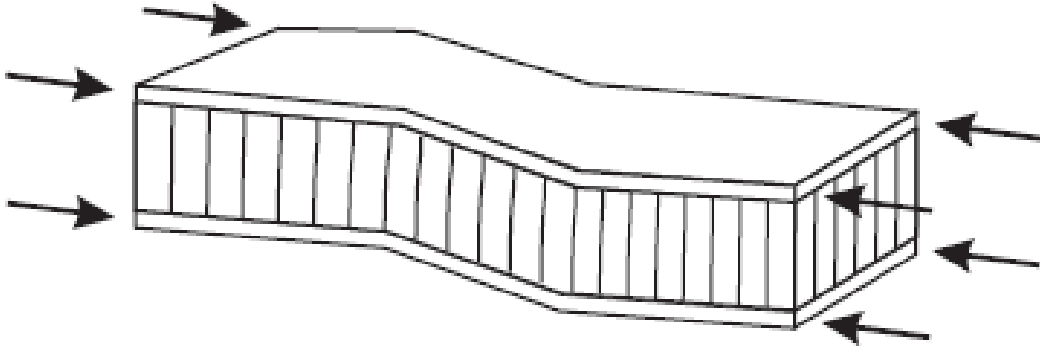


Figure 8.5: Shear : detail [5]

Shear crimping will occur in axially compressed cylindrical sandwiches when $V_c \geq 2$, where

$$V_c = \frac{\sigma_o}{\sigma_{crimp}} \quad (8.16)$$

and the two stresses are

$$\sigma_o = \eta E_f \frac{h}{R} \frac{2\sqrt{t_1 t_2}}{\sqrt{1 - \nu_e^2 (t_1 + t_2)}} \quad (8.17)$$

$$\sigma_{crimp} = \frac{h^2}{(t_1 + t_2)t_c} G_{xz} \quad (8.18)$$

The quantities present in the equation of σ_o are:

- η plasticity reduction factor
- E_f Young's modulus of facings
- h distance between middle surfaces of facings
- R radius to middle surface of cylindrical sandwich panel
- t_1 and t_2 thicknesses of faces
- ν_e Elastic Poisson's ratio of facings
- t_c height of core
- G_{xz} Core shear modulus

Chapter 9

Results and data analysis - FEM correlation

Once the tests have been done, it is time to correlate the results with the FEM models and prediction previously made. In a first moment, the FEM model is done starting from the CATIA CAD, and it is given to the solver, in this case MSC Nastran, to calculate stress and deformation through the component; this is an early step to evaluate which areas are the most stressed and the most subjected to wide deformation.

In this chapter tests results will be compared to FEM ones, where the modeled coupons have been loaded with the effective ultimate loads to which the real coupons crushed: this step is really important to verify the quality of the model. In fact, if the FEM results do not match with the effective test, a review of the model is requested, or at least a few considerations will be needed to justify possible differences.

9.1 Coupon 1

For the first coupon, as for the following ones, it has to be investigated the rupture and it is necessary to understand which components led to that particular failure. As shown before, the first coupon is subjected to lateral and axial loads, so that it will see compression and lateral bending. As the figure 9.1 demonstrates, the failure happened in the bracket area, leaving the inserts intact.

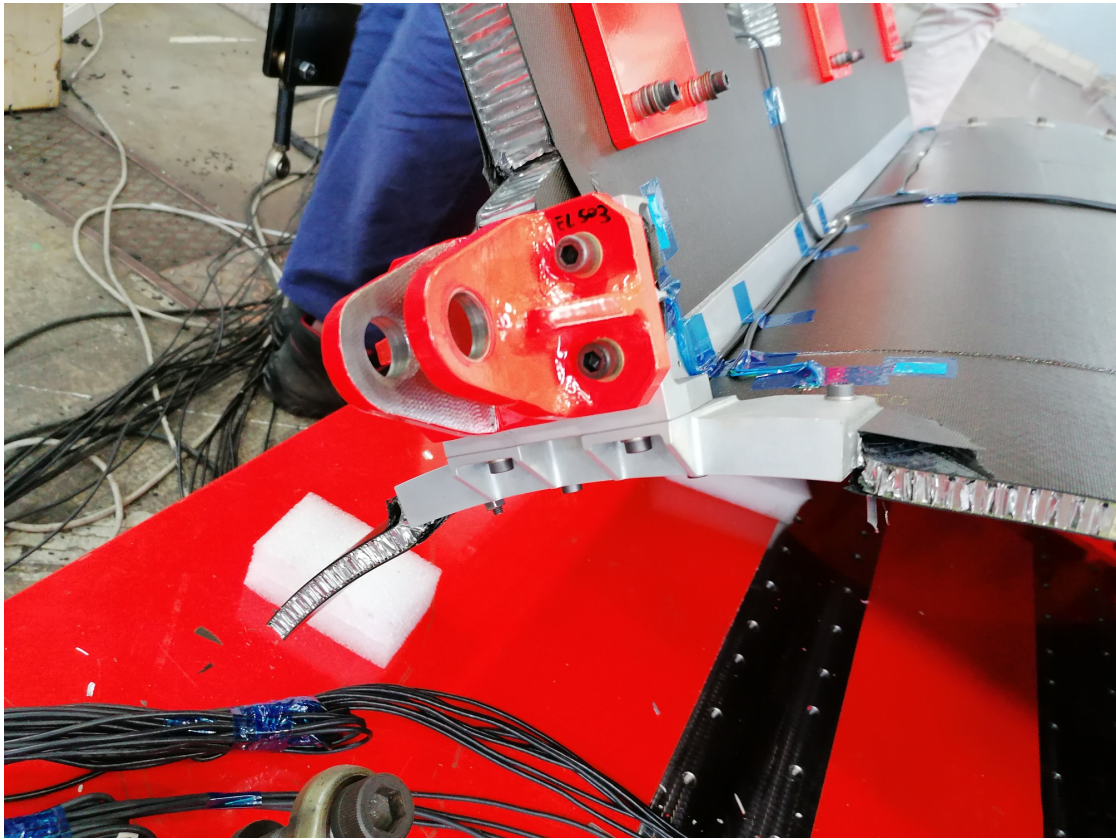


Figure 9.1: Coupon 1 - Rupture detail around brackets area - *Courtesy of TAS-TO*

This on the one hand certifies the resistance of the inserts and the junction, on the other it is asking to verify that the model is effectively stressed in the upper areas of the coupon. To do so, it is requested to analytically calculate the margin of security of the laminate, of the honeycomb and of the inserts.

For the laminate, the Hoffman Theory has been applied to identify the failure index FI ; this value, however, only indicates if the laminate breaks or withstands the load intact, but does not give a concrete measure of "how much" the skins could still bear. In other words, if the failure index has a value less than one, the conditions of allowable are accepted, but they are not, it does not mean that the margin is necessarily negative: when the FI is around the unity, in fact, the margin could be positive, which indicates that the laminate, in the analysed position is unbroken.

Furthermore, it is important to specify that the Hoffmann criteria is not a progressive failure one, so it does not give a detailed indication of the ply rupture, but it just indicates when the overall laminate comes to rupture.

At first, it is checked the inserts margin of security, to verify that the model

is in accordance with the coupon failure. To better understand the numbering of the inserts and to make them easier to identify, the figure 9.2 gives a quick view of their position in the model (1 to 10 for the Y shear web and 11 to 20 for the X one)

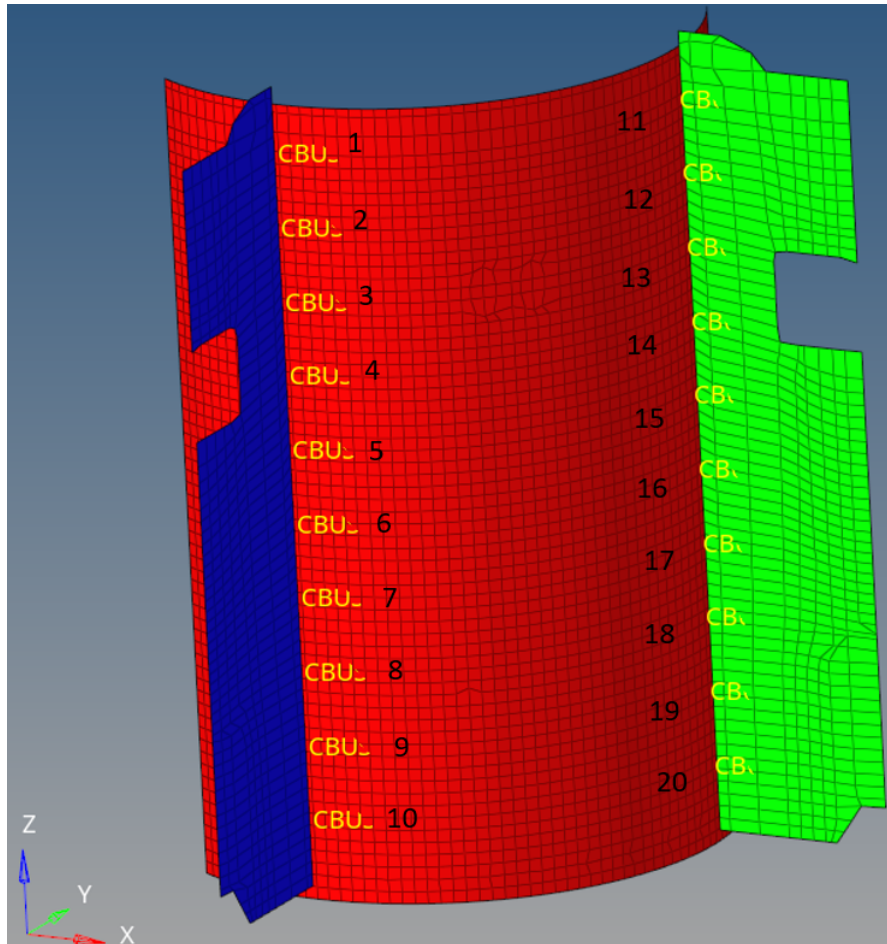


Figure 9.2: Numbering of inserts

The test highlights that there is no rupture of the inserts, but only of the lamina around the brackets area: the table 9.1 confirms this entirety of the inserts, except for the first one on the Y shear web. This failure, however, is ascribable to the mesh size, in fact the interested element is next to the bracket area but to the first insert too, so the transmission of the stresses is not perfectly distributed: a more detailed division of the area, with element whose surface is smaller, could better represent the behavior of the zone, leading probably to a positive margin of safety for the first insert.

		COUPON 1 -AXIAL+LATERAL- SUBCASE 6				
		ELEMENT ID	FORCE X	RIS YZ	RIS MOMENT YZ	Mos
		-	[N]	[N]	[Nm]	-
Inserti Y	1	70400321	-1.24E+03	4.31E+03	7.24E+01	-0.13
	2	70400322	-1.27E+03	3.22E+03	5.74E+01	0.09
	3	70400323	-1.20E+03	2.91E+03	4.62E+01	0.13
	4	70400324	-1.10E+03	2.95E+03	3.33E+01	0.31
	5	70400325	-1.09E+03	2.44E+03	1.98E+01	0.62
	6	70400326	-1.07E+03	1.62E+03	8.27E+00	0.94
	7	70400327	-1.02E+03	1.05E+03	2.97E+01	0.57
	8	70400328	-8.49E+02	1.14E+03	5.86E+01	0.05
	9	70400329	-2.93E+02	2.49E+03	9.05E+01	-0.28
	10	70400330	1.57E+03	6.13E+03	1.35E+02	-0.53
Inserti X	11	70400341	-1.17E+03	4.36E+03	6.53E+01	0.03
	12	70400342	-1.22E+03	3.24E+03	5.05E+01	0.30
	13	70400343	-1.17E+03	2.94E+03	4.13E+01	0.60
	14	70400344	-1.08E+03	2.97E+03	2.99E+01	1.20
	15	70400345	-1.07E+03	2.42E+03	1.72E+01	2.75
	16	70400346	-1.07E+03	1.59E+03	9.46E+00	11.37
	17	70400347	-1.03E+03	1.01E+03	3.05E+01	1.48
	18	70400348	-8.71E+02	1.13E+03	5.73E+01	0.26
	19	70400349	-3.02E+02	2.55E+03	8.52E+01	-0.17
	20	70400350	1.57E+03	6.31E+03	1.24E+02	-0.46

Table 9.1: Insert margin of safety of coupon 1

Although there was not rupture around inserts area during the test, as confirmation for lamina and honeycomb, the margin of safety of both of them is shown in the following tables: the first take into account the location of inserts which connect the central cylinder with the shear web build along the Y direction, the second are for the location of inserts that connect the cylinder with the shear web along the X axis.

COUPON 1 - INSERTS OF Y SHEAR WEB				
INSERT	sigma_x	sigma_y	FI	MoS
1	-222.2	33.8	1.413	0.08
2	-189.2	57.5	2.700	0.50
3	-253.7	67.5	3.434	0.44
4	-240.6	52.8	2.457	1.55
5	-216.3	40.6	1.741	1.95
6	-196.2	28.2	1.130	2.17
7	-193.7	48.9	2.163	1.95
8	-238.4	73.7	3.864	0.24
9	-389.6	99.4	6.238	-0.51
10	-688.9	111.5	7.966	-0.76

Table 9.2: Margin of safety of the lamina around inserts location of Y shear web

COUPON 1 - AXIAL + LATERAL				
		shear_xz	shear_yz	MoS
SHEAR WEB Y LOCATION	1	9.18E+05	1.40E+06	0.34
		1.19E+06	1.44E+06	0.19
	2	7.24E+05	1.51E+06	0.36
		1.04E+06	1.44E+06	0.26
	3	6.48E+05	1.37E+06	0.50
		9.53E+05	1.28E+06	0.40
	4	5.66E+05	1.15E+06	0.77
		8.44E+05	1.05E+06	0.65
	5	4.89E+05	9.54E+05	1.12
		7.32E+05	8.62E+05	0.96
6	5.70E+05	4.18E+05	2.05	
	5.70E+05	6.94E+05	1.47	
7	7.43E+05	6.73E+05	1.18	
	4.41E+05	7.37E+05	1.63	
8	8.91E+05	9.28E+05	0.71	
	5.45E+05	9.87E+05	1.01	
9	9.36E+05	1.10E+06	0.54	
	5.81E+05	9.22E+05	1.06	
10	1.62E+06	2.17E+06	-0.18	
	2.11E+06	2.43E+06	-0.31	

Table 9.3: Margin of safety of the honeycomb around inserts location of Y shear web

COUPON 1 - INSERTS OF X SHEAR WEB				
INSERT	sigma_x	sigma_y	FI	MoS
11	-213.4	38.0	1.605	0.10
12	-193.6	51.5	2.314	0.19
13	-181.5	52.6	2.364	0.36
14	-227.3	55.0	2.572	0.75
15	-198.4	41.3	1.754	2.08
16	-172.3	24.2	0.936	2.57
17	-170.2	48.8	2.131	2.20
18	-202.4	67.3	3.355	0.24
19	-432.2	109.1	7.251	-0.61
20	-745.6	138.8	11.130	-0.80

Table 9.4: Margin of safety of the lamina around inserts location of X shear web

COUPON 1 - AXIAL + LATERAL				
		shear_xz	shear_yz	MoS
SHEAR WEB X LOCATION	11	1.13E+06	1.34E+06	0.26
		1.00E+06	1.41E+06	0.30
	12	9.51E+05	1.55E+06	0.24
		7.92E+05	1.47E+06	0.36
	13	8.82E+05	1.42E+06	0.34
		7.58E+05	1.33E+06	0.48
	14	7.86E+05	1.21E+06	0.56
		7.18E+05	1.11E+06	0.70
	15	6.86E+05	1.01E+06	0.83
		7.01E+05	9.17E+05	0.93
	16	6.50E+05	7.46E+05	1.23
		6.83E+05	6.54E+05	1.32
	17	7.20E+05	7.84E+05	1.07
		6.26E+05	8.62E+05	1.10
	18	5.90E+05	1.07E+06	0.86
		8.39E+05	1.14E+06	0.58
	19	7.83E+05	1.22E+06	0.55
		5.97E+05	1.18E+06	0.72
	20	1.96E+06	2.29E+06	-0.26
		1.65E+06	2.62E+06	-0.27

Table 9.5: Margin of safety of the honeycomb around inserts location of X shear web

In particular, tables 9.2 and 9.3 present the MoS of the laminate and of the honeycomb for the Y shear web, while table 9.4 and 9.5 show the margin of safety calculated for the X shear web. It is possible to notice that around inserts 9 and 10, and 19 and 20 the laminate comes to rupture according to the model, while only around the lower inserts, 10 and 20, the honeycomb breaks: this is not a truthful

reproduction of the test, it is probably an issue connected to the constraints of the lower part of the coupon, which is not able to deform enough under the loads and it brings the piece to brake in those areas. In this case, it is possible to modify the position of the constraints, for example lowering them by a row of CQUAD element, or to change the method of reading of the results, from the centroid to the four nodes of the element: this is a smart solution because it permits to overcome eventual numerical errors which generates higher stresses than the actual ones.

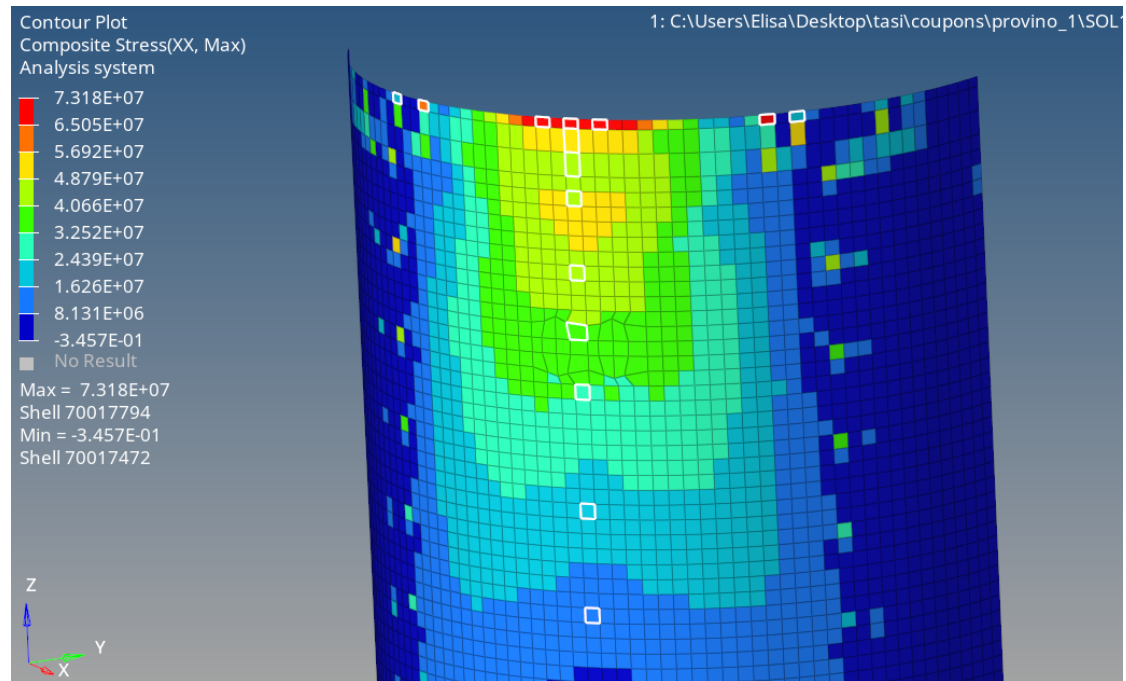


Figure 9.3: FEM detail of the failure zone in accordance to the test

Now that it is verified that there is no failure of the inserts and it is congruent with the results of the test, it is time to investigate the rupture zone around the brackets, to understand if it happened due to the overcoming of the allowable of the laminate, of the honeycomb or both of them. The FEM in particular identifies a concentration of stress in the upper part of the cylinder, between the two brackets.

The margin of safety, as shown in the following figures 9.6 e 9.7, demonstrate that the coupon breaks due to the structural failure of the skin around the entire analyzed area, while the honeycomb fails only for two of the considered elements, therefore it is not the main cause of the rupture. Anyhow, the localized failure of the honeycomb contributes to the failure of the entire zone

COUPON 1 - FAILURE ZONE				
FAILURE ZONE AND CENTRAL	ID	shear_xz	shear_yz	MoS
	70017900	1.35E+06	3.26E+05	0.51
	70017937	1.36E+06	2.38E+06	-0.17
	70018014	7.90E+05	7.48E+03	1.63
	70017803	8.02E+05	2.96E+05	1.46
	70017997	4.87E+05	1.23E+04	3.27
	70018069	4.97E+05	4.42E+04	3.17
	70017727	2.50E+05	5.53E+04	7.15
	70017747	2.59E+05	1.70E+04	7.03
	70017792	4.37E+05	5.51E+04	3.73
	70017794	1.52E+05	9.77E+03	12.68
	70018465	1.42E+05	1.67E+05	9.10
	70019027	4.33E+05	8.96E+03	3.81
	70019028	5.50E+05	3.58E+04	2.78
	70018324	3.88E+05	2.44E+06	-0.06
70018360	6.17E+05	3.48E+05	2.01	

Table 9.6: Honeycomb MoS for elements around the rupture zone

COUPON 1 - FAILURE ZONE				
ELM ID	sigma_x	sigma_y	Fl	MoS
70017900	-210.430	70.994	0.418	-0.60
70017937	-176.440	130.900	9.223	-0.33
70017803	-355.190	244.860	9.738	-0.88
70017794	-372.570	255.090	9.945	-0.89
70018465	-362.230	249.700	9.960	-0.88
70018324	-210.540	155.540	12.323	-0.45
70018360	-199.980	75.394	0.379	-0.62
70019027	-315.810	209.550	14.045	-0.86
70019028	-307.780	194.150	18.119	-0.83
70017792	-255.970	204.270	19.684	-0.79
70017727	-271.150	177.430	15.456	-0.78
70017747	-276.870	151.250	11.827	-0.76
70018069	-257.730	133.430	9.608	-0.74
70017997	-217.030	107.437	6.758	-0.64
70018014	-174.460	86.537	4.801	-0.49

Table 9.7: Laminate MoS for elements around the rupture zone

9.2 Coupon 2

For coupon 2, three different types of test have been carried out: *pullout*, *axial traction* and *bending*. For each of them, the same considerations of Coupon 1 were made and the results are shown below.

9.2.1 Coupon 2 - Pullout test

The pullout test highlights that, although it was done trying to distribute the 33175 N load equally on all inserts, a certain moment has established, causing the type of rupture shown in figure 9.4



Figure 9.4: Photo of the coupon 2 after pullout test - *Courtesy of TAS-TO*

To have a coherent view, insert number 1 is the first starting from the top and insert 10 the last one at the bottom, for the pullout test, as illustrated in the next figure 9.5

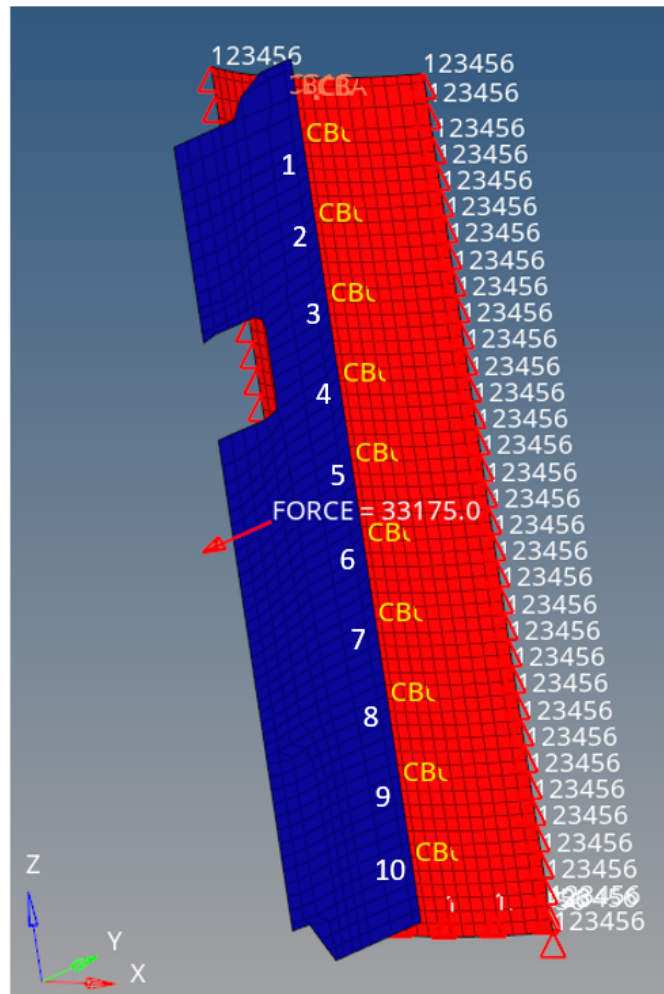


Figure 9.5: Position of the inserts for pullout test

From the test, it is possible to see that the failure interests the insert zone, while the panel itself seems to be intact; however, from the image and in general from the broken coupon, it can not be told which component comes first to brake, so it is necessary to study every margin of safety to understand it. Starting from the skin, the Hoffmann theory has been applied, and the results of the analysis shows that it does not occur failure throughout the laminate, as next table demonstrates [9.8](#)

COUPON 2 - PULLOUT - INSERTS				
INSERTS	sigma_x	sigma_y	FI	MoS
1	-164.45	34.353	1.361	0.02
	-116.16	42.262	1.702	0.25
2	-91.025	40.997	1.611	0.34
	-77.462	115.17	7.374	1.79
3	-72.358	38.082	1.445	0.43
	-72.402	39.6	1.521	0.49
4	-66.957	37.928	1.431	0.46
	-69.641	37.895	1.432	0.52
5	-67.826	36.399	1.358	0.49
	-70.29	37.642	1.421	0.56
6	-60.786	35.046	1.286	0.56
	-65.197	35.101	1.293	0.64
7	-59.884	32.362	1.161	0.65
	-61.842	33.605	1.220	0.72
8	-57.629	32.219	1.151	0.71
	-58.124	32.428	1.161	0.76
9	-58.08	32.142	1.149	0.74
	-62.37	32.967	1.191	0.83
10	-131.01	30.976	1.170	0.31
	-92.576	32.483	1.199	0.68

Table 9.8: Positive MoS highlights that the laminate stays unbroken

Honeycomb is another component to analyze, in particular around the zone of the inserts, in fact it could happen to witness the breakup of the inserts due to the honeycomb failure: once the honeycomb is compromised, the potting is no more efficient and the insert can not stay in place. This is what happened for the analyzed pullout test, the honeycomb in the area of the insert has a general low margin of safety, really close to zero. The zones around first and second insert show a negative margin, which means that a rupture occurs (table 9.9); as a consequence, the load is redistributed in the remaining 8 inserts. The honeycomb around the third insert sees now an increase of load, which will lead to failure. This is not explicitly demonstrate, but a multi - step analysis would confirm this statement.

COUPON 2 - PULLOUT - CASE 1 ULTIMATE				
		shear_xz	shear_yz	MoS
INSERT LOCATION	1	1.56E+06	2.13E+06	-0.15
		1.57E+06	2.07E+06	-0.14
	2	1.22E+06	1.92E+06	-0.01
		1.22E+06	1.91E+06	-0.01
	3	1.18E+06	1.85E+06	0.03
		1.18E+06	1.84E+06	0.03
	4	1.17E+06	1.81E+06	0.04
		1.17E+06	1.81E+06	0.04
	5	1.13E+06	1.77E+06	0.07
		1.13E+06	1.76E+06	0.07
	6	1.07E+06	1.68E+06	0.13
		1.07E+06	1.67E+06	0.13
	7	1.01E+06	1.58E+06	0.20
		1.01E+06	1.58E+06	0.20
	8	9.87E+05	1.54E+06	0.23
		9.90E+05	1.54E+06	0.23
	9	9.82E+05	1.51E+06	0.25
		9.85E+05	1.51E+06	0.24
	10	1.42E+06	1.69E+06	0.00
		1.43E+06	1.73E+06	-0.01

Table 9.9: Collapsing of the first and second inserts leads to the rupture of the following

COUPON 2 - PULLOUT - CASE 1 ULTIMATE				
	ELEMENT ID	FORCE X	RIS FORCE YZ	Mos
	-	[N]	[N]	-
1	70400321	-4.07E+03	1.12E+03	0.02
2	70400322	-3.61E+03	6.93E+02	0.16
3	70400323	-3.46E+03	8.66E+00	0.21
4	70400324	-3.41E+03	4.98E+02	0.23
5	70400325	-3.33E+03	1.73E+02	0.26
6	70400326	-3.15E+03	1.26E+02	0.33
7	70400327	-2.96E+03	1.67E+02	0.41
8	70400328	-2.89E+03	5.79E+02	0.44
9	70400329	-2.86E+03	4.99E+02	0.46
10	70400330	-3.43E+03	3.51E+01	0.22

Table 9.10: Margin of safety, which demonstrates the integrity of the inserts, despite the failure occurred in that area

In this situation, the margin of safety calculated for the inserts would not be enough to guarantee the correct prevision of failure, in fact as the figure 9.10 shows,

every inserts has positive margin, so they do not directly break, their collapse is due to the honeycomb one.

9.2.2 Coupon 2 - Axial Traction test

In this coupon, unlike the pullout one, the first insert is considered to be the one situated in the lower part of the cylindrical panel, while the last one, number ten, is at the top of the structure; this numbering is adopted to reflect the actual breaking order predicted for the inserts, as shown in figure 9.6

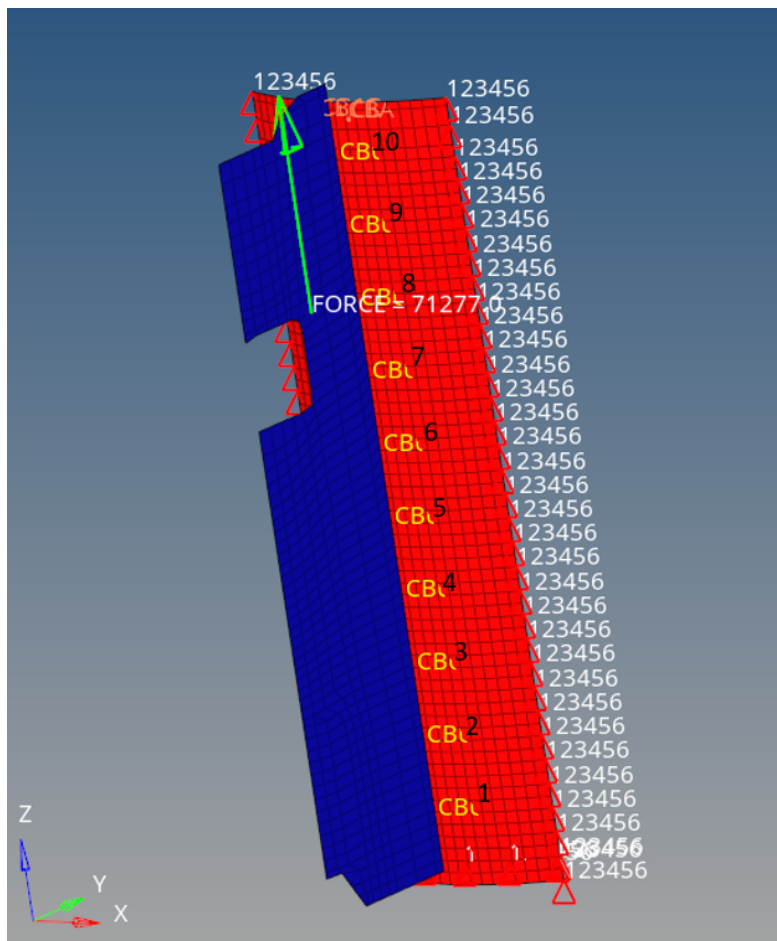


Figure 9.6: Numbering of the inserts for axial traction test

The ultimate load for this coupon is 71277 N, result achieved from the test. The figure 9.7 shows that nine inserts out of the breaks under the ultimate load, and the last one probably too, even though it is not totally visible: the processing of the part will investigate this possibility.



Figure 9.7: Axial traction coupon immediately after the test - *Courtesy of TAS-TO*

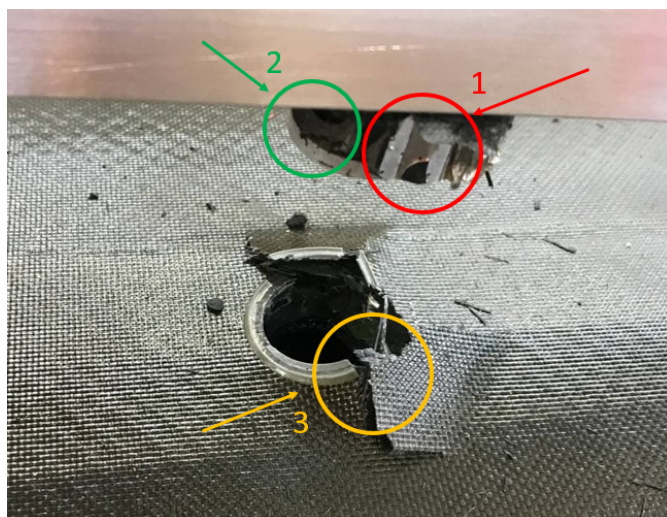


Figure 9.8: Detail of the failure zone - *Courtesy of TAS-TO*

A vision of detail is provided to better analyze the failure zone and which components have been involved during the rupture, considering that no bending or momentum was involved during the test (9.8): in the first area, a piece of honeycomb can be seen out of the panel, attached to the insert; in the second zone, a black structure is identified around the insert and it is the potting, out of its location, but still connected to the aluminium insert. Finally the laminate is broken and different plies are lifted.

As for the previous test, inserts, honeycomb and laminate margin of safety are calculated to understand which components contribute to the break.

COUPON 2 - AXIAL TRACTION - INSERTS				
INSERTS	sigma x	sigma y	FI	MoS
1	-135.3	123.2	8.287	0.74
	-141.35	125.29	8.515	0.83
2	-107.129	82.819	4.415	0.89
	-108.713	84.018	4.515	1.02
3	-105.501	53.559	2.337	1.51
	-106.7	54.318	2.385	1.65
4	-103.356	31.691	1.176	2.50
	-101.453	32.131	1.195	2.69
5	-109.362	9.3577	0.348	3.93
	-110	9.46	0.351	3.97
6	-196.13	19.547	0.213	0.23
	-200.42	19.855	0.216	0.20
7	-277.09	47.619	0.378	-0.44
	-284.46	48.334	0.369	-0.45
8	-330	70.158	0.499	-0.61
	-339.57	71.159	0.488	-0.62
9	-391.49	96.987	0.619	-0.72
	-403.37	98.285	0.608	-0.72
10	-466.29	127.82	1.329	-0.78
	-484.77	129.91	1.298	-0.79

Table 9.11: Margin of safety for laminate around insert area

The table 9.11 exposes a positive margin for the skins in the insert area, from 1 to 6 and than a negative ones, so it seems that the failure does not start from here, but once it happens, the rupture is propagated along the structure from the seventh insert onward. The honeycomb around the first insert is the first to yield, and the corresponding margin is negative; from the second on, the margin is positive, but it is again close to zero, so that it can easily turn negative once the honeycomb in the location 1 is compromised, and the load is distributed between the still intact components. The insert number ten shows a negative margin, since the constraints are probably too conservatives and they do not reflect the effective behavior of the coupon.

COUPON 2 - AXIAL - CASE 2 ULTIMATE				
		shear_xz	shear_yz	MoS
INSERT LOCATION	1	2.46E+06	2.80E+06	-0.41
		2.45E+06	9.61E+05	-0.20
	2	1.08E+06	1.53E+06	0.20
		1.07E+06	4.41E+05	0.83
	3	7.46E+05	1.01E+06	0.78
		7.39E+05	2.96E+05	1.65
	4	5.00E+05	6.24E+05	1.78
		4.94E+05	1.87E+05	2.99
	5	2.62E+05	2.39E+05	5.16
		2.55E+05	7.81E+04	6.87
6	3.35E+05	4.30E+04	5.18	
	3.27E+05	2.68E+05	4.13	
7	8.70E+05	7.51E+05	0.89	
	8.64E+05	7.72E+05	0.88	
8	6.50E+05	1.18E+06	0.68	
	6.44E+05	1.14E+06	0.72	
9	1.09E+06	1.56E+06	0.18	
	1.08E+06	1.52E+06	0.20	
10	1.77E+06	2.27E+06	-0.23	
	1.76E+06	2.17E+06	-0.21	

Table 9.12: Margin of safety of the honeycomb around the insert area

The honeycomb around the first insert is the first to yield, and the corresponding margin is negative; from the second on, the margin is positive, but it is again close to zero, so that it can easily turn negative once the honeycomb in the location 1 is compromised, and the load is distributed between the components still intact.

COUPON 2 - AXIAL TRACTION - CASE 2 ULTIMATE							
		ELEMENT ID	FORCE X	MOMENT X	RIS YZ	RIS MOMENT YZ	Mos1
		-	[N]	[Nm]	[N]	[Nm]	-
10	70400330	-5.41E+03	-1.20E+00	7.66E+03	2.19E+01	-0.28	
9	70400329	-2.77E+03	-3.93E-01	7.29E+03	4.34E+01	-0.01	
8	70400328	-1.82E+03	-4.35E-01	7.29E+03	4.47E+01	-0.02	
7	70400327	-1.11E+03	-4.43E-01	7.36E+03	4.25E+01	-0.01	
6	70400326	-3.85E+02	-4.89E-01	7.54E+03	3.93E+01	-0.11	
5	70400325	5.84E+02	-5.27E-01	7.52E+03	3.50E+01	-0.03	
4	70400324	1.53E+03	-5.11E-01	7.76E+03	3.87E+01	-0.04	
3	70400323	2.21E+03	-4.75E-01	7.31E+03	3.88E+01	-0.05	
2	70400322	2.92E+03	-4.36E-01	6.43E+03	3.32E+01	-0.15	
1	70400321	4.25E+03	-8.54E-01	5.13E+03	1.12E+01	-0.10	

Table 9.13: Margin of safety of the inserts

To dispel any doubt, the table 9.13 shows a negative margin for every single insert, obtained without a redistribution of the load, because the first one applied is already enough to break all of them.

9.2.3 Coupon 2 - Bending test

The bending test presents a failure at the lowest ultimate loads between the applied, 5701 N; the numbering of the inserts follows the one chosen for the axial traction test. As a result of the test, the shear web is bent as the figure 9.9 explains, and in the same picture is possible to see how the inserts are lifted up, but they still connect the shear web and the cylindrical panel section. The failure is not as evident as it was in the other tests, because apparently the skins are intact and the inserts too: the deformed component is the cleat, made of AA 7075 Aluminium alloy, and modeled through CBAR elements.

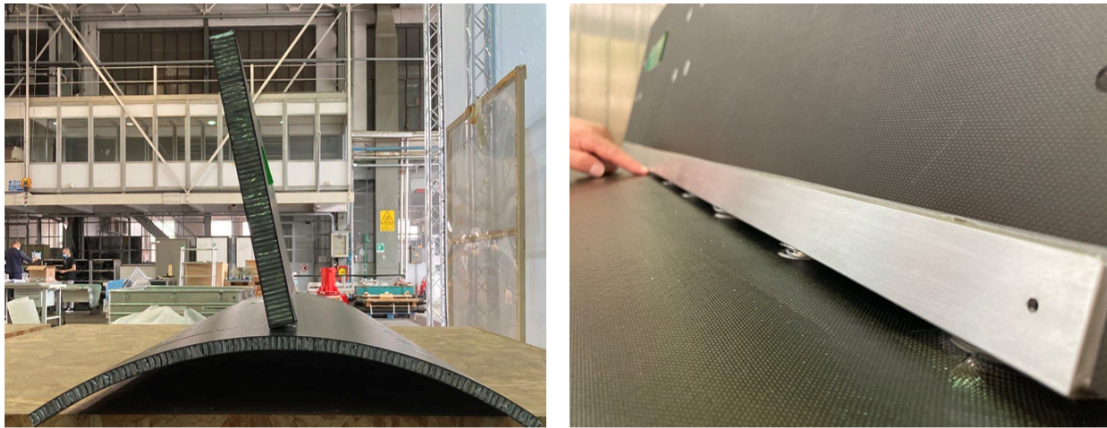


Figure 9.9: Result of the bending test and general view of the insert area - *Courtesy of TAS-TO*

In particular (9.10) the cleat seems to yield around the insert, reaching plastic deformation and in some cases the cleat is ripped, leaving the rest of the component without evident signs of breaking, except for insert 1 and 2, which show a slight ripple of the skins



Figure 9.10: (a) Detail of the first insert, with the broken skin, (b) an insert which reached plastic deformation, (c) difference between two consecutive insert locations, where the cleats break in two distinct ways - *Courtesy of TAS-TO*

According to the test, the processing of the forces for the inserts shows that every insert cracks under the applied load, but it is necessary to explore the role of the skins and the honeycomb around inserts. The honeycomb, in particular, is undamaged and it is in agreement with the test (table 9.14)

COUPON 2 - LATERAL - CASE 4 ULTIMATE				
		shear_xz	shear_yz	MoS
INSERT LOCATION	1	6.14E+05	8.96E+05	1.06
		5.60E+05	8.96E+05	1.13
	2	5.43E+05	8.39E+05	1.25
		5.42E+05	8.37E+05	1.25
	3	5.23E+05	8.02E+05	1.35
		5.23E+05	8.03E+05	1.34
	4	5.26E+05	8.09E+05	1.33
		5.27E+05	8.09E+05	1.33
	5	5.33E+05	8.23E+05	1.29
		5.35E+05	8.24E+05	1.29
	6	5.19E+05	7.99E+05	1.36
		5.23E+05	8.02E+05	1.35
	7	5.03E+05	7.73E+05	1.43
		5.07E+05	7.75E+05	1.42
	8	5.08E+05	7.85E+05	1.40
		5.14E+05	7.86E+05	1.39
	9	5.22E+05	8.20E+05	1.31
		5.37E+05	8.24E+05	1.28
	10	5.16E+05	9.02E+05	1.17
		6.12E+05	8.91E+05	1.07

Table 9.14: Honeycomb MoS indicates an intact core after the test

Regarding the skin (table 9.15), the margin of safety calculated is negative for every insert location, while the test point out that only the first insert involves the

breaking of the laminate, so it can be said that the modelization is conservative compared to the real test results.

COUPON 2 - LATERAL BENDING - INSERTS				
INSERTS	sigma_x	sigma_y	FI	MoS
1	-183.7	58.619	1.949	-0.52
	-146.3	57.563	2.626	-0.40
2	-189.2	59.356	1.979	-0.53
	-145.2	58.652	2.695	-0.40
3	-180.4	56.793	2.004	-0.51
	-144.1	56.111	2.533	-0.40
4	-172.7	56.177	2.005	-0.50
	-140.8	55.308	2.479	-0.41
5	-182.6	58.366	2.043	-0.52
	-143	57.728	2.633	-0.41
6	-187	60.544	2.051	-0.54
	-139.7	59.686	2.756	-0.41
7	-184.8	58.971	2.075	-0.52
	-145.2	58.234	2.668	-0.42
8	-179.3	58.146	2.088	-0.52
	-144.1	57.398	2.614	-0.42
9	-192.5	60.775	2.117	-0.54
	-148.5	60.159	2.796	-0.43
10	-200.2	63.987	2.156	-0.56
	-154	64.229	3.074	-0.44

Table 9.15: Margin of safety of the skins around the insert area

COUPON 2 - LATERAL - CASE 4 ULTIMATE						
ELEMENT ID	FORCE X	MOMENT X	RIS YZ	RIS MOMENT YZ	Mos1	
-	[N]	[Nm]	[N]	[Nm]	-	
10	70400330	2.64E-01	1.38E+01	5.53E+02	7.40E+01	-0.28
9	70400329	3.98E-01	-1.41E+00	6.95E+02	7.05E+01	-0.01
8	70400328	-9.41E-03	-3.39E+00	4.58E+02	6.97E+01	-0.02
7	70400327	-1.22E-01	2.80E+00	3.82E+02	6.96E+01	-0.01
6	70400326	9.73E-02	7.78E+00	5.34E+02	7.08E+01	-0.11
5	70400325	2.81E-01	2.29E+00	6.88E+02	7.16E+01	-0.03
4	70400324	2.20E-02	-2.82E+00	5.29E+02	7.16E+01	-0.04
3	70400323	-1.93E-01	3.38E+00	4.28E+02	7.17E+01	-0.05
2	70400322	7.83E-02	8.66E+00	6.24E+02	7.31E+01	-0.15
1	70400321	6.25E-01	2.96E+00	8.10E+02	7.71E+01	-0.10

Table 9.16: Margin of safety of the inserts

Finally, the insert MoS indicates a failure for every insert, as in table 9.16, but it can not be particularly demonstrative of the real failure occurred, because the most

important components to analyze, in this case, are the cleats. After a recovery of the forces is done, for the CBAR involved, it is necessary to compare the von Mises stress with the AA7075 Ultimate strength allowable, to calculate the margin of safety. The sum of forces arising from every insert lead to a negative margin of safety for the cleat, meant as the long joint connecting the shear web with the cylindrical sandwich panel. The cleat, in particular, presents signs of yield and rupture around the inserts, from the third onward, while the analytical calculation shows a failure for the first and second insert too: this is not a problem, it just means that the mathematical model is conservative. As the table 9.17 shows, the cleats fails at yield and at ultimate too.

COUPON 2 - -LATERAL - - CLEATS				
SUM MOM X	SUM MOM Z	SUM RIS YZ	MoS YIELD	MoS ULTIMATE
34.073837	-719.59732	5701.010507	-0.42	-0.27

Table 9.17: Margin of safety of the cleat

9.3 Coupon 3

The third coupon depicts the attachment to the LVA ring, and it was tested to traction and it failed under a force of 60300 N. The figure 9.11 shows the order in which the inserts have been processed.

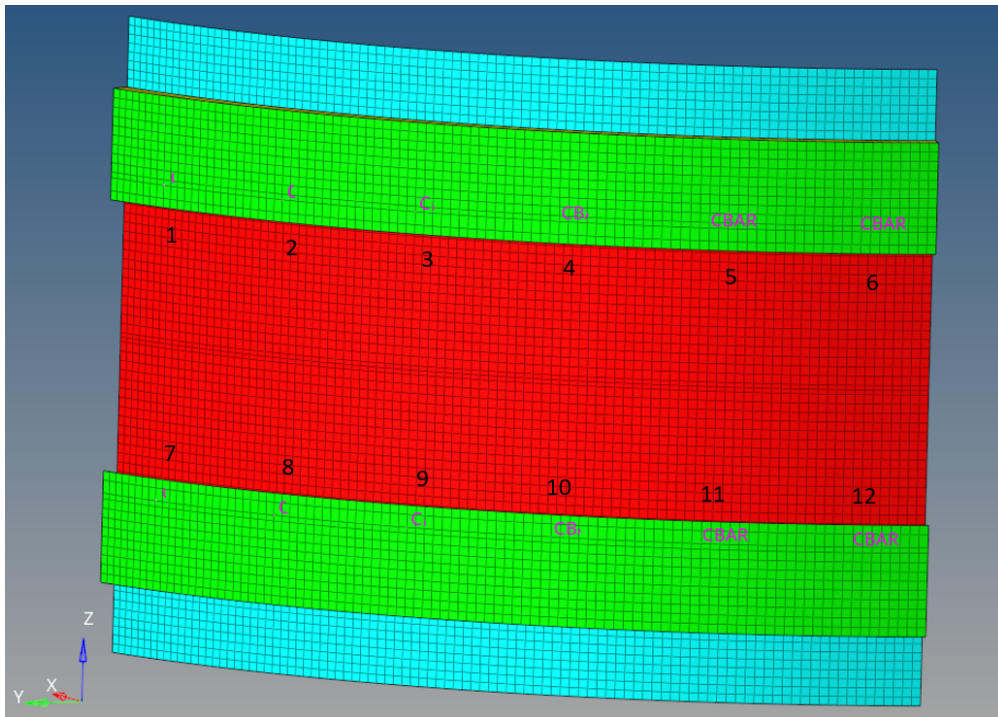


Figure 9.11: Numbering of inserts - *Courtesy of TAS-TO*

This coupons presents a kind of rupture different from all the others seen before; from the picture 9.12 in fact, no sign of fracture is visible from the skin or the honeycomb, but the hole of the insert oval, which means that the part failed by bearing.

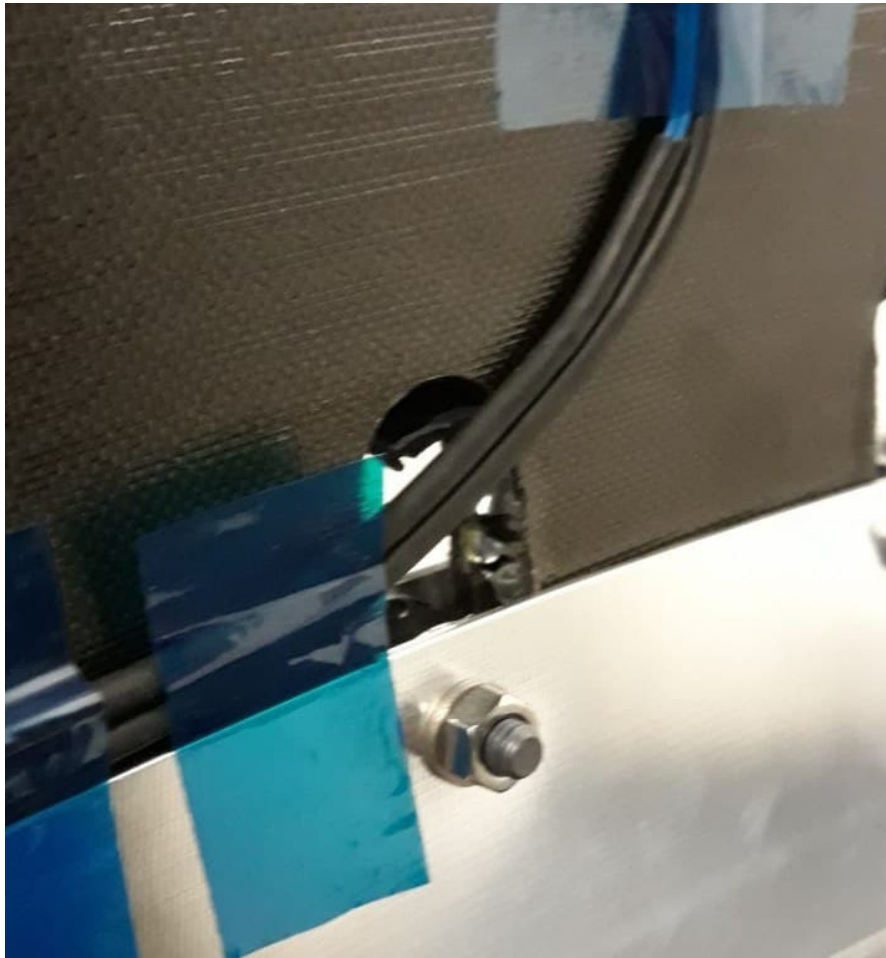


Figure 9.12: Bearing of the hole - *Courtesy of TAS-TO*

Even though the failure has been identified, a check of the laminate and honeycomb failure mode must be done, as well as for the inserts. The margin of safety of the inserts was higher than one for every location, as reported in the table [9.18](#) and the test results confirm this analysis. In the same way, the honeycomb stayed in place and did not failed, as reported in figure [9.19](#)

COUPON 3 - ULTIMATE TRACTION - CASE 2					
	ELEMENT ID	AXIAL	RIS SHEAR	MAX MOMENT	Mos
	-	[N]	[N]	[Nm]	-
1	14672	3.01E+02	5.25E+03	3.62E+01	0.38
	14673	4.38E+02	5.01E+03	2.93E+01	0.55
2	14675	4.48E+02	4.93E+03	1.96E+01	0.59
	14676	4.38E+02	4.89E+03	1.96E+01	0.60
3	14677	4.27E+02	5.04E+03	1.99E+01	0.55
	14678	3.09E+02	5.15E+03	1.99E+01	0.52
4	14679	3.01E+02	5.23E+03	3.63E+01	0.38
	14680	2.77E+02	4.98E+03	3.45E+01	0.45
5	14681	2.55E+02	4.87E+03	3.37E+01	0.49
	14682	2.54E+02	4.85E+03	3.36E+01	0.49
6	14683	2.88E+02	5.05E+03	3.47E+01	0.44
	14684	3.05E+02	5.26E+03	3.63E+01	0.38
7	14685	2.67E+02	5.05E+03	3.47E+01	0.44
	14686	2.50E+02	4.85E+03	3.36E+01	0.49
8	14687	2.47E+02	4.87E+03	3.37E+01	0.49
	14688	2.67E+02	4.99E+03	3.46E+01	0.45
9	14689	3.02E+02	5.23E+03	3.64E+01	0.38
	14690	3.27E+02	5.12E+03	3.03E+01	0.52
10	14691	4.29E+02	5.00E+03	2.92E+01	0.56
	14692	4.57E+02	4.93E+03	2.84E+01	0.59
11	14693	4.51E+02	4.89E+03	2.83E+01	0.60
	14694	4.29E+02	5.03E+03	2.91E+01	0.55
12	14695	3.11E+02	5.15E+03	3.02E+01	0.52
	14696	3.08E+02	5.12E+03	3.04E+01	0.52

Table 9.18: MoS of the inserts

COUPON 3 - ULTIMATE TRACTION - CASE 2 ULTIMATE				
		shear_xz	shear_yz	MoS
INSERT LOCATION	1	7.29E+04	1.97E+04	29.41
		5.00E+04	6.57E+04	28.63
	2	1.63E+05	1.41E+05	10.12
		9.55E+04	1.31E+05	14.14
	3	2.56E+05	2.16E+05	6.13
		1.03E+05	2.31E+04	20.72
	4	2.41E+05	2.24E+05	9.20
		1.05E+05	2.45E+04	20.28
	5	2.03E+05	1.94E+05	7.62
		9.90E+04	2.14E+04	21.62
	6	7.27E+04	1.18E+05	20.52
		5.74E+04	3.19E+04	34.62
	7	7.68E+04	2.02E+04	27.93
		4.02E+04	5.52E+04	34.91
	8	9.63E+04	1.30E+05	14.17
		1.43E+05	1.20E+05	11.81
	9	2.15E+05	1.99E+05	7.19
		1.03E+05	1.45E+05	12.75
	10	2.13E+05	2.06E+05	7.13
		1.04E+05	1.46E+05	12.67
	11	2.04E+05	1.96E+05	7.48
		7.07E+04	1.04E+05	18.59
	12	7.66E+04	1.20E+05	16.37
		2.57E+04	4.25E+04	48.85

Table 9.19: Margin of safety of the honeycomb around the insert area

. From the laminate point of view, skins have been processed and analyzed in the area around the insert location, where the failure happened, but they still resist to the stress, table 9.20

COUPON 3 - AXIAL TRACTION - INSERTS				
INSERTS	sigma_x	sigma_y	FI	MoS
1	-415.47	1.5774	0.522	1.87
	-191.73	12.683	0.543	2.03
2	-358.49	2.6136	0.464	0.21
	-179.96	9.4259	0.428	2.23
3	-342.76	2.5443	0.440	0.38
	-172.59	10.6381	0.456	2.37
4	-340.12	2.4904	0.435	0.37
	-181.28	8.3193	0.398	2.21
5	-342.43	2.4662	0.438	0.31
	-197.34	2.4365	0.259	1.96
6	-415.8	1.5642	0.539	11.13
	-192.06	1.1759	0.220	1.97
7	-412.39	1.6104	0.535	0.86
	-203.06	8.3369	0.421	1.81
8	-199.87	2.5454	0.265	1.92
	-342.43	2.5212	0.439	0.37
9	-337.04	2.5817	0.449	0.50
	-176.99	9.2114	0.416	2.22
10	-335.39	2.5256	0.446	0.48
	-186.34	7.0499	0.365	2.06
11	-347.49	2.6653	0.450	0.32
	-179.63	9.1124	0.418	2.23
12	-411.07	1.5906	0.515	0.86
	-201.63	8.5041	0.427	1.89

Table 9.20: Margin of safety of the laminate around insert area

. Other parts to be checked are the upper and lower fork, made of aluminium AA7075; for this margin of safety is enough to find the von Mises stresses from the post processing, around the insert area, and compare them with the ultimate stress allowbles, and for completeness with the yield stress too. The test results show the fork completely intact, which suggests that the bearing failure interest the cylindrical sandwich section.

Superior external fork					Superior internal fork				
INSERTO	ELM ID	vonMises [MPa]	MoS yield	MoS ultimate	INSERTO	ELM ID	vonMises [MPa]	MoS yield	MoS ultimate
1	6568	1,37E+02	1,31	1,92	1	5414	2,77E+02	0,14	0,44
	6563	1,25E+02	1,54	2,21		5417	2,57E+02	0,23	0,56
2	6444	1,31E+02	1,43	2,06	2	5265	2,59E+02	0,22	0,54
	6352	1,23E+02	1,58	2,25		5090	2,41E+02	0,32	0,66
3	6203	1,28E+02	1,48	2,13	3	4949	2,47E+02	0,28	0,62
	6228	1,22E+02	1,60	2,28		4941	2,34E+02	0,36	0,71
4	5992	1,27E+02	1,49	2,14	4	4838	2,48E+02	0,28	0,61
	5987	1,21E+02	1,61	2,29		4841	2,34E+02	0,36	0,71
5	5868	1,30E+02	1,44	2,07	5	4689	2,55E+02	0,24	0,57
	5776	1,23E+02	1,57	2,24		4518	2,58E+02	0,23	0,55
6	5627	1,26E+02	1,51	2,17	6	4373	2,70E+02	0,17	0,48
	5645	1,38E+02	1,30	1,90		4365	2,58E+02	0,23	0,55

Table 9.21: Upper fork margin of safety for aluminum in the insert area

Inferior external fork					Inferior internal fork				
INSERTO	ELM ID	vonMises [MPa]	MoS yield	MoS ultimate	INSERTO	ELM ID	vonMises [MPa]	MoS yield	MoS ultimate
7	14538	1,26E+02	1,53	2,19	7	13382	2,77E+02	0,14	0,44
	14531	1,24E+02	1,56	2,23		13385	2,57E+02	0,23	0,56
8	14412	1,31E+02	1,43	2,06	8	13233	2,59E+02	0,22	0,54
	14320	1,23E+02	1,57	2,24		13058	2,41E+02	0,31	0,66
9	14171	1,28E+02	1,49	2,14	9	12917	2,48E+02	0,28	0,61
	14196	1,22E+02	1,60	2,29		12909	2,34E+02	0,36	0,71
10	13960	1,27E+02	1,49	2,15	10	12806	2,49E+02	0,28	0,61
	13955	1,21E+02	1,62	2,30		12809	2,34E+02	0,35	0,71
11	13836	1,30E+02	1,43	2,07	11	12657	2,56E+02	0,24	0,56
	13744	1,24E+02	1,57	2,24		12482	2,41E+02	0,32	0,66
12	13595	1,26E+02	1,51	2,17	12	12341	2,71E+02	0,17	0,48
	13620	1,26E+02	1,52	2,18		12333	2,58E+02	0,23	0,55

Table 9.22: Lower fork margin of safety for aluminum in the insert area

. Finally, according to the test, bearing results show a failure for each insert, table 9.23

COUPON_3 - BEARING				
N	ELM ID	RIS SHEAR	MoS	
-	-	[N]	-	
INSERTI	1	14672	4.79E+03	-0.48
		14673	4.57E+03	-0.45
	2	14675	4.49E+03	-0.44
		14676	4.46E+03	-0.44
	3	14677	4.59E+03	-0.45
		14678	4.69E+03	-0.47
	4	14679	4.77E+03	-0.47
		14680	4.54E+03	-0.45
	5	14681	4.45E+03	-0.44
		14682	4.42E+03	-0.43
	6	14683	4.60E+03	-0.46
		14684	4.80E+03	-0.48
	7	14685	4.61E+03	-0.46
		14686	4.42E+03	-0.43
	8	14687	4.45E+03	-0.44
		14688	4.55E+03	-0.45
	9	14689	4.77E+03	-0.47
		14690	4.67E+03	-0.46
	10	14691	4.56E+03	-0.45
		14692	4.49E+03	-0.44
	11	14693	4.46E+03	-0.44
		14694	4.59E+03	-0.45
	12	14695	4.69E+03	-0.47
		14696	4.67E+03	-0.46

Table 9.23: Bearing results for cylindrical sandwich panel around inserts

9.4 Adhesive joint Mos

Since there was not any sign of failure from the adhesive point of view, neither during tests or from analytical calculation, the following table 9.24 resumes the cleat's

margin of safety, largely positive for every coupon and for every load configuration, according to the Hart-Smith theory.

		MoS
Coupon 1	y shear web	9.91
	x shear web	14.02
Coupon 2	pullout	13.51
	axial traction	4.94
	bending	98.02

Table 9.24: Margin of safety for adhesive joint 1 and 2

Chapter 10

Conclusions

The work done and presented in this Master Thesis Report presents a part of test campaign carried out on HE-R1000 Platform. It has provided the ultimate loads and failure modes of main structural components necessary for HE-R1000 satellite structure. In particular, the coupons highlighted the correct structural behaviour that has been observed in the Static Qualification phase of HE-R1000 platform. Thanks to accurate study of load cases of HE-R1000 by means FEM simulations, the three scale coupons have been accurately selected taking into account the effective real dimensions and the structural symmetries that include the main load paths of HE-R1000 structure. The coupons predicted correctly the load paths and the possible failure mode that in HE-R1000 structure will occur if the Qualification loads increment.

A summary of coupon's test results is made; every coupon withstood the Qualification Load, except for the lateral bending test of Coupon 2, and an Ultimate load is recorded. The test campaign have been concluded successfully leading at the Static Qualification of HE-R1000 Structure. The work treated and illustrated in this work highlighted the importance conducted by coupons and the main components tested in order to better define the Design Concept. About the FEM simulations of the coupons, the mathematical models have been capable to predicted accurately the real behaviour of the Design. In some cases, they showed overestimated predicted values compared to the test read ones, but this effect can be considered as a conservative approach, because it leads to a lower Margin of Safeties. In other cases, in few areas, the FEM simulations underestimated the predicted values compared to the test readings, but these local effects are not significant because in those cases additional safety factor have been take into account in the Strength Analysis. However, this effects of overestimation and underestimation are intrinsic of Element Finite formulations and, in particular, they are due to the presence of rigid elements of connection which introduce concentrate loads and generate a peak of strains. Vice-versa, the difference of considerable stiffness

between rigid elements and 2D shell elements with the adequate mechanical properties leads to underestimate the strain/stress. In any case, these local events don't affect the goodness of global behaviour of the mathematical models, that are consider sufficiently accurate. The success of the test object of this academic work is demonstrated by following results, obtained from strain gauges below reported:

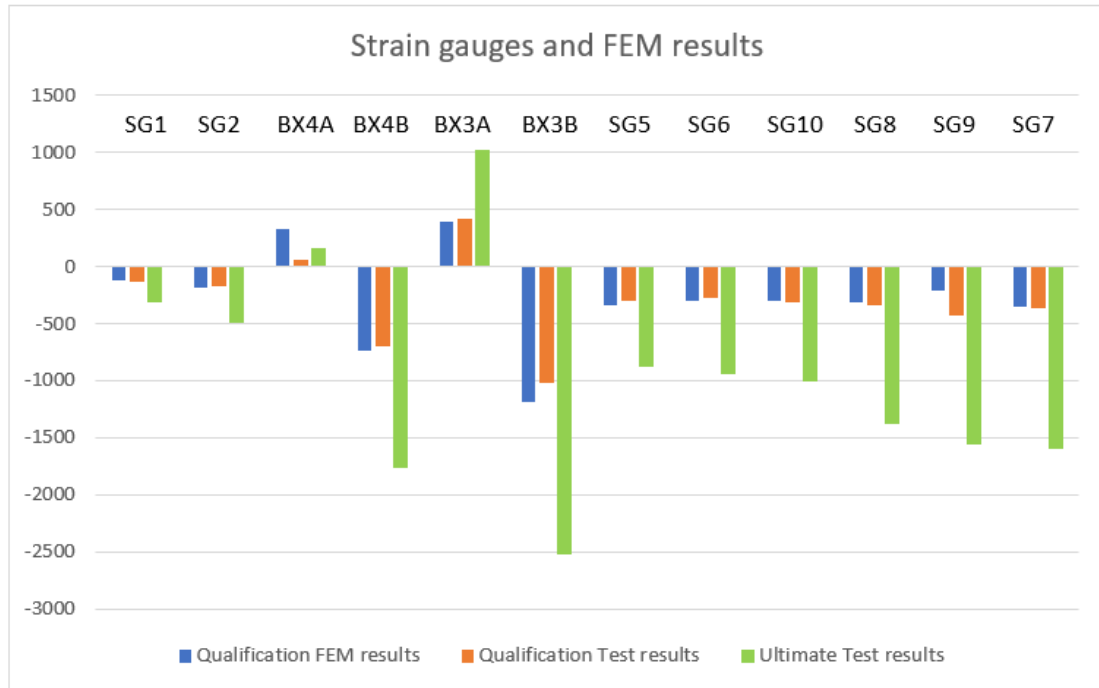


Figure 10.1: Strain gauges readings for Qualification and Ultimate load with respect to FEM qualification prediction values

The results can be considered reliable and coherent to the reality, due to the instrumentation adopted: out of 10 strain gauges adopted, and 12 measurement collected, 10 of them are less than 15% distant from the predicted FEM results, so a percentage of 83% of the total used, fig. 10.1 Moreover, a brief summary of ultimate failure loads reach in coupons test are reported:

- Coupon 1: Ultimate Collapse load reached is 35489N for each LURA bracket, and 7250N for each lateral clamp
- Coupon 2: this coupon needs to be further divided in three cases, one for each sample and corresponding test
 - Pull Out test: this tension test gave back an Ultimate load of 33175N

- Axial: Ultimate Collapse load for this test is 71277N
- Bending: this coupon was not able to reach Qualification Load and broke under a load of 5701 N
- Coupon 3: for this model, 2 samples were created and both of them overcome the Qualification Load, in particular the one subjected to traction reached 60300N before the rupture.

From the data recovered by coupons' test, compared to tested qualification load cases of HE-R1000, it is possible to declare:

1. The ultimate loads recovered on Coupon 1 fully covered the axial Qualification loads of HE-R1000. The expected failure mode is in line with FEM prevision. Moreover, strains which have been read on the Cylindrical part, at Ultimate load, demonstrate high strength capability and no local buckling phenomena and Euler instability occurs.
2. The ultimate loads recovered on the Coupons 2 demonstrate as follow:
 - The ultimate pull out recovered test fully covered the maximum qualification radial load of HE-R1000
 - The ultimate axial recovered load fully covered the maximum axial qualification load of HE-R1000
 - The ultimate lateral recovered load is approximately similar to qualification load of HE-R1000.
3. The ultimate loads recovered on the Coupons 3 demonstrate that the junction between Cylinder and LVA Ring fully covered the qualification loads reached in HE-R1000 qualification process.

From this academic study carried out in TAS-I company in TORINO site, it can be deduced the capability of HE-R1000 to sustain the loads over the Qualification level. The obtained result is important since it can be considered the starting point for future enhancement of the payload configuration.

grazie agli accurati studi dei load case di HER1000 tramite le simulazioni fem, sono stati accuratamente selezionati tre coupons,

Bibliography

- [1] Soyuz at Guiana Space Centre User's Manual
- [2] <http://isogridcomposites.com/about/>
- [3] HE-R1000 PRODUCT - Structure Design Description and Mechanical Analysis Report *L. Manfredi*
- [4] Tecnologie e materiali Aerospaziali *G. Sala, L. Di Landro, A. Airoidi, P. Bettini*
- [5] HexWeb™ HONEYCOMB SANDWICH DESIGN TECHNOLOGY
- [6] ECSS-E-HB-32-22A *Space engineering - Insert design handbook*
- [7] Appunti del corso Tecnologie Aerospaziali *Professor G. Romeo - Politecnico di Torino*
- [8] NASA CR-1122335 ADHESIVE-BONDED DOUBLE-LAP JOINTS *L. J. Hart-Smith*
- [9] HE-R1000 Test Specification Material and Structural component characterization *L. Manfredi*
- [10] ASTM-D1002 - Standard Test Method for Apparent Shear Strength of Single-Lap-Joint Adhesive Bonded Metal Specimens by Tension Loading (Metal to Metal)
- [11] ASTM-D5868 - Standard Test Method for Lap Shear Adhesion for reinforced plastic (FRP) Bonding
- [12] NASA CR-1457 - Manual for structural Stability analysis of Sandwich Plates and Shells *R. T. Sullins, G. W. Smith, E. E. Spier*
- [13] Caratterizzazione meccanica di un pannello sandwich per l'interno di un aeromobile *Tesi di laurea magistrale, Mattia Ioni*

- [14] ASTM C364 - Standard Test Method for Edgewise Compressive Strength of Sandwich Construction
- [15] NSTS 08307 - NASA Space Transportation system: Space Shuttle Criteria for Pre-loaded bolts

Acknowledgements

I wish to dedicate this space to all the people who got involved not only in this project, but in this journey too.

My thanks go to my thesis professor, M. Gherlone, for the availability and support, and to my co-rapporteur Luigi Manfredi, for dedication, patience and time spent for my growth during this project.

A thanks go to Gabriele, for the essential help given and for his kindness, and to Sofia, Tommaso, Luca and Damiano for their presence and the laugh during those hysterical study sessions. To all the friends who touched my path in these years, to the close ones and to the distant ones, thank you for sharing your time.

A huge, special thanks to my family, for the support and the patience demonstrated, for standing my breakdown and for cheering me up even when I thought I could not manage. I love you all.

To mom and dad, for the love and the encouragement and to my Bugo, my best friend despite the teasing, always by my heart

To my man, Mario, for your being there during this journey and for those to come.